UNIVERSITY OF WEST BOHEMIA
FACULTY OF APPLIED SCIENCES

BIOMECHANICAL MUSCULOSKELETAL MODEL

Ing. Linda Havelková

A doctoral thesis submitted in fulfilment of the requirements for the degree of doctor in Applied Mechanics

Supervisor: doc. Ing. Luděk Hynčík, Ph.D.
Department of Mechanics

Plzeň 2016

ZÁPADOČESKÁ UNIVERZITA

FAKULTA APLIKOVANÝCH VĚD

Biomechanický svalově-kosterní model

Ing. Linda Havelková

Disertační práce k získání akademického titulu doktor v oboru

Aplikovaná mechanika

Školitel: doc. Ing. Luděk Hynčík, Ph.D.

Katedra mechaniky

Plzeň 2016

Declaration of Authorship

I, Linda Havelková, declare that this work titled, 'Biomechanical musculoskeletal model', is my own. I confirm that where any part has previously been published, this has been clearly stated. When I have already presented some parts, this is always clearly attributed. When I have quoted from the work of others, the source is always given.

Signed:

_____

Date:

_____

Acknowledgements

Foremost, I would like to express my appreciation and thanks to my supervisor doc. Ing. Luděk Hynčík, Ph.D. for the continuous support of my study and research, for motivation and enthusiasm. This work was accomplished during my Ph.D. study at the Department of Mechanics of the Faculty of Applied Sciences of the University of West Bohemia in Pilsen. The kind support of the department's stuff is greatfully acknowledged. Further, my thanks belong to my colleagues from the New Technologies - Research Centre for their useful advice.

Next, I would like to thank to the department of doc. PaedDr. Karel Jelen, CSc. from the Faculty of Physical Education and Sport of Charles University, Prague, for the experimental support. I also thank to MUDr. Milan Novák, the head doctor at Radiology department at City Hospital, Pilsen, PRIVAMED Inc and to MUDr. Boris Pauček, Ph.D., the head doctor at Medihope - MR diagnostic center Military Hospital, Olomouc for the MRI data of healthy subjects.

My great acknowledgement belongs also to the AnyBody Research Group, Aalborg, Denmark, headed by Prof. John Rasmussen, Ph.D. for the big support and help during my study internship in their group.

Last but not the least, I would like to thank a lot to my family for the indispensable support.

Abstract

Presented thesis work is focused on musculoskeletal modeling, especially on muscle forces and moment arms calculation using the new method for muscle path determination. The main contribution is the new torus-obstacle method development limiting the lacks of existing methods for muscle trajectory calculation. The method is developed to model the correct muscle trajectory in any joint configuration. It is based on obstacle-set method. However, the new torus obstacles are implemented instead of standard obstacles such as spheres and cylinders to improve the original process of muscle wrapping. This method also enables the automatic calculation of muscle lines attachments; positions, rotation and radius of torus obstacles originated from MRI and respecting the input number of muscle lines. The torus-obstacle method also considers the muscle bulging up as well as changes of muscle shapes influenced by surrounding muscles.

The case of this study is to create the simple shoulder model in MATLAB including the deltoid muscle and using developed torus-obstacle method. Thanks that, the implementation, usage, advantages and disadvantages of presented method are shown. The bones are modeled by rigid bodies connected by real joints; the real muscle behavior is simulated by Hill-type model. For purpose of this work, the scapula and the clavicle are fixed. The muscle complex is replaced by elastic frictionless muscle lines of action generating the same force along the whole band and wrapping around the neighboring structures replaced by torus obstacles. The humeral abduction and forward flexion till 90° are simulated to validate the model and also the wrapping method. The paths of muscle lines, muscle forces, actual lengths and the muscle moment arms are compared to the similar models published in literature, to the electromyography measurement and to two shoulder models built in AnyBody Modeling System.

The results show the successful validation of major actuators of abduction and forward flexion. The new torus-obstacle method is suitable for all human body joints especially for complicated joints as shoulder complex, for all muscles - thick, thin, shallow, long, short etc. Presented study also introduces briefly the anatomy and physiology of the shoulder complex, offers the research of existing shoulder models and methods for muscle path definition and describes the multibody spatial dynamics in more details. In conclusion, developed torus-obstacle method designed for muscle trajectory computation in musculoskeletal modeling seems to be useful tool.

Keywords: musculoskeletal modeling, shoulder complex, obstacle-set method, Hill-type model, deltoid muscle, torus.

Abstrakt

Předkládaná práce je zaměřena na svalově-kosterní modelování, především pak na výpočet svalových sil a ramen momentů při libovolném pohybu s využitím nové metody určení průběhů svalů. Jejím hlavním přínosem je vývoj unikátní metody založené na svalovém obepínání anuloidů, která výrazně snižuje nedostatky již existujících metod pro určení svalových trajektorií. Metoda je vyvinuta pro výpočet korektního tvaru svalu při jakékoliv konfiguraci kloubů. Je založena na obecně známé metodě svalového obepínání série překážek tvořených tuhými geometrickými tvary a nahrazujících okolní tkáně, obecně známá jako *metoda obstacle-set*. Z důvodu vylepšení původní metody byly překážky tvaru koule či válce nahrazeny anuloidy. Nově vzniklá metoda dále umožňuje automatický výpočet umístění svalových úponů; pozic, natočení a poloměrů jednotlivých anuloidů; nárůst aktuálního fyziologického průřezu svalu během kontrakce či změny tvaru svalu s ohledem na sousedící svalové skupiny. Veškerá geometrie metody je založena na MRI a počtu uvažovaných svalových vláken.

Dílčím cílem studie je vytvořit jednoduchý model ramene v programu MATLAB, který obsahuje pouze dvojhlavý sval pažní a je založen na nově vyvinuté metodě obepínání anuloidu. Touto cestou je prezentována implementace, použití, výhody a nevýhody této metody. Kosti modelu jsou nahrazeny tuhými tělesy spojenými reálnými klouby; skutečné chování svalů je simulováno modelem Hillova typu. Pro potřeby této práce jsou pohyby lopatky a klíční kosti zanedbány. Svalový komplex je prezentován elastickými svalovými vlákny zanedbatelného tření generující stejnou sílu po celé své délce a obepínající sousední struktury nahrazené anuloidy. Pro validaci modelu a metody obepínání anuloidu je simulován pohyb pažní kosti - abdukce a přední flexe do úhlu 90°. Trajektorie svalových vláken, síly ve svalech, aktuální délka a momentová ramena svalů jsou poté porovnána s výsledky obdobných modelů prezentovaných v literatuře, s elektromyografickým měřením a se dvěma modely ramene sestavených v programu AnyBody Modeling System.

Výsledky prokazují úspěšnou validaci hlavních akčních členů abdukce a přední flexe ramene. Nová metoda svalového obepínání anuloidů je vhodnou metodou pro simulaci všech kloubů lidského těla - především pro komplikované klouby jako je např. ramenní komplex, či pro všechny typy svalů - silný, slabý, plochý, dlouhý, krátký, aj. Prezentovaná studie také stručně představuje anatomii a fyziologii ramenního komplexu, nabízí rešerši existujících ramenních modelů a metod pro výpočet svalové trajektorie a do větších detailů popisuje dynamiku vázaných mechanických systémů v prostoru. Závěrem lze říci, že metoda svalového obepínání anuloidů je užitečným nástrojem při svalově-kosterním modelování.

Klíčová slova: svalově-kosterní modelování, ramenní komplex, metoda obstacle-set, svalové obepínání, model Hillova typu, dvojhlavý sval pažní, anuloid.

Kurzfassung

Diese Arbeit beschäftigt sich mit der muskuloskelettalen Modellierung besonders mit der Berechnung der Muskelaktivitäten und Kraftarmen während der beliebigen Bewegung, wenn die Bestimmungsmethode der Muskelverlafen benutzt ist. Ihr Hauptbeitrag ist die Entwicklung der unikal Methode, die auf dem Muskelumwinden des Torus beruhend ist. Die präsentierte Methode stammt aus einer bekannten Methode, die allgemein als *obstacle-set* Methode bekannt ist. Bei dieser Methode sind die benachbarten Strukturen durch die festen Körper ersetzen (wie z.B. durch eine Kugel, einen Zylinder oder ein Ellipsoid). Danach umwinden die Muskelfasern diese Körper um die umliegenden Gewebe zu vermeiden. Die neu entwickelte Methode des Musckelumwindenes ersetzt diese Körper durch einen Torus. Sie ermöglicht auch die automatische Berechnung der Position der Muskelansätze und der Torus. Nicht in der letzten Reihe erhalt sie den Anstieg der vertikalen Querschnittsfläche während der Muskelkontraktion und die Änderung der Muskelform im Hinblick auf die benachbarten Muskeln. Die Geometrie der Methode stammt aus MRI und aus der Zahl der Muskelfasern.

Das Teilziel ist ein einfaches Schultermodel zu schaffen, das nur einen Muskel Deltoideus enthält und das auf der neuen Methode für Muskelumwinden beruhend ist. Auf diese Weise die Implementierung, die Benutzung, die Vorteilen und die Nachteilen der Methode präsentieren sind. Die Knochen sind durch die festen Körper im Model ersetzen; das Muskelverhalten ist mit dem Hill Muskelmodel simuliert. Das Schlüsselbein und das Schulterblatt sind fixiert. Der Schulterkomplex ist mit den elastischen Fasern präsentiert; die keine Friktion haben, die die gleiche Muskelkraft auf die ganzen Länge generieren und die Torus-hindernisse umwinden. Diese Methode und ebenso das Schultermodel sind bei zwei Bewegungen validiert - mit der Abduktion und der Flexion bis 90°. Die Trajektorien der Muskelfasern, die Muskelkräfte und die Muskelkraftarmen sind danach mit der Literatur, der EMG Messung und mit zwei Schultermodellen, die im AnyBody Modeling System gebaut sind, verglicht.

Die Ergebnisse ergeben, dass die Validierung des Hauptaktionselements erfolgreich ist. Diese neue Methode für Muskelumwinden ist geeignet für Gelenksimulation - vor allem für komplizierte Gelenke wie z.B. Schulterkomplex. Diese Studie präsentiert auch die Anatomie und die Physiologie des Schulterkomplexes, bietet die Recherche der existieren ähnlichen Modellen und Methoden an und beschreibt die Dynamik der gebunden festen Körper im 3D. Zum Schluss kann man sagen, dass diese neue Methode für Muskelverlaufen Bestimmung ein nützliches Mittel im muskuloskelettalen Modellierung ist.

Schlüsselworten: muskuloskelettale Modellierung, Schulterkomplex, Obstacle-set Methode, Muskelumwinden, Hill Muskelmodel, Muskel Deltoideus, Torus.

Contents

List of Tables

List of Figures

Part I

INTRODUCTION

Chapter 1

Musculoskeletal Biomechanics, Purpose and Overview of Thesis

1.1 Background

With increase of the standard of living and of the age of population, it is put the growing emphasis on the topics of health and comfort such as medical care improvement, optimization of rehabilitation, reliable prediction of some injury and diseases, useful prevention, workplace ergonomics, and many others. To achieve the most accurate results in this areas and to speed up the progress, the new innovative methods are used. However, the experimental methods such as electromyography are very often invasive, painful, time-consuming, expensive, etc. In addition, they are usually space-demanding, limited by ethics and law, depending on the high number of participants, etc.

Because of these disadvantages, the use of the biomechanical virtual human body models is becoming increasingly popular. Computer modeling is a valuable tool that allows researchers to simulate all inner and outer processes of the human body in any details. For example, it is possible to calculate the muscle forces generated in the skeletal muscle during elbow flexion as well as to model the calcium regulation of this muscle contraction. The biomechanical models are already indispensable especially for description of complex structure such as shoulder joint or for complicated simulations. For instance, to date, the computer models are still the only one means for the estimation of muscle forces, certainly outside laboratory conditions [71]. Many models describing the human body musculoskeletal system have been already developed - from simple two-dimensional (2D) to complex three-dimensional (3D) models [31].

1.2   Musculoskeletal Modeling

The musculoskeletal system of human body is very complex. From medical point of view it consists of four main subsystems - central nervous system, muscles, skeletal system and proprioceptors (feedback of central nervous system). The precise coordination of these helps to permit body movements while also to keep the body center of gravity in balance.

In computer modeling, the human body is often represented by mechanical system. Central nervous system is usually replaced by some optimization methods. Muscles are mostly represented by forces and considered to be actuators without any mass properties. Bones are modeled by rigid bodies connected by mechanical joints corresponding well with the real anatomy and physiology. The bone geometry and positions of muscle attachments are commonly based on MRI (magnetic resonance imaging) or on VHP (Visible Human Project) [38].

The musculoskeletal models help in clinical practices to prevent some problems, to improve the strategy of rehabilitation, to diagnose orthopedic pathologies, etc. These are also used in sport to optimize the sport performance; in research and education to describe the anatomy and physiology of human musculoskeletal system in more details; in ergonomics to optimize the structure of working machines and tools; and many others.

1.3   Importance of Correct Muscle Path Modeling

Musculoskeletal human body models are commonly used to calculate the forces transmitted by muscles, ligaments and articular surfaces at the joints during movements [37, 56]. The results of these studies are extremely sensitive to the muscle path definitions. For the given joint configuration, the muscle paths determinate the lengths, muscle moment arms, forces as well as torques of muscles at the given joint [37, 44].

Each musculoskeletal model is required to include some mathematical model for muscle path definition. The representation of that determines muscle's sites and trajectory between them. This factor directly influences the direction of the force applied to the bone. Moreover, the muscle length parameter influence the muscle's force-length properties determining the force capacity of individual muscle. In conclusion, the model of muscle path influence significantly the results of musculoskeletal modeling studies [110].

Three distinctly different models are mainly used to represent the muscle path in the body - (1) the straight-line model, (2) the centroid-line model (usually using the via-points) and (3) the obstacle-set method. In the first method, the muscle lines are straight lines going between the attachments [13, 22, 29]. This method is easy to implement, however, it has not meaningful results when the muscles intersect the surrounding structures. In the second method, the muscle line goes along the locus of cross-sectional centroid of given muscle [27, 84, 104]. This method produces a more

realistic description of the muscle line shapes. Several approaches have been already developed to approximate the centroid-line of muscle. The most common method is called via-point method. The method introduces effective via points at specific locations along the centroid path. The muscle path is then given by straight lines between these points, origins and insertions. Nevertheless, the points are fixed to the bones even as the joint moves. This approach is reasonable for simple revolute joints. But, it is not adequate for complex joints having more than one degree of freedom. The third approach, the obstacle-set method, idealizes the muscle as a frictionless elastic bands moving freely over neighboring anatomical constraints replaced by regular-shaped rigid bodies such as spheres and ellipsoids [37]. The last method is very useful but it has still some limits such as - each muscle lines requires many obstacles; the muscle lines behave independently of the other muscles; the muscle lines slide over the obstacles too much; they fall down from the obstacles very often; the positions of obstacles are not calculated automatically; the muscle bulging up is neglected; the obstacle placement does not work for all arbitrary joint configurations; etc. Therefore, the new torus-obstacle method was developed in this study to limit the lacks of existing methods of muscle path definition.

1.4   Purpose of Thesis

Presented thesis is focused on musculoskeletal modeling, especially on muscle path definition. The first task is to prepare review of existing methods for muscle trajectory determination.

The main aim is to develop the new torus-obstacle method to eliminate or at least limit the lacks of existing approaches. This is the main contribution of this study. The method offers the automatic calculation of position of muscle attachments, the locations and diameters of torus obstacles, both based on MRI and on the number of muscle lines of action set by user. The method considers the muscle bulging up and the muscle paths also respect the surrounding muscles. This method is useful in general, for all arbitrary joint movements.

The next purpose of this work is to model the shoulder joint to show the usage of the new torus-obstacle method, to verified and validate the results, to express its advantages and disadvantages. In reality, the shoulder complex is the most complicated joint with the largest range of motion. Therefore, right the torus-obstacle method is suitable to use for this muscle path modeling. At the end of work, the method is validated using the MRI data, literature, EMG measurement, etc.

1.5   Overview of Thesis

The **Part I** is focused on the background of this work, introduces the musculoskeletal modeling in general and highlights the importance of correct muscle path calculation. This section describes content of each individual part of this study.

The **Part II** also called *State of the Art* is focused on the anatomy and physiology of the shoulder joint and deltoid muscle; on the existing shoulder models dividing into two main groups and on the muscle wrapping methods defining the muscle trajectory. This part is divided into three chapters.

In Chapter 2, the anatomy and physiology of shoulder complex are described. The structure of shoulder complex is briefly reported the shapes of bones, the all joints, their movements and range of motion. Some medical problems and joint stability of such a complicated joint are also mentioned. The deltoid muscle is depicted in more details its attachments, functions, individual parts as well as pathological changes.

In Chapter 3, the short review of existing shoulder models is offered. Two main groups are considered the mechanical and computer models. Their advantages as well as disadvantages are summarized.

In Chapter 4, the most used methods for muscle path calculation are introduced. Their principles, advantages and disadvantages are stated. The new torus-obstacle method is originally based on the obstacle-set method [37] and thus, this method is described in more details.

The **Part III** also called *Methods* describes the equations of multibody spatial dynamic; some essential methods of biomechanical modeling of human body and the new torus-obstacle method. This part if divided into three chapters as following described in more details.

In Chapter 6, the forward and inverse dynamics of multibody spatial movements are explained in more details. The fundamental equations are obtained from literature [83]. The Principal of Virtual Work as well as mass moment of inertia are also mentioned. The constrained dynamics considering the spherical joint is explained.

In Chapter 7, some biomechanical methods for human body modeling used in this work are evaluated. The redundant problem of biomechanics caused by higher number of unknown muscle forces than the number of equations of motion is solved by constrained optimization technique. The next topic of this chapter is the Hill-type muscle model. The simplified three elementary model is used to simulate the real behavior of skeletal muscle. The k-means method is also represented. This method is thereafter used to calculate the positions of muscle attachments and torus obstacles. The muscle moment arms estimation is included. The clinically-useful definition is introduced.

In Chapter 8, the new torus-obstacle method is developed. Firstly, the assumptions and advantages of this method are denoted. The method is described in few steps in all details. This chapter also demonstrates how the torus obstacle parameters (such as position, rotation, radius) are calculated. The method denotes also the process of muscle bulging up and the influence of muscle geometry on the other surrounding muscles.

The **Part IV** also called *Results* contains the results of model of human deltoid muscle and shows the validation tests of the shoulder model and that the new torus-obstacle method. This part is divided in two chapters.

In Chapter 9, the model of shoulder joint involving the deltoid muscle is depicted. The model is defined in all details. The process of geometry reconstruction is demonstrated. The positions of muscle attachments and torus obstacles are summarized in clear tables. The local and global coordinate systems are introduced. The mass moment of inertia is also evaluated. The optimization process with the used cost function are included. All parameters of muscle model are implemented. The simulations of abduction and forward flexion are exposed. The figures of muscle lines in different joint position are shown. The resulting muscle forces, actual muscle length and muscle moment arms generated during both movements are represented. At the end of chapter, the motion capture data and EMG processing are incorporated. In addition, the shoulder model built in AMS for model validation is specified.

In Chapter 10, the results of validation are denoted.

The **Part V** also called *Discussion and Conclusion* represents the final study evaluation.

Part II

STATE OF THE ART

Chapter 2

Anatomy and Physiology
of the Shoulder Complex

The human upper limb has wide range of motion. The main function of this complex system is essentially holding and manipulation. The upper limb is attached to the trunk by the pectoral girdle - the only point of articulation being at the sternoclavicular joint. Between the trunk and hand, there are the series of highly mobile joints and the system of levers. The precise cooperation of this structure allows the hand to be almost in any point in space. The most complicated system of upper arm is sure the shoulder. Complex consists of three bones and three joints. The shoulder complex is not easy defined because of complicated movements, anatomy and physiology [102].

2.1   Shoulder Complex

The shoulder complex consists of three bones - the clavicle, the scapula and the humerus, see Fig. 2.1. The clavicle extends laterally and horizontally across the neck from manubrium to the acromion. The shaft is sinuous, being convex forwards in its medial two-thirds and concave forward lateral to this. The clavicle is unlike typical long bone. The scapula is a flat, triangular bone; overlaps in part from the second to seventh ribs on the posterolateral thoracic aspect. The acromion belong to three processes of scapula (spinous, acromial and coracoid). This process is situated forwards, almost at the right angle, from the lateral end of the spine. This part includes the acromioclavicular facet and principal areas of attachments of the coracoacromial ligaments and deltoid muscle [30]. The humerus represents the longest and largest bone of the upper limb. Proximally and round humeral head form with the scapular glenoid cavity an enarthrodial articulation. The distal end also called condylar is adapted to the elbow joint of connection of forearm bones.

The connection of the upper limb bones is ensured by three joints - the sternoclavicular (SC), the acromioclavicular (AC) and the glenohumeral (GH), see Fig. 2.1. The SC joint involves the

sternal end of clavicle and the sternal clavicular notch, together with the adjacent superior surface of the first costal cartilage, [102]. The one part is convex vertically and slightly concave anteroposteriorly; the next joint part is reciprocally curved. However, these two parts are not fully congruent. The shape of the articular surface permits movement in approximately anterioposterior and vertical planes and some rotation around the long clavicle axis till about 30° [55]. The AC joint is between the clavicular acromial end and the medial acromial margin. This is approximately the plane connection; but either surface is slightly convex, the other is reciprocally concave. The movements of AC joint are almost the same as mentioned in SC joint. Therefore, the cooperation of these joints allows the scapular rotation till 60°. In the case, when the angle between the superior scapular border and the clavicular shaft reaches the angle 90°, the scapular rotation is further ensured by the SC joint. The GH joint also called shoulder joints represents the connection between the shallow scapular glenoid fossa and the roughly hemispherical humeral head. This joint is skeletally too weak. The joints stability depends for support of surrounding muscles more than on its shape. The humeral convexity exceeds in area that of the glenoid concavity such that only very small area opposes the glenoid in any position (about 1/3). Therefore, the good rotator muscles and GH ligaments are required for shoulder stability. On the other hand, this limitation offers the very wide range of joint movements. This spherical joint has three degrees of freedom - rotation around three orthogonal axes (flexion - extension, abduction - adduction, circumduction, medial and lateral rotation). The GH abduction is stated about 90° [55]. About 70° further abduction occurs at the contribution of SC and AC joints. The full abduction is then about 160° and more. In the forward flexion, the humerus swings at right angle to the scapular plane. Further, the scapular movements are needed. Thanks this cooperation, the 180° of elevation becomes possible. The movements of shoulder joint are usually extended by other special movements of scapula - (1) elevation and depression, when the scapula slides over the thoracic cage up and down; (2) protraction, when the scapula goes forward round the thoracic wall - this ability is used by pushing especially; (3) retraction, when the scapula goes backward and (4) lateral rotation of scapula, that increases the range of humeral elevation by turning the glenoid cavity to face almost directly up.

Because of shoulder complex complicatedness, its anatomy and physiology etc., this system is prone to many injuries, diseases, pathological changes and other problems. The most frequently is the dislocation, usually with the arm abduction. In the case of traumatic dislocation, the further complications are common such as stretching of GH ligaments [89], dysfunction of glenoid attachments [10], detachments of the anterior and inferior glenoid labrum thereby creating the typical Blankart lesion [102] or the loss of the shoulder joint mobility compensated by increasing scapular movements, and many others.

2.2 Deltoid Muscle

The external contour of the shoulder is produced by the deltoid muscle, see Fig. 2.2. It belongs to the skeletal muscles consisting of parallel bundles of long and multinucleate fibres, [102]. These muscles are sometimes called voluntary muscles, because the movements in which they participate are initiated mainly by central nervous system (CNS). Exactly, the CNS determinates which muscle will contribute and which activity with to the given movement. There is a long list of decision criteria such as the fatigue, health, the history of movement, the plans of motion, etc.
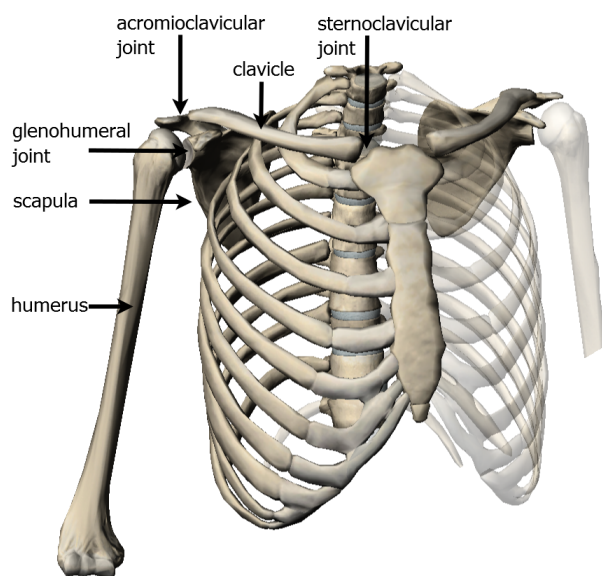
FIGURE 2.1: The bones and joints of shoulder complex (Muscle Premium - Visible Body, Boston, 2014).
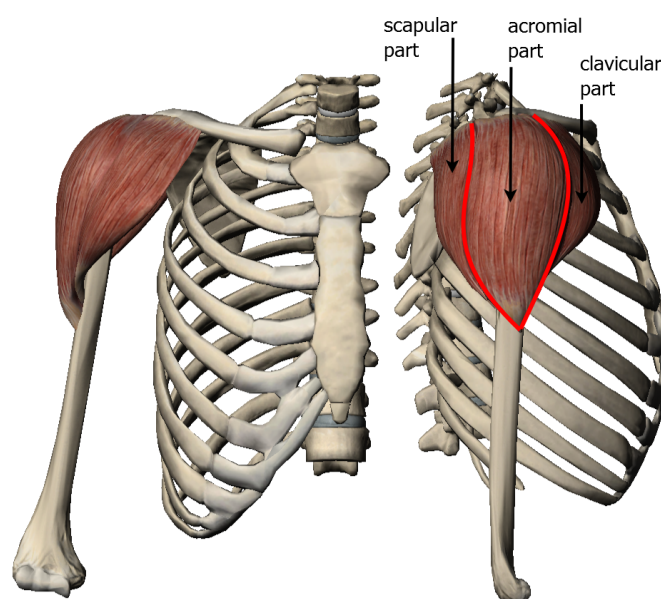
FIGURE 2.2: The deltoid muscle (Muscle Premium - Visible Body, Boston, 2014).

The deltoid muscle is a thick triangular skeletal muscle. This muscle has three origins (1) the anterior border and superior surface of the lateral third of the clavicle; (2) the lateral margin and superior surface of the acromion and (3) the lower edge of the crest of the scapular spine [102]. As mentioned in the same source, the fibers converge inferiorly to the deltoid tuberosity, on the lateral aspect of the humeral midshaft. According to these three origins, the muscle is divided in three parts clavicular (CL), acromial (AC) and scapular (SC), respectively, see Fig. 2.2.

These muscle parts can act independently as well as together. The CL muscle part in cooperation with pectoralis major ensures the forward flexion of humerus and medial rotation. The SC part assists to latissimus dorsi and teres major in backward flexion and lateral rotation. The AC muscle part is the main humeral abductor.

The deltoid muscle has naturally some clinical complications. For example, the lesions affecting the nerve cause atrophy of deltoid muscle, the acromion then appears to be more prominent, the distance between the acromion and the humeral head is increased and it leads to the GH joint dislocation, [102]

Chapter 3

Shoulder Models

Historically, most models and simulations of human body were focused on the hip and the knee joints. These joints had an interest of clinical and industrial researchers because of their common replacements.

The upper extremity motions are more variable than the locomotive movements of the lower limb. While two-dimensional analysis of gait can reasonably characterize leg kinematics, such a simplified treatment of the shoulder joint is not adequate [77].

Existing models can be categorized into two groups in general: mechanical shoulder models and computer numerical models. Mechanical shoulder models usually consist of stuffs representing bones and muscles. The bones are mostly obtained from cadavers or replaced by wood or plastic stuff. Muscles are usually represented by hemp threads. The computer technology allowed to develop numerical models eliminating lacks of mechanical models.

Research activity involving numerical models of the shoulder is dramatically increasing. The main aim is to better understand shoulder joint motions and pathologies. The number of publications involving this type of modeling exponentially increases, see Fig. 3.1. Models are usually used for ergonomics, clinical practice to develop therapeutic strategies, crash tests simulation, etc.
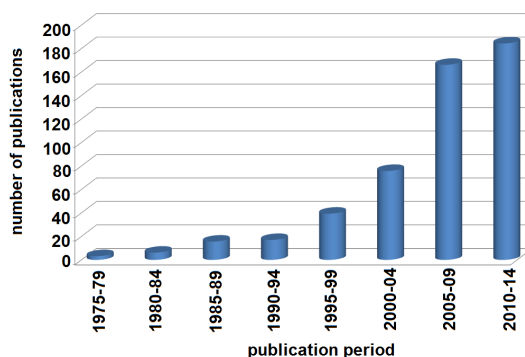
FIGURE 3.1: Number of publications focused on shoulder modeling, listed on PubMed (National Center for Biotechnology Information, U.S. National Library of Medicine, USA).

3.1 Mechanical Shoulder Models

The first famous mechanical shoulder models were developed at the end of the 19th century. In these models, the muscles of shoulder specimens were replaced by hemp threads. Scapular movements were usually not considered. The models were used to prescribe shoulder joint positions and to record the resulting changes in length of individual muscles.

One of the most famous thread models is Fick's model [34]. The scapular movements were not considered. The main usage of this model was the prescription of shoulder joint positions and muscle moment arms and torques calculation. Mollier's shoulder model [67] belongs also to the thread models. The muscles of an arm-thoracis specimen were connected to large lever arms. The scapulothoracis joint was already considered. Shiino's [86] and Strasser's [90] models improved the Fick's model. Muscle power was calculated providing that the muscle tension decreases linearly with an increase muscle length. Hvorslev's model [51] constructed cadaveric shoulder specimens. The model involved a frame consisting of the thorax, the spine and the pelvis. The scapula was rotated around a metal rod attached to the rig cage of the cadaver. Direct measurements of arm position were performed.

Later shoulder models modeled mechanism movable in two dimensions only. These studies described merely the motions of the humerus with respect to a non-moving scapula. These models such as DeLuca's [25] and Poppen's [76] model were too oversimplified. Therefore, they did not provide a realistic results and they also did not describe shoulder activities in more details.

The real shoulder models are still constructed such as described in [33, 109], see Fig. 3.2 and Fig. 3.3. Models consist of cadaveric specimens or of epoxy mannequin. Muscles are usually represented by wire cables or threads without muscle properties.
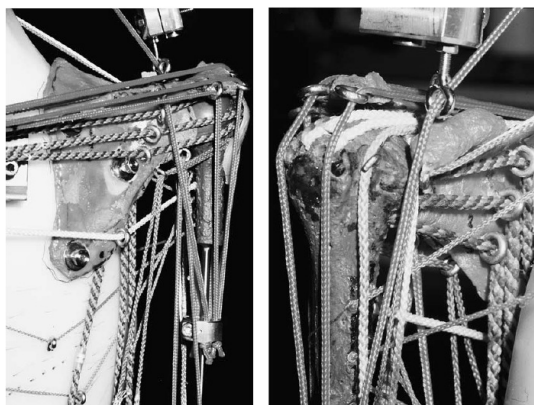
FIGURE 3.2: The Favre's model, [33].
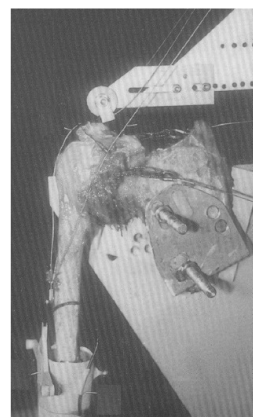
FIGURE 3.3: The Wuelker's model, [109].

In general, mechanical models have many lacks summarized follows:

- *deterioration of soft tissues* - the cadaveric tissues have to be kept in special chemicals and temperature to prevent or minimize their deterioration. Even so, the postmortem tissues change significantly their physical and chemical properties.

- *time-consuming* - preparation of experiment, measurements and subsequent data processing take a lot of time. Moreover, some mistakes occurring during the modeling process could be uncorrectable and thus, the model could be simply destroyed.

- *spatial-consuming* - the special laboratory and tools are necessary to construct the model. In addition, the storeroom is suitable to save the model. Furthermore, these places demand the special conditions for correct storage such as specific temperature, humidity, pressure, etc.

- *stuff-consuming* - an assembling of mechanical model requires some special stuffs such as pathologist to remove bones from cadaver, anatomist to reconstruct the joint structure, technical expert to build the model, etc.

- *not possible to repeat the measurements* - it is not possible to repeat the measurement with the same external conditions such as the pressure, the temperature, the size and the direction of external loading, etc.

- *not possible to scale* - the results obtained from the experiment correspond to the properties of measured object. It is not possible to change any anthropometrical parameters, to implement any injuries or pathologies and the like.

- *muscles without real properties* - the muscles are usually substituted by wire cables, by threads or by cadaveric muscle. Thus, it is not possible to create the muscle lines with the real muscle properties such as length-tension relationship, force-velocity relationship, etc.

- *ethical limitation* - in many countries (such as Czech Republic), the agreement of ethical commission is essential to use some cadaveric specimens.

- *painful* - some in vivo experiments are also perform to avoid inaccuracies of cadaveric modeling. Such measurements are usually very uncomfortable and painful.

- *financially-consuming* - real models are often too expansive (to get cadavers or stuff to build the model, to have an available space of the laboratory and the storeroom, to have some financial reward for employees, etc.)

- *difficult to transport* - it is too complicated to transport the mechanical models because of their weight, size and fragility.

3.2   Computer Shoulder Models

At the second half of 20th century, IT development started the new stage of shoulder modeling. Computer models were designed to calculate moment arms and the load distribution at the shoulder joint, to prescribe the muscle activity and muscle forces. One of the first models was the Wood's shoulder model [107]. This model digitized the anatomy of shoulder and elbow muscles and calculated trajectory data for each muscle.

Simulation performed by numerical models allow investigation of aspects that are otherwise difficult or impossible to quantify such as overcoming technical limits (deterioration of tissues, adequate placements of sensors), ethical limits (invasiveness and short supply of specimens).

Depending on the aspect of shoulder function, various modeling approach can be selected. Existing computer models can be broadly categorized into two groups: rigid body models and deformable models. The rigid body models can simulate kinematics and collisions between entities, musculoskeletal actions and joint reaction forces to address issues in joint stability, etc. Deformable models account stress-strain distributions in the component structures.

Rigid Shoulder Models

Rigid body models idealize the skeletal system by solid segments connected by kinematic constrains. These models could be furthermore divided into two groups according to the model structure: (1) without muscles and (2) considering muscles.

The first group of models neglects muscles and ligaments. Such models are used to estimate joint moments during a specific motion, to describe the trajectories of components, to assess the range of joint movements. The models may be used especially in optimization of rehabilitation, prevention of joint injuries, specification of diagnosis and for ergonomics applications. The following literature list summarizes some examples of scientific articles concerning this kind of shoulder complex: [8, 57, 65, 91, 113].

The models respecting the muscles are usually focused on muscle force estimation technique consisted mainly of optimization methods. Such models are used to compute muscle forces and activity distribution using inverse dynamics, to estimate joint reaction forces and moments, to prescribe some muscle fatigue, etc. The muscle wrapping method is usually implemented to accurate the results. Some of this kind of models are described in [18, 28, 38, 46, 50, 80, 97, 99, 114], see Fig. 3.4.

Finite-Element Shoulder Models

The finite element method is used to simulate the deformations of complex system that are otherwise difficult to assess. This allows to model complex materials phenomena such as nonlinear elastic and viscoelastic behavior or plastic deformations. The main limitations usually are boundary conditions and material properties. Most models implement the idealized material properties [4, 98].
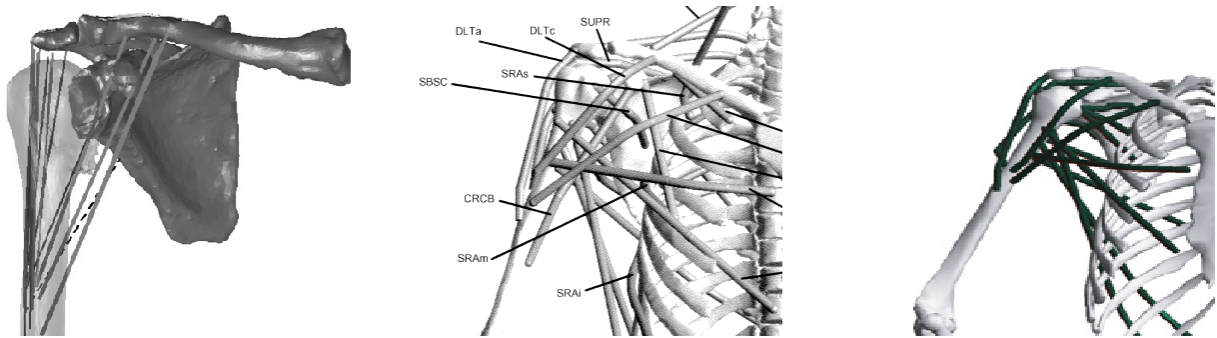
FIGURE 3.4: Rigid shoulder models involving muscles; left: Helm's [72], Garner's [38] and Yu's [114] model.

These models are developed for instance to optimize the shape of implant component [17] or unconventional fixation type [69], to compare cemented and uncemented prosthesis fixation [40], to test the influence of cement thickness [20, 49], see Fig. 3.5..
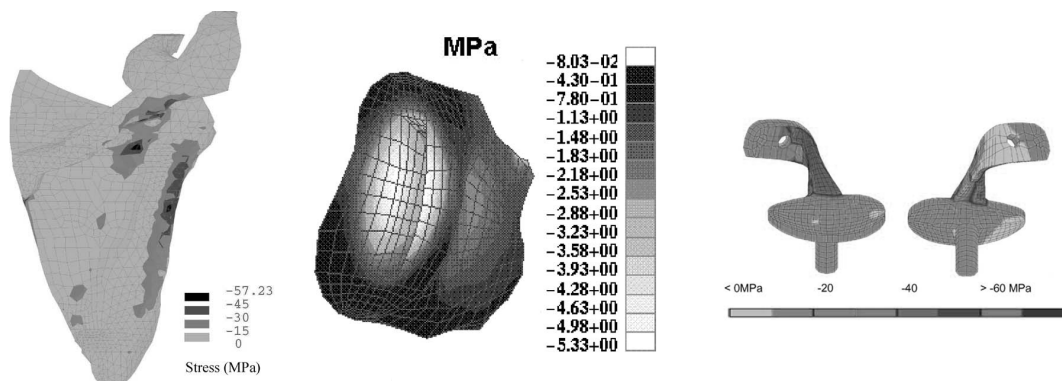
FIGURE 3.5: Finite-element models; left: Gupta's [40] - principal normal stress distribution during humeral abduction, Cauteau's [20] - maximal stresses in the thick cement mantle with the central load in glenohumeral joint, Murphy's [69] - minimum stress in acromion implant for abduction.

Chapter 4

Muscle Wrapping Methods

Two absolutely different models have been already developed to represent the paths of muscles in body: (1) the straight-line model and (2) the centroid-line model. The first model considered only straight lines joining the muscle attachments. The second one represents the muscle path by a line that passes through the locus of cross-sectional centroids of the muscle. Several approaches have been used to approximate the centroid-line for all joint configurations such as via-point method, obstacle-set algorithm or linked-plane obstacle-set method. The special group of muscle path representation is the finite-element models [82], [22].

4.1 Straight-Line Method

In the straight-line model [13, 22, 29, 82], the muscle path is modeled by a straight line connecting directly the muscle attachments. The muscle origin and insertion have the fixed positions located in the local coordinate systems of bones. When the joint moves, the muscle attachments move as well and cause the shortening or elongating of the muscle line. This model is very easy to implement. However, it may not provide meaningful results. In fact, the muscles wrap usually around some bones, muscles and other tissues. Thus, the muscle lines have absolutely wrong shape and length, see Fig. 4.1. The straight-line algorithm could be applied to muscles that are short and straight. If the muscle path becomes more complex, this method becomes unsuitable.
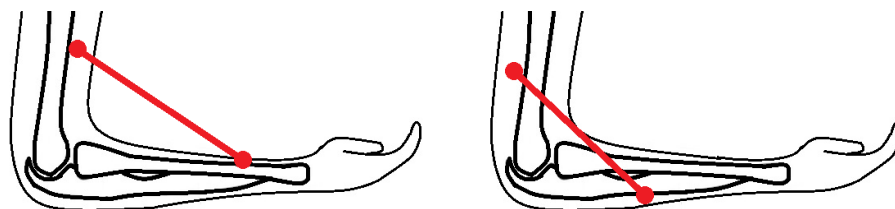
FIGURE 4.1: Straight-line method focused on muscle path estimation.

4.2 Centroid-line model

4.2.1 Via-Points Method

The via-points method introduces effective attachment sites called via-points at specific position along the centroid muscle line [27, 84, 104]. The muscle path is represented by series of straight-line segments passing through the via-points. According to the real anatomy, the muscle shape is also influenced by surrounding structure considered bones, joints, other muscles, organs, etc. The via-points represent the position of these obstacles. When the straight-line of muscle may intersect some obstacle, the via-point becomes active and deforms the muscle path. Otherwise, when the straight-line of muscle is not close to the obstacle, the via-point becomes inactive and the muscle is represented by only one straight line. The via-points method is also very easy to apply. Nevertheless, it has a lot of limitations such as unrealistic muscle shape, see Fig. 4.2.
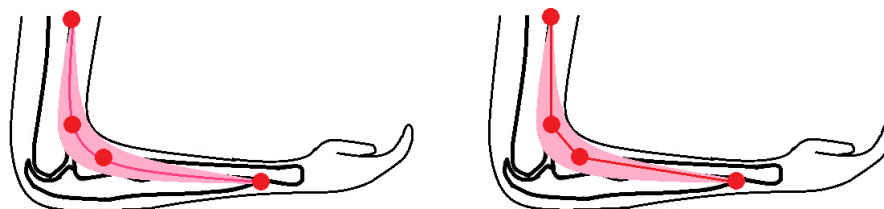
FIGURE 4.2: Via-points method focused on muscle path estimation. Left: via-points situated along the centroid muscle line; right: the straight-lines between via-points.

4.2.2 Obstacle-Set Method

The obstacle-set method was developed by Garner and Pandy [36, 37], based on the study of van der Helm [97]. This method simulates the muscle paths wrapping around some simplified obstacles, see Fig 4.4.

The method is based on three assumptions: (1) the muscle force acts along the locus; (2) the muscle can be idealized as a frictionless elastic band that moves freely over neighboring anatomical structures; (3) the surrounding anatomical structures constraining the muscle path can be represented by regular shape such as spheres, cylinders, ellipsoids and their combination modeled by rigid bodies.

The skeleton is modeled as a set of rigid bodies (bones) connected by joints. For a given configuration of joints, the following parameters are fully described and considered inputs: (1) the relative position and orientation of each bone; (2) muscle origin and insertion; (3) position, orientation, and geometrical parameters of obstacles such as center and radius. The obstacle-set algorithm can be described in following steps, see Fig. 4.3:

- *To decide if the obstacle is active or not.* The wrapping condition changes depending on actual joint configuration, because the muscle attachments are fixed to the bones and the obstacle

via-points are fixed to the obstacles. Mathematically, this condition is defined in terms of the angle formed by the muscle path as it wraps over the obstacle. The wrapping angle is formed by three points: the obstacle via-point T, the center of obstacle, the via-point S, see Fig. 4.3. If the wrapping angle is greater or equal to 180°, the wrapping should not occur.

- *To find the via-points, Q and T, associated with the obstacle.* The obstacle via-points are located on the surface of the obstacle and in the plain defined by muscle attachments, *P and S*, and the center of obtacle. To ensure the minimum muscle path, the straight line segment that joins the obstacle via-points to their neighboring muscle attachments, *P or S*, has to be tangent to the obstacle surface. Nevertheless, there are two solutions corresponding to two possible directions which path can be taken around the obstacle: right-handed and left-handed sense. This problem is solved by giving the signed value to the radius of obstacle. In this way, positive and negative values for radius would correspond to right-handed and left-handed wrapping, respectively.

- *To calculate the minimum length of muscle between obstacle via-points, Q and T.* The curved line is based on geometry of respective obstacle.

- *To calculate the length of whole muscle path from origin to insertion.* The final muscle path is defined by series of straight-line ST, curved-line TQ, and straight-line QP, segments connected by via-points. The length of straight-line segments *PQ and TS*, may be computed simply as a distance between the respective points. The arc length QT, is found using the geometrical rules of respective obstacle (e.g. for single sphere - law of cosines).
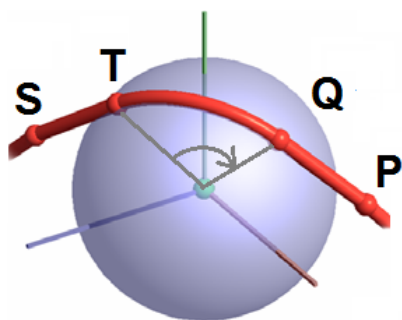
FIGURE 4.3: Obstacle-set method for muscle path calculation (fixed muscle attachments: S, P and obstacle via-points: T,Q), [37].
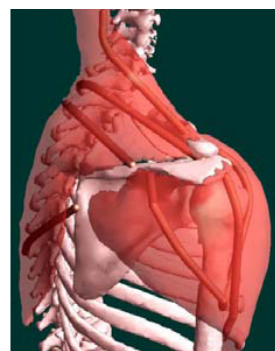
FIGURE 4.4: Obstacle-set method used to represent the path of deltoid and trapezius muscles, [37].

The obstacle-set method also has some limitations in simulation of broad muscle or complicated joint configuration such as: (1) each muscle line requires usually more than three obstacles. And thus, the algorithm is time consuming. (2) Each muscle path stays in its own surfaces and behaves independently. In real anatomy, muscle fibers of one muscle act interactively. (3) Some muscle lines slip off the obstacle very often, when the joint is moved. (4) The obstacle-set placement does not work for all arbitrary joint configurations.

4.2.3 Linked-Plane Obstacle-Set Method

The linked-plane obstacle-set method is developed by Bo Xu [12]. It is based on obstacle-set method mentioned in the previous section. In addition, each muscle band is defined to lie in its own muscle path plane, see Fig. 4.5 and 4.6. The broad muscles are represented by a number of muscle bands consisting of a straight-line, a curved-line and another straight-line. The curved-line wraps around the sphere and simultaneously lies in the muscle path plane. The position and orientation of this plane depends on the current joint configuration and on the other planes of the muscle bands.

This algorithm of muscle wrapping implements the interconnectivity between muscle band and avoids the slipping problem that occurs in the obstacle-set method. Nevertheless, the linked-plane obstacle-set algorithm has a number of limits such as: (1) the positions of muscle attachments are oversimplified. The real contact area is not taken into account and the points are considered in one line. (2) The distribution of muscle bands is not defined in whole 3D muscle shape. Only the middle surface is used. And thus, it is not possible to simulate the changes in muscle volume during contractions. (3) The muscle shapes is still not satisfying - especially in the extreme positions of shoulder joint. (4) The obstacles and via-points are defined only for some constrained movements - shoulder abduction up to 90°.
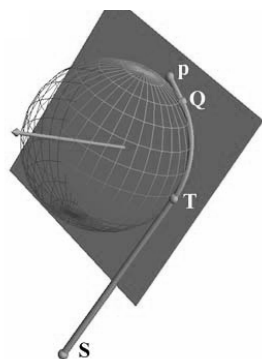
FIGURE 4.5: The linked-plane obstacle-set algorithm, [12].
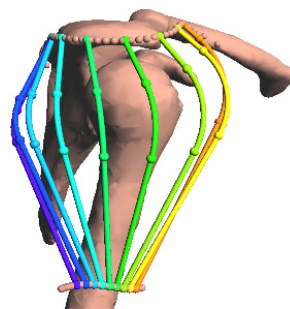
FIGURE 4.6: Lateral view of the deltoid muscle, [12].

4.3 Finite Element Method

The finite element algorithm was developed by Blemker et al. [11, 58]. The method is based on MR images of each individual muscle. The finite element mesh of whole muscle is constructed to define geometrical parameters of each muscle band. A template mesh that is in the shape of a cube is created, see Fig. 4.7. The template mesh undergoes a mapping process predefined by some conditions to create a target mesh. The final mesh represents already the geometry of one unit of the specific muscle band. The nodes of mesh represent the via-points of muscle bands connected by straight-lines. This model can represent muscles with complex. In cooperation with mechanics of muscle tissue, connectivity between muscle band and surface contact with surrounding anatomical

structure, the simulation using this model show really realistic results. It is possible to generate simulation at any arbitrary joint configuration. Nevertheless, the model has also some limits such as: (1) too many input parameters; (2) numerous path of the muscle band; both disadvantages considerably increasing the computation time (almost 10 hours for a single muscle).
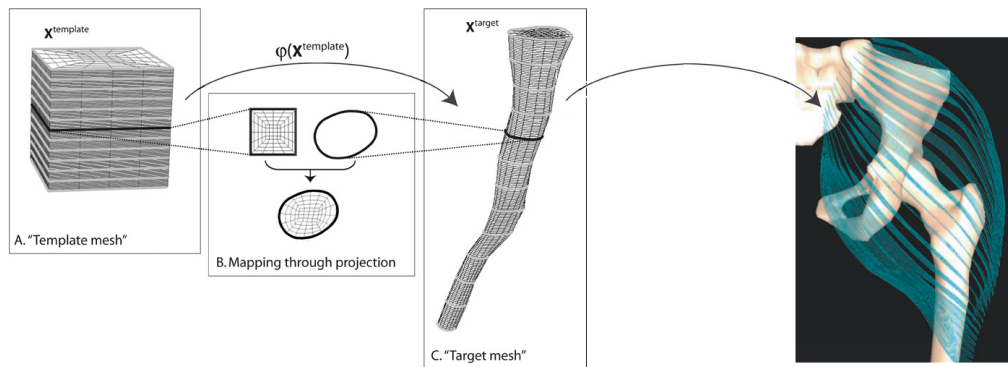
FIGURE 4.7: Process of finite-element method used for gluteus maximus muscle, [11].

Part III

METHOD

Chapter 5

Multibody Spatial Dynamics

In the spatial analysis, the unconstrained motion of a rigid body is defined by six coordinates - three coordinates defining the position of the reference point of the rigid body and three coordinates defining its orientation. Unlike the 2D motion, the rotation in the 3D analysis is not commutative and the sequence of rotation performing has to be taken into account. In addition, the angular velocities are not the time derivatives of a set of orientation coordinates. The angular velocities are expressed in terms of a selected set of orientation coordinates and their time derivatives. Several methods how to describe the orientation of the rigid body has been already published [15, 83, 100]. In this chapter, the methods describing equations of motion in 3D are presented. The configuration of rigid body is described by a set of generalized coordinates defining the global position vector and orientation. In general, these coordinates are independent. The relationships between the angular velocity and the time derivatives of the generalized coordinates are estimated to define the absolute velocity and acceleration vectors of an arbitrary rigid body point. This kinematics is used to develop the dynamic equations of motion. In the 3D, the equations are much more complex in comparison with 2D movement. Thus, the definition of derivation of the dynamic equations of motion as well as the mass matrix of spatial system are simplified - the reference point is selected to be the body center of mass, as defined in literature [83]. This case leads to the formulation of the Newton-Euler equations. Therefore, there is no inertia coupling between the translation and rotation of the rigid body.

5.1 Forward Dynamics

In the dynamics of mechanical systems, there are two different types of analysis - forward and inverse dynamics. In the forward dynamics, the all forces producing the motion are known and the aim is to calculate the position, velocities and acceleration. The accelerations are determined by the laws of motion. The integrated accelerations are then used to calculate the velocities and positions. In

most cases, the solution is difficult to obtain and thus, the numerical integration methods are usually used.

5.1.1 General Displacement and Finite Rotations

In the spatial analysis, the unconstrained motion of the rigid body is described by six independent coordinates - three for translation, three for rotation. The translation motion of whole rigid body is defined by the displacement of one selected point, so called reference point, fixed to the rigid body. In the case of pure translational movement, the orientation of the body does not change. Thus, all points of the rigid body have the same velocity. Otherwise, the kinematics of the rigid body is fully described within the sum of translation motions of the referent point and relative rotations around this particular point. As shown in Fig. 5.1, the global position vector of an arbitrary point of rigid body can be written as

$$\mathbf{r}^i = \mathbf{R}^i + \mathbf{A}^i \bar{\mathbf{u}}^i, \tag{5.1}$$

where $\mathbf{r}^i$ is the position vector of arbitrary point respecting the global coordinate system XYZ, $\mathbf{R}^i$ is the global position vector of the origin of the local body reference frame $X^iY^iZ^i$, $\mathbf{A}^i$ is the transformation matrix from the local coordinate system to the global coordinate system, $\bar{\mathbf{u}}^i$ is the position vector of the arbitrary body point respecting the local coordinate system and $i = 1, 2, \ldots, n_b$, where n_b is a number of rigid bodies linked in kinematic chain or tree structure. The $\mathbf{A}^i$ matrix is a 3×3 matrix. The vectors $\mathbf{r}^i$, $\mathbf{R}^i$ and $\bar{\mathbf{u}}^i$ are three-dimensional defined as

$$\mathbf{r}^i = \begin{bmatrix} r_x^i & r_y^i & r_z^i \end{bmatrix}^T, \tag{5.2}$$

$$\mathbf{R}^i = \begin{bmatrix} R_x^i & R_y^i & R_z^i \end{bmatrix}^T, \tag{5.3}$$

$$\bar{\mathbf{u}}^i = \begin{bmatrix} \bar{u}_x^i & \bar{u}_y^i & \bar{u}_z^i \end{bmatrix}^T = \begin{bmatrix} x^i & y^i & z^i \end{bmatrix}^T. \tag{5.4}$$
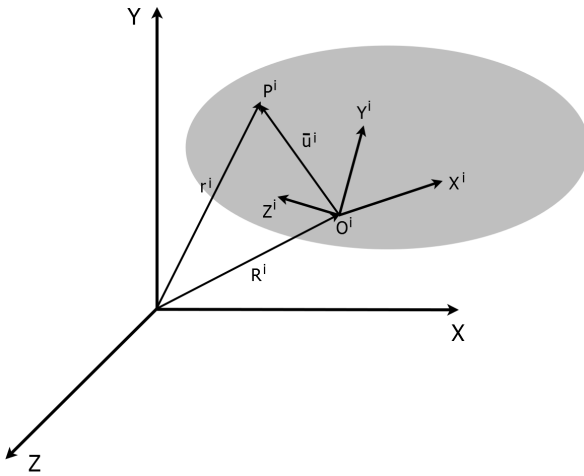
FIGURE 5.1: General coordinates of rigid body situated in 3D.
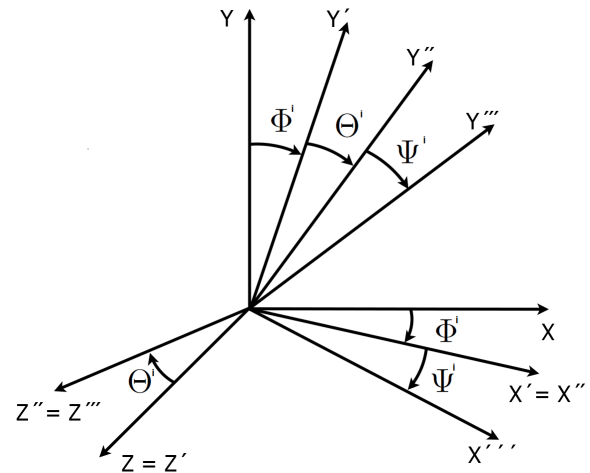
FIGURE 5.2: Euler angles.

The three-dimensional rotation of multibody system is very often described by independent Euler angles; ϕ^i, θ^i and ψ^i, see Fig. 5.2. The angles represent three successive rotations about three axes. Thanks that, the coordinate system can reach any orientation. Considering the global coordinate system XYZ and the local system $X^iY^iY^i$, the sequence of rotation starts by rotation the system $X^iY^iY^i$ an angle ϕ^i about the Z axis. In this case, the transformation (rotation) matrix is given by

$$\mathbf{A}_1^i = \begin{bmatrix} cos\phi^i & -sin\phi^i & 0 \\ sin\phi^i & cos\phi^i & 0 \\ 0 & 0 & 1 \end{bmatrix}. \tag{5.5}$$

Then the system $X^iY^iY^i$ is rotated an angle θ^i about the X' axis. In this case, the transformation matrix is given by

$$\mathbf{A}_2^i = \begin{bmatrix} 1 & 0 & 0 \\ 0 & cos\theta^i & -sin\theta^i \\ 0 & sin\theta^i & cos\theta^i \end{bmatrix}. \tag{5.6}$$

Finally, the system $X^iY^iY^i$ is rotated an angle ψ^i about the Z'' axis. In this case, the transformation matrix is given by

$$\mathbf{A}_3^i = \begin{bmatrix} cos\psi^i & -sin\psi^i & 0 \\ sin\psi^i & cos\psi^i & 0 \\ 0 & 0 & 1 \end{bmatrix}. \tag{5.7}$$

The final orientation of the system $X^iY^iY^i$ is defined in the global system XYZ by the matrix A^i given by follows

$$\mathbf{A}^i = \mathbf{A}_1^i \mathbf{A}_2^i \mathbf{A}_3^i, \tag{5.8}$$

$$\mathbf{A}^i = \begin{bmatrix} cos\psi^i cos\phi^i - cos\theta^i sin\phi^i sin\psi^i & -sin\psi^i cos\phi^i - cos\theta^i sin\phi^i cos\psi^i & sin\theta^i sin\phi^i \\ cos\psi^i sin\phi^i + cos\theta^i cos\phi^i sin\psi^i & -sin\psi^i sin\phi^i + cos\theta^i cos\phi^i cos\psi^i & -sin\theta^i cos\phi^i \\ sin\theta^i sin\psi^i & sin\theta^i cos\psi^i & cos\theta^i \end{bmatrix}. \tag{5.9}$$

5.1.2 Velocity and acceleration

The absolute velocity of an arbitrary point on the rigid body is obtained by differentiating the general displacement vector defined by Eq. 5.1 with respect to time. The velocity is then given by

$$\dot{\mathbf{r}}^i = \dot{\mathbf{R}}^i + \dot{\mathbf{A}}^i \bar{\mathbf{u}}^i. \tag{5.10}$$

Using the orthogonality of the transformation matrix, the time derivatives is given by

$$\dot{\mathbf{A}}^i = \tilde{\boldsymbol{\omega}}^i \mathbf{A}^i, \tag{5.11}$$

where $\tilde{\boldsymbol{\omega}}^i$ is a skew symmetric matrix that can be written as

$$\tilde{\boldsymbol{\omega}}^i = \begin{bmatrix} 0 & -\omega_3^i & \omega_2^i \\ \omega_3^i & 0 & -\omega_1^i \\ -\omega_2^i & \omega_1^i & 0 \end{bmatrix}. \tag{5.12}$$

The $\omega_1^i, \omega_2^i, \omega_3^i$ are called the components of the angular velocity vector $\boldsymbol{\omega}^i$, that is

$$\boldsymbol{\omega}^i = \begin{bmatrix} \omega_1^i & \omega_2^i & \omega_3^i \end{bmatrix}^T. \tag{5.13}$$

Substituting this relationships into Eq. 5.10 yields

$$\dot{\mathbf{r}}^i = \dot{\mathbf{R}}^i + \tilde{\boldsymbol{\omega}}^i \mathbf{A}^i \bar{\mathbf{u}}^i \quad \text{or} \quad \dot{\mathbf{r}}^i = \dot{\mathbf{R}}^i + \tilde{\boldsymbol{\omega}}^i \mathbf{u}^i \quad \text{or} \quad \dot{\mathbf{r}}^i = \dot{\mathbf{R}}^i + \boldsymbol{\omega}^i \times \mathbf{u}^i, \tag{5.14}$$

where

$$\mathbf{u}^i = \mathbf{A}^i \bar{\mathbf{u}}^i, \tag{5.15}$$

is the position vector $\bar{\mathbf{u}}^i$ represented in global coordinate system. The equation of the absolute acceleration can be obtained by differentiating the Eq. 5.10 with respect to time. The acceleration is then given by

$$\ddot{\mathbf{r}}^i = \ddot{\mathbf{R}}^i + \ddot{\mathbf{A}}^i \bar{\mathbf{u}}^i. \tag{5.16}$$

were $\ddot{\mathbf{A}}^i$ is in following form

$$\ddot{\mathbf{A}}^i = \dot{\tilde{\boldsymbol{\omega}}}^i \mathbf{A}^i + \tilde{\boldsymbol{\omega}}^i \dot{\mathbf{A}}^i. \tag{5.17}$$

The angular velocity, $\boldsymbol{\omega}^i$, defined in the global coordinate system can be also expressed in terms of Euler angles and their time derivative as

$$\boldsymbol{\omega}^i = \mathbf{G^i} \dot{\boldsymbol{\theta}}^{\mathbf{i}}, \tag{5.18}$$

where $\boldsymbol{\theta}^i$ is the set of Euler angles defined as

$$\boldsymbol{\theta}^i = \begin{bmatrix} \phi^i & \theta^i & \psi^i \end{bmatrix}^T, \tag{5.19}$$

and the matrix $\mathbf{G^i}$ is defined as

$$\mathbf{G^i} = \begin{bmatrix} 0 & cos\phi^i & sin\theta^i sin\phi^i \\ 0 & sin\phi^i & -sin\theta^i cos\phi^i \\ 1 & 0 & cos\theta^i \end{bmatrix}. \tag{5.20}$$

The columns of the matrix $\mathbf{G^i}$ represent unit vectors along axes about which the Euler angles rotations are performed. These vectors are defined in the fixed coordinate system. Using already mentioned equations, the absolute velocity of an arbitrary point of the body can be expressed in terms of Euler angles as

$$\dot{\mathbf{r}}^i = \dot{\mathbf{R}}^i - \tilde{\mathbf{u}}^i \mathbf{G}^i \dot{\boldsymbol{\theta}}^i, \tag{5.21}$$

where $\tilde{\mathbf{u}}^i$ is the skew symmetric matrix defined as

$$\tilde{\mathbf{u}}^i = \begin{bmatrix} 0 & -u_z^i & u_y^i \\ u_z^i & 0 & -u_x^i \\ -u_y^i & u_x^i & 0 \end{bmatrix}. \tag{5.22}$$

The absolute velocity can bee also expressed using matric partitioning as

$$\dot{\mathbf{r}}^i = \begin{bmatrix} \mathbf{I} & -\tilde{\mathbf{u}}^i \mathbf{G}^i \end{bmatrix} \begin{bmatrix} \dot{\mathbf{R}}^i \\ \dot{\boldsymbol{\theta}}^i \end{bmatrix} \quad \text{or} \quad \dot{\mathbf{r}}^i = \begin{bmatrix} \mathbf{I} & -\mathbf{A}^i \tilde{\bar{\mathbf{u}}}^i \bar{\mathbf{G}}^i \end{bmatrix} \begin{bmatrix} \dot{\mathbf{R}}^i \\ \dot{\boldsymbol{\theta}}^i \end{bmatrix}. \tag{5.23}$$

The matrix $\bar{\mathbf{G}}^i$ is the matrix $\mathbf{G}^i$ defined in local coordinate system and is defined by

$$\bar{\mathbf{G}}^i = \mathbf{A}^{iT} \mathbf{G}^i \quad \text{or} \quad \bar{\mathbf{G}}^i = \begin{bmatrix} sin\theta^i sin\psi^i & cos\psi^i & 0 \\ sin\theta^i cos\psi^i & -sin\psi^i & 0 \\ cos\theta^i & 0 & 1 \end{bmatrix}. \tag{5.24}$$

5.1.3 Generalized Inertia Forces - The Principle of Virtual Work

There are several methods how to construct the dynamic equations of motion for rigid body moving in 3D space. In this study, the principle of virtual work in dynamics is used to find the differential equations describing the body motion. Based on Eq. 5.23, the virtual change of the body position of the arbitrary body point is given by

$$\delta\mathbf{r}^i = \begin{bmatrix} \mathbf{I} & -\mathbf{A}^i \tilde{\bar{\mathbf{u}}}^i \bar{\mathbf{G}}^i \end{bmatrix} \begin{bmatrix} \delta\mathbf{R}^i \\ \delta\boldsymbol{\theta}^i \end{bmatrix}. \tag{5.25}$$

The virtual work, δW_i^i, of the inertia forces of the rigid body is given by

$$\delta\mathbf{W}_i^i = \int_{V^i} \rho^i \ddot{\mathbf{r}}^{i^T} \delta\mathbf{r}^i \, \mathrm{d}V^i, \tag{5.26}$$

where ρ^i is the mass density and V^i is the volume of the rigid body. This can be also written as

$$\delta\mathbf{W}_i^i = \begin{bmatrix} \ddot{\mathbf{q}}^{i^T} \mathbf{M}^i - \mathbf{Q}_\nu^{i^T} \end{bmatrix} \delta\mathbf{q}^i, \tag{5.27}$$

where $\mathbf{Q}^i_\nu$ is a vector of inertia forces that absorbs terms that are quadratic in the velocities, defined later in Eq. 5.37 and the vector of generalized coordinates of the body are defined as

$$\mathbf{q}^i = \begin{bmatrix} \mathbf{R}^{iT} & \boldsymbol{\theta}^{iT} \end{bmatrix}^T. \tag{5.28}$$

$\mathbf{M}^i$ is the symmetric mass matrix defined by the form

$$\mathbf{M}^i = \begin{bmatrix} \mathbf{m}^i_{RR} & \mathbf{m}^i_{R\theta} \\ \mathbf{m}^i_{\theta R} & \mathbf{m}^i_{\theta\theta} \end{bmatrix}. \tag{5.29}$$

where

$$\mathbf{m}^i_{RR} = m^i\mathbf{I}, \quad \text{or} \quad \mathbf{m}^i_{\theta\theta} = \bar{\mathbf{G}}^{iT}\bar{\mathbf{I}}^i_{\theta\theta}\bar{\mathbf{G}}^i. \tag{5.30}$$

$\tilde{\mathbf{I}}^i_{\theta\theta}$ is a 3×3 symmetric matrix called the inertia tensor of the rigid body (described in Chapter 5.1.4 in more details) given by

$$\bar{\mathbf{I}}^i_{\theta\theta} = \begin{bmatrix} i_{xx} & i_{xy} & i_{xz} \\ & i_{yy} & i_{yz} \\ symm & & i_{zz} \end{bmatrix}. \tag{5.31}$$

where i_{xx}, i_{yy}, i_{zz} are the moments of inertia and i_{xy}, i_{xz}, i_{yz} are the products of inertia. The mass matrix is very often simplified. The reference point of the local coordinate system of the rigid body is suitable to situate in the body mass center (called centroidal body coordinate system). In this case, the mass matrix becomes more simple

$$\mathbf{m}^i_{R\theta} = \mathbf{m}^{iT}_{\theta R} = 0. \tag{5.32}$$

5.1.4   Mass Moment of Inertia

The upper arm, involved in presented model, is considered to be composed of skin, soft tissue (muscles, tendons, veins, etc.) and bone. Moreover, the bony section contains a canal at the center. The simplified structure of the upper arm is shown in Fig. 5.3. All tissues are approximated by cylindrical bodies with ellipsoidal cross sections areas. The mass moments of inertia for the upper arm complex are then estimated using a superposition technique given by following forms, published in [78]

$$\begin{aligned} I_{xx}(skin) &= \tfrac{\pi\rho_s}{12}\left[(a_s b_s l_s)\left(3b_s^2 + l_s^2\right) - (a_{st}b_{st}l_{st})\left(3b_{st}^2 + l_{st}^2\right)\right], \\ I_{yy}(skin) &= \tfrac{\pi\rho_s}{12}\left[(a_s b_s l_s)\left(3a_s^2 + l_s^2\right) - (a_{st}b_{st}l_{st})\left(3a_{st}^2 + l_{st}^2\right)\right], \\ I_{zz}(skin) &= \tfrac{\pi\rho_s}{4}\left[(a_s b_s l_s)\left(a_s^2 + b_s^2\right) - (a_{st}b_{st}l_{st})\left(a_{st}^2 + b_{st}^2\right)\right], \end{aligned} \tag{5.33}$$

$$\begin{aligned} I_{xx}(soft\ tissue) &= \tfrac{\pi\rho_{st}}{12}\left[(a_{st}b_{st}l_{st})\left(3b_{st}^2 + l_{st}^2\right) - (a_b b_b l_b)\left(3b_b^2 + l_b^2\right)\right], \\ I_{yy}(soft\ tissue) &= \tfrac{\pi\rho_{st}}{12}\left[(a_{st}b_{st}l_{st})\left(3a_{st}^2 + l_{st}^2\right) - (a_b b_b l_b)\left(3a_b^2 + l_b^2\right)\right], \\ I_{zz}(soft\ tissue) &= \tfrac{\pi\rho_{st}}{4}\left[(a_{st}b_{st}l_{st})\left(a_{st}^2 + b_{st}^2\right) - (a_b b_b l_b)\left(a_b^2 + b_b^2\right)\right], \end{aligned} \tag{5.34}$$

$$I_{xx}(bone) = \frac{\pi\rho_b}{12}\left[(a_b b_b l_b)\left(3b_b^2 + l_b^2\right) - (a_c b_c l_c)\left(3b_c^2 + l_c^2\right)\right],$$
$$I_{yy}(bone) = \frac{\pi\rho_b}{12}\left[(a_b b_b l_b)\left(3a_b^2 + l_b^2\right) - (a_c b_c l_c)\left(3a_c^2 + l_c^2\right)\right], \quad (5.35)$$
$$I_{zz}(bone) = \frac{\pi\rho_b}{4}\left[(a_b b_b l_b)\left(a_b^2 + b_b^2\right) - (a_c b_c l_c)\left(a_c^2 + b_c^2\right)\right],$$

where a, b and l are the half width, depth and length of the cylinders, respectively; ρ is the mass density; s, st, b and c denote the skin tissue, soft tissue, bone and canal, respectively.

The final mass moment inertia of the whole upper arm complex is the sum of skin, soft tissue and bone as (sum of Eq. 5.33, 5.34 and 5.35)

$$I_{xx}(upper\ arm) = I_{xx}(skin) + I_{xx}(soft\ tissue) + I_{xx}(bone),$$
$$I_{yy}(upper\ arm) = I_{yy}(skin) + I_{yy}(soft\ tissue) + I_{yy}(bone), \quad (5.36)$$
$$I_{zz}(upper\ arm) = I_{zz}(skin) + I_{zz}(soft\ tissue) + I_{zz}(bone).$$
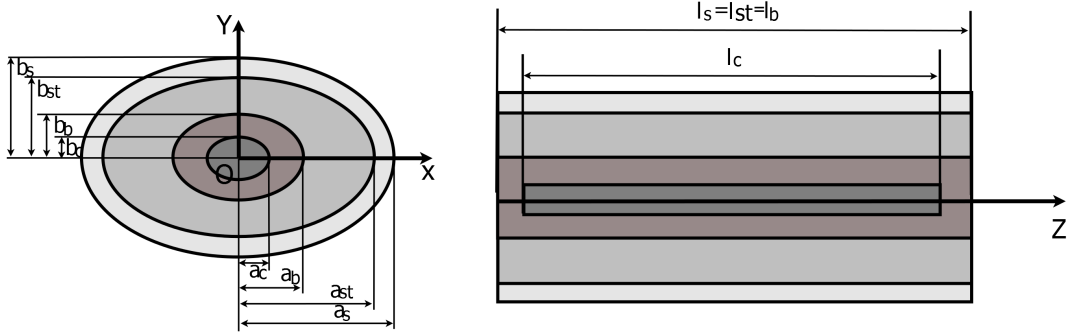
FIGURE 5.3: The upper arm segment is approximated by cylinders with ellipsoidal cross sectional areas. The segment consists of skin, soft tissue, bone and canal.

5.1.5 Centrifugal and Generalized Applied Forces

The centrifugal forces can be written as

$$\mathbf{Q}_\nu^i = \begin{bmatrix} (\mathbf{Q}_\nu^i)_R \\ (\mathbf{Q}_\nu^i)_\theta \end{bmatrix} = \begin{bmatrix} \mathbf{0} \\ -\bar{\mathbf{G}}^{iT}[\boldsymbol{\varpi}^i \times \bar{\mathbf{I}}_{\theta\theta}^i \boldsymbol{\varpi}^i + \bar{\mathbf{I}}_{\theta\theta}^i \dot{\bar{\mathbf{G}}}^{iT} \dot{\boldsymbol{\theta}}^i] \end{bmatrix}. \quad (5.37)$$

In the case of centroidal coordinate system, there is no inertia coupling between the translation and the rotation of the rigid body. Therefore, in this special case, the element $(\mathbf{Q}_\nu^i)_R$ is equal to zero.

The examples of generalized applied forces are the gravity, motor torque, muscle forces, etc. The forces can be again defined by the principle of virtual work. The force vector, $\mathbf{F^i}$ acting at a point, P^i, on the rigid body defined in the global coordinates can be written as

$$\delta\mathbf{W}_e^i = \mathbf{F}^{iT}\delta\mathbf{r}_P^i. \quad (5.38)$$

Using the previous equations, this relationship can be transform to

$$\delta \mathbf{W}_e^i = \mathbf{F}_R^{i^T} \delta \mathbf{R}^i + \mathbf{F}_\theta^{i^T} \delta \boldsymbol{\theta}^i. \tag{5.39}$$

In the situation, when the set of forces, $\mathbf{F}_1^i, \mathbf{F}_2^i, \ldots, \mathbf{F}_n^i$, acts at the body points with the position vectors, $\mathbf{r}_1^i, \mathbf{r}_2^i, \ldots, \mathbf{r}_n^i$, and a set of moments, $\mathbf{M}_1^i, \mathbf{M}_2^i, \ldots, \mathbf{M}_n^i$, respectively, the virtual work can be written as

$$\delta \mathbf{W}_e^i = \mathbf{F}_1^{i^T} \delta \mathbf{r}_1^i + \mathbf{F}_2^{i^T} \delta \mathbf{r}_2^i + \cdots + \mathbf{F}_{nF}^{i^T} \delta \mathbf{r}_n^i + \left(\mathbf{M}_1^i + \mathbf{M}_2^i + \cdots + \mathbf{M}_{nM}^i \right)^T \mathbf{G}^i \delta \boldsymbol{\theta}^i. \tag{5.40}$$

This equation can be also written as

$$\delta \mathbf{W}_e^I = \left(\mathbf{Q}_e^i \right)_R^T \delta \mathbf{R}^i + \left(\mathbf{Q}_e^i \right)_\theta^T \delta \boldsymbol{\theta}^i, \tag{5.41}$$

where $(\mathbf{Q}_e^i)_R$ and $(\mathbf{Q}_e^i)_\theta$ are the vectors of generalized forces associated with the generalized translation and rotation coordinates. These vector are given by

$$\left(\mathbf{Q}_e^i \right)_R = \mathbf{F}_1^i + \mathbf{F}_2^i + \cdots + \mathbf{F}_{nF}^i = \sum_{k=1}^{nF} \mathbf{F}_k^i, \tag{5.42}$$

$$\left(\mathbf{Q}_e^i \right)_\theta = \mathbf{G}^{i^T} \left[\mathbf{M}_1^i + \mathbf{M}_2^i + \cdots + \mathbf{M}_{nM}^i + \mathbf{u}_1^i \times \mathbf{F}_1^i + \mathbf{u}_2^i \times \mathbf{F}_2^i + \cdots + \mathbf{u}_n^i \times \mathbf{F}_n^i \right]$$

$$= \mathbf{G}^{i^T} \left[\sum_{l=1}^{nM} \mathbf{M}_l^i + \sum_{r=1}^{nF} (\mathbf{u}_r^i \times \mathbf{F}_r^i) \right], \tag{5.43}$$

where nF is a number of acting forces and nM is the number of acting moments.

5.1.6 Equations of Motion

Unconstrained Dynamics

Dynamic equations of motion are developed using the principle of virtual work. The virtual work of the inertia forces, $\delta \mathbf{W}_i^i$, is given by Eq. 5.27. The virtual work of the applied forces, $\delta \mathbf{W}_i^i$, is given by Eq. 5.41. For the unconstrained motion, these virtual works are equal. Therefore, this leads to following relationship

$$\mathbf{M}^i \ddot{\mathbf{q}}^i = \mathbf{Q}_e^i + \mathbf{Q}_\nu^i. \tag{5.44}$$

This expression can be also written in the matrix form as

$$
\underbrace{\begin{bmatrix} \mathbf{m}^i_{RR} & \mathbf{m}^i_{R\theta} \\ \mathbf{m}^i_{\theta R} & \mathbf{m}^i_{\theta\theta} \end{bmatrix}}_{\mathbf{M}^i} \underbrace{\begin{bmatrix} \ddot{\mathbf{R}}^i \\ \ddot{\boldsymbol{\theta}}^i \end{bmatrix}}_{\ddot{\mathbf{q}}^i} = \underbrace{\begin{bmatrix} (\mathbf{Q}^i_e)_R \\ (\mathbf{Q}^i_e)_\theta \end{bmatrix}}_{\mathbf{Q}^i_e} + \underbrace{\begin{bmatrix} (\mathbf{Q}^i_\nu)_R \\ (\mathbf{Q}^i_\nu)_\theta \end{bmatrix}}_{\mathbf{Q}^i_\nu}.
\tag{5.45}
$$

Constrained Dynamics

There are several approaches how to formulate the dynamics equations of motion of constrained multibody systems. In this study, the so called augmented formulation is used [83]. The dynamics equations are formulated in terms of a set of dependent and also independent coordinates. The constrictions are added by joints decreasing the number of degrees of freedom. The kinematic relationships describing mechanical joints and specified motion trajectories are implemented to the system of differential equations using the technique of Lagrange multipliers. This approach leads to a large system of equations that can be solved by numerical computer methods.

In general, the multibody system involves n_b connected bodies. The body configuration is described by the absolute Cartesian coordinates, $\mathbf{R}^i$, and the orientation coordinates, $\boldsymbol{\theta}^i$. The final vector of the generalized coordinates is then

$$
\mathbf{q}^i = \begin{bmatrix} \mathbf{R}^{iT} \boldsymbol{\theta}^{iT} \end{bmatrix}^T.
\tag{5.46}
$$

The kinematic relationships describing the constraints can be written as follows

$$
\mathbf{C}(\mathbf{q}, t) = 0.
\tag{5.47}
$$

The velocity equations can be computed by differentiating Eq. 5.47 as

$$
\mathbf{C_q}\dot{\mathbf{q}} = -\mathbf{C}_t,
\tag{5.48}
$$

were $\mathbf{C_q}$ is the constraint Jacobian matrix and $\mathbf{C}_t$ is the vector of partial derivatives of the constraint equations with respect to the time given by follows

$$
\mathbf{C}_t = \frac{\partial \mathbf{C}}{\partial t}.
\tag{5.49}
$$

The acceleration equations can be obtained by differentiating the Eq. 5.48 with respect to time as

$$
\mathbf{C_q}\ddot{\mathbf{q}} = \mathbf{Q}_d,
\tag{5.50}
$$

where $\mathbf{Q}_d$ is a vector that absorbs terms that are quadratic in the velocities and it is defined as

$$\mathbf{Q}_d = \left[-\sum_{\alpha=1}^{n}\sum_{j=1}^{n} C_1^{j\alpha}\dot{\mathbf{q}}^j\dot{\mathbf{q}}^\alpha \quad -\sum_{\alpha=1}^{n}\sum_{j=1}^{n} C_2^{j\alpha}\dot{\mathbf{q}}^j \quad \cdots \quad -\sum_{\alpha=1}^{n}\sum_{j=1}^{n} C_r^{j\alpha}\dot{\mathbf{q}}^j \right]^T. \tag{5.51}$$

The derivatives of constraint equation with respect to particulat generalized coordinteas are given by

$$C_i^{j\alpha} = \frac{\partial^2 C_i}{\partial q^j \partial q^\alpha}. \tag{5.52}$$

To add the kinematic constraint equations to the differential equations of motion, the technique of Lagrange multipliers is used. The final equations can be written in matrix form as

$$\mathbf{M}^i\ddot{\mathbf{q}}^i - \mathbf{C}_{\mathbf{q}^i}^T\boldsymbol{\lambda} = \mathbf{Q}_e^i + \mathbf{Q}_\nu^i, \tag{5.53}$$

that can be also written in matrix form

$$\begin{bmatrix} \mathbf{M} & \mathbf{C}_{\mathbf{q}}^T \\ \mathbf{C}_{\mathbf{q}} & \mathbf{0} \end{bmatrix} \begin{bmatrix} \ddot{\mathbf{q}} \\ -\boldsymbol{\lambda} \end{bmatrix} = \begin{bmatrix} \mathbf{Q}_e + \mathbf{Q}_\nu \\ \mathbf{Q}_d \end{bmatrix} \tag{5.54}$$

When the mathematical model is formulated, the main problem is to select the suitable solution method. The special transformation method published in [41] is used in this study. The index of the differential algebraic equation is transformed into the underlying ordinary differential equation using the elimination of Lagrange multipliers. The goal is to avoid the computation of the multipliers. Thus, the acceleration is expressed from the first Eq. 5.54 as

$$\ddot{\mathbf{q}} = \mathbf{M}^{-1}\left(\mathbf{Q}_e + \mathbf{Q}_\nu + \mathbf{C}_q^T\boldsymbol{\lambda}\right). \tag{5.55}$$

Substituting this form into the second Eq. 5.54, the following relationship can get

$$\mathbf{C}_{\mathbf{q}}\mathbf{M}^{-1}\left(\mathbf{Q}_e + \mathbf{Q}_\nu + \mathbf{C}_{\mathbf{q}}^T\boldsymbol{\lambda}\right) = \mathbf{Q}_d. \tag{5.56}$$

After some processing, the expression of Lagrange multipliers can be given by

$$\boldsymbol{\lambda} = \left(\mathbf{C}_{\mathbf{q}}^T\mathbf{M}^{-1}\mathbf{C}_{\mathbf{q}}^T\right)^{-1}\left[\mathbf{Q}_d - \mathbf{C}_{\mathbf{q}}\mathbf{M}^{-1}\left(\mathbf{Q}_e + \mathbf{Q}_\nu\right)\right]. \tag{5.57}$$

Finally, the vector of Lagrange multipliers can be eliminated and the acceleration can be written as

$$\ddot{\mathbf{q}} = \mathbf{M}^{-1}\left[\mathbf{Q}_e + \mathbf{Q}_\nu + \mathbf{C}_{\mathbf{q}}^T\left(\mathbf{C}_{\mathbf{q}}\mathbf{M}^{-1}\mathbf{C}_{\mathbf{q}}^T\right)^{-1}\left(\mathbf{Q}_d - \mathbf{C}_{\mathbf{q}}\mathbf{M}^{-1}\left(\mathbf{Q}_e + \mathbf{Q}_\nu\right)\right)\right]. \tag{5.58}$$

The equation can be solved by the standard numerical integration methods. However, it can be numerically unstable especially for the case of higher number of connected bodies. Some methods for the numerical integration of ordinary differential equations are reviewed e.g. in [9, 35].

Spherical Joint

In the dynamical system, the kinematic constrains are divided into two groups: joint and driving constrains. Driving constraints describe the specified motion trajectories. Joint constraints define the connection between the system bodies. The joints eliminate the degrees of freedom. The spherical joint shown in Fig. 5.4 eliminates the freedom of relative translations. It allows only three degrees of freedom for relative rotations. The kinematic constraints of the spherical joint can be written as

$$\mathbf{C}\left(\mathbf{q}^i, \mathbf{q}^j\right) = \mathbf{R}^i + \mathbf{A}^i \bar{\mathbf{u}}_P^i - \mathbf{R}^j - \mathbf{A}^j \bar{\mathbf{u}}_P^j = 0, \tag{5.59}$$

where i and j are two bodies connected by spherical joint, $\mathbf{R}^i$ and $\mathbf{R}^j$ are the global position vectors of the origins of the local coordinate systems of the bodies, $\mathbf{A}^i$ and $\mathbf{A}^j$ are the transformation matrices of these bodies, $\bar{\mathbf{u}}_P^i$ and $\bar{\mathbf{u}}_P^j$ are the local position vectors of the joint points and P is the point of joint.
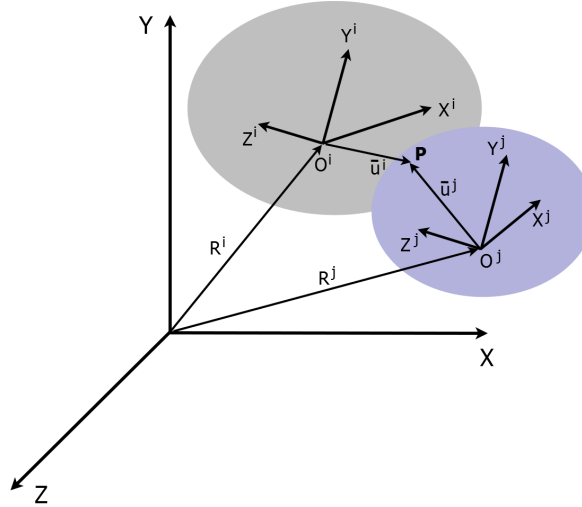
FIGURE 5.4: The spherical joint.

In the case of spherical joint, the Jacobian matrix can be expressed as

$$\mathbf{C}_{\mathbf{q}} = \left[\mathbf{C}_{\mathbf{q}}^i, \mathbf{C}_{\mathbf{q}}^j\right] = \left[\mathbf{I}, \mathbf{A}^i \tilde{\bar{\mathbf{u}}}_P^{iT} \bar{\mathbf{G}}^i, -\mathbf{I}, -\mathbf{A}^i \tilde{\bar{\mathbf{u}}}_P^{iT} \bar{\mathbf{G}}^i\right]. \tag{5.60}$$

5.2 Inverse Dynamics

In the inverse dynamics, the trajectories of given movement are known and the aim is to calculate the forces producing the desired motion. The process of solving this kind of analysis is to define

a kinematically driven system by introducing set of driving constraints of given motion. Thus, the position, velocities and accelerations are determined using the standard kinematic analysis. The coordinates, velocities and accelerations are known and therefore, the system can be solved as a set of algebraic equations to compute the driving forces required to generate the prescribed motion. Hence, it is expected that when these forces are again used to drive the system, the given motion trajectories are obtained.

The unknown force vector is given by Eq. 5.54 as

$$\mathbf{Q}_e = \mathbf{M}\ddot{\mathbf{q}} - \mathbf{C}_{\mathbf{q}}^T \boldsymbol{\lambda} - \mathbf{Q}_\nu, \tag{5.61}$$

where all parameters are known for prescribed motion. Moreover, from the Eq. 5.43 is clear that

$$(\mathbf{Q}_e)_\theta = \mathbf{G}^T \left[\sum_{r=1}^{nF} (\mathbf{u}_r \times \mathbf{F}_r) \right]. \tag{5.62}$$

Considering the vector of gravity, the final equation is written as

$$\sum_{r=1}^{nF} (\mathbf{u}_r \times \mathbf{F}_r) = \left(\mathbf{G}^T \right)^{-1} (\mathbf{Q}_e)_\theta - \mathbf{u}_g \times \mathbf{F}_g, \tag{5.63}$$

where $\mathbf{F}_g$ is the vector of gravitation force, $\mathbf{u}_g$ is its moment arm and $\mathbf{F}_r$ are the unknown external forces. To get the unequivocal solution, the next conditions have to be added. Thus, the unknown forces are computed in the known direction, $\mathbf{n}_k = (n_{xr}, n_{yr}, n_{zr})$. In presented study, this direction is given by muscle trajectories. The vector size is given by following form

$$\|\mathbf{n}_r\| = \sqrt{n_{xr}^2 + n_{yr}^2 + n_{zr}^2} \tag{5.64}$$

The unit vector is then given by

$$\mathbf{e}_{nr} = \frac{n_{xr}}{\|n_r\|}\mathbf{i} + \frac{n_{yr}}{\|n_r\|}\mathbf{j}\frac{n_{zr}}{\|n_r\|}\mathbf{k}, \tag{5.65}$$

where $\mathbf{i}, \mathbf{j}, \mathbf{k}$ are the unit vectors in the direction of the x, y, z axes of a three dimensional Cartesian coordinate system.

And thus, the unknown force vector can be then written as

$$\mathbf{F}_r = \|F_r\|\mathbf{e}_{nr}. \tag{5.66}$$

To get the final expression of the unknown external forces, the substitution of Eq. 5.66 into the Eq. 5.63 is used.

Chapter 6

Biomechanical Modeling of Human Body

6.1 Inverse Dynamic Analysis Underdetermined Biomechanical System

In the chapter 5, it has been demonstrated how the equations of motion of rigid body in 3D can be applied. The inverse dynamic analysis was also introduced to find the system of equations describing the external muscle forces ensuring the considered movement. However, to calculate the muscle forces, the underdetermined mechanical system with redundant nature is solved. So there are more unknowns to calculate than available equations of motion. In this chapter, the mean aim is to solve the underdetermined biomechanical system and to find the muscle forces. Afterwards, the redundant problem in biomechanics is identified. The muscles are associated with muscle model simulated the muscle activation-contraction dynamics. Namely, the Hill-type muscle model is used. The underdetermined system is solved by optimization method. This process and used tools are also presented.

6.1.1 The Redundant Problem in Biomechanics

In the complex of human body, almost every joint is crossed by several muscles or muscle groups. From the physiological point of view, more muscles cooperate in the joint position or motion than it is necessary. Moreover, different muscle activation patterns can generate the same body posture or movement. The selection of muscle and their activity is ensured by central nervous system. Its decision-making criterions are fatigue, the set of tasks being already performed and the objectives to be achieved. The redundant problem in biomechanics, historically termed in [112], is the problem of underdetermined system. This problem is solved by optimization techniques that find, from the infinite set of solutions, the optimal one.

6.1.2 Optimization

The inverse dynamics problem with the muscle actuators is underdetermined system. It presents an infinite set of solutions. In real physiology, the central nervous system effectively adopts only one of them. From mathematical point of view, there are several methods how to find right this one. The first technique is to reduce the number of unknowns until the number of available equations. The second one is to increase the number of equations until the number of unknowns. However, these approaches lose important information regarding the unknowns that were grouped or removed. Moreover, it is very difficult to find the additional equations [92]. The third approach is to find the one solution from all possible that minimizes the given objective (also called cost) function. This function is usually subjected to a number of restrictions and constrictions. In this study, the optimal distribution of muscle forces during some body movements and position is computed using the constrained optimization method. The used technique is explained in [6, 53, 88] in more details.

General Optimization Problem

The general optimization problem can be expressed as

$$
\begin{aligned}
Control\ variables: &\quad \mathbf{x}\,(x_i) &\quad i = 1, 2, \ldots, n_F \\[2ex]
Minimize: &\quad \mathcal{F}\,(\mathbf{x}) \\[2ex]
Subject\ to: &\quad f_k\,(\mathbf{x}) = 0 &\quad k = 1, 2, \ldots, n_{cc} \\
&\quad f_l\,(\mathbf{x}) \geq 0 &\quad l = 1, 2, \ldots, n_{ic} \\
&\quad x_i^{lower} \leq x_i \leq x_i^{upper}
\end{aligned}
\tag{6.1}
$$

where $\mathbf{x}$ is the vector of control unknowns variables, $\mathcal{F}(\mathbf{x})$ is the objective function to be minimized, $F_k(\mathbf{x})$ are the equality constraints (total number n_{ce}), $F_l(\mathbf{x})$ are the inequality constraints (total number n_{ie}), x_i^{lower} and x_i^{upper} are the side constraints. In the optimization, the total number of constraint equations is essentially smaller than the number of control variables (i.e. $n_F > n_{cc}$ and $n_F > n_{ie}$). The equality constraints represent the underdetermined system of equations and vector $\mathbf{x}$ represents the unknown muscle forces.

If the objective function and the constraint function depend linearly on the control variables, the optimization problem is linear. Otherwise, the problem is non-linear. To purpose of musculoskeletal modeling, the linear problem is considered to be inadequate in the estimation of the force sharing problem - not predicting the co-activation of agonists and antagonists [92]. For this reason, the redundant problem in biomechanics is formulated as constrained non-linear.

Cost-Function and Constrained Optimization

The minimization of the objective function replaces the physiological criteria adopted by the central nervous system - which muscle and which activation will be used to produce the given movements or to keep the body posture. So many different objective functions have been already used to solve the redundant problem in biomechanics [19, 21, 23, 112]. The reason is that the objective function has too complicated role. It should be able to consider the physiological activity, to reflect the pathological and fatigue of human body, to include relevant physiological characteristics as well as to introduce the future plans of activities. In addition, from the mathematical point of view, the objective function should be numerically stable and the computation time should be acceptable. Some examples of objective functions commonly used, non-linear are presented follows

- The sum of the squares of individual active muscle forces [92]

$$\mathcal{F} = \sum_i \left(F_{CE}^i \right)^2 . \tag{6.2}$$

  This function finds the energy minimization. However, it does not include any physiological capabilities. Originally, the function is developed for applications to the human locomotion.

- The sum of the cube of the individual average muscle stresses [21]

$$\mathcal{F} = \sum_i \left(\sigma_{CE}^i \right)^3 = \sum_i \left(\frac{F_{CE}^i}{PCSA^i} \right)^3 , \tag{6.3}$$

  where $PCSA$ is the physiological cross sectional area of the individual muscle. This function is based on quantitative force-endurance relationship and on experimental results. It includes the physiological information - the muscle physiological cross sectional area. Thus, this function should be able to predict co-activation of muscles.

- The sum of the square of the individual normalized muscle forces [75]

$$\mathcal{F} = \sum_i \left(\frac{F_{CE}^i}{F_{max}^i} \right)^2 . \tag{6.4}$$

  This function also includes the physiological information - the maximal isometric force that each muscle is able to produce.

Alternatively, the objective function, Eq. 6.2, can also be the sum of the instantaneous muscle power of the sum of the square of the total reaction forces at the joints. These objective functions and many others are presented in literature such as in [19, 23, 92].

These three objective functions, Eq. 6.2, 6.3 and 6.4, were tested in previous work [95]. The basic 2D three-body segment musculoskeletal model of the upper limb was modeled. The static analysis and

optimization method was used to calculate the muscle forces needed to keep the given static position. In that work, the optimization problem was solved by Python optimization package providing several commonly known algorithms. Namely the Sequential Least Squares Programming (SLSQP) algorithm was used. The SLSQP optimizer is based on the slightly modified version of Lawson and Heuson's nonlinear least-squares solver [59]. It was shown that all functions have the same results. However, the second one, Eq. 6.3, has the significantly lowest number of iterations. Therefore, this function is also used in presented study.

In inverse dynamics, the constraint equations, that the control variables have to fulfill, are presented by the equations of motion. So, all constraints are of equality type. In addition, the lower and upper limits are given by real anatomy - $F_i^{lower} = 0$ (the muscle can only pull, it can not push), $F_i^{upper} = F_{i_{max}}$ (the maximal muscle force that can be generated by the individual muscle). The optimization problem defined in this work is then given by following formula

$$
\begin{aligned}
Control\ variables: \quad &\mathbf{F}\left(F_i\right) && i = 1, 2, \ldots, n_F \\[2mm]
Minimize: \quad &\mathcal{F} = \sum_i \left(\frac{F_{CE}^i}{PCSA^i}\right)^3 \\[2mm]
Subject\ to: \quad &\sum_{r=1}^{nF} \left(\mathbf{u}_r \times \mathbf{F}_r\right) = \left(\mathbf{G}^T\right)^{-1} \left(\mathbf{Q}_e\right)_\theta - \mathbf{u}_g \times \mathbf{F}_g \\[2mm]
&0 \leq F_i \leq F_{i_{max}}
\end{aligned}
\tag{6.5}
$$

6.2 Muscle Model

The Hill-type muscle bar model was used to simulate the behavior of the skeletal muscle [45]. The model lacks accuracy in the description of some specific phenomena such as the drop of active force at high elongation speeds and the detailed understanding of muscle construction especially the reactions of contractile proteins. However, the Hill-type model has the basic structure, it is suitable for calculation of the peak value of muscle force with the reasonable accuracy, the computation is not time-consuming and the model does not require large range of input parameters. It describes the muscle in terms of its macroscopic elongation, the shortening or lengthening velocities and the neural excitation level.

The Hill-type model consists of a contractile element CE and a parallel visco-elastic element $PE + DE$. The contractile element represents the active force generated by the muscle during muscle contraction. The parallel element simulates the passive muscle properties. It consists of a nonlinear spring PE and a linear dashpot DE. The final model structure is depicted in Fig. 6.1. The muscle force is then written as

$$
F_{Mus} = F_{CE} + F_{PE} + F_{DE}.
\tag{6.6}
$$
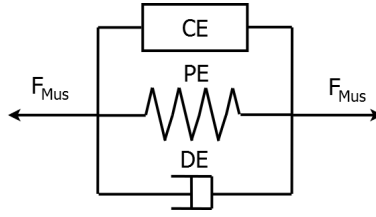
FIGURE 6.1: Hill-type muscle model.

The contractile force is a function of instantaneous muscle length L, instantaneous elongation or contraction rate ν and the values of the active muscle state $N_a(t)$. The contractive muscle force is given by the following form

$$F_{CE}(x, \nu, t) = N_a(t) F_L(x) F_\nu(\nu),$$ (6.7)

where $F_L(x)$ is the force-length characteristic of the muscle at the $\nu = const.$ and $N_a = const.$, F_ν is the force-velocity characteristic at $L = const.$ and $N_a = const.$

The muscle force-length property is shown in Fig. 6.2. Apparently, this relation exhibits a maximum at the optimal muscle length, L_{opt}. When the muscle is shorter or longer, its active force drops. It is also assumed, that the CE force is equal zero when the muscle length exceeds the values $0.5 L_{opt}$ during the shortening. This fact can be explained by sarcomeres appearance during the muscle deformation. On the other hand, when the muscle continues to elongate the total force increase again due to passive properties of the element PE. The concavity of the muscle force-length characteristic is determinated by the parameter C_{sh}. In the most cases, the parameter $C_{sh} = 0.3 - 0.5$. In the current study, the CE force is modeled using the formula given by [7] as

$$F_L(x) = F_{max} exp\left(-\left(\frac{\frac{L}{L_{opt}} - 1}{C_{sh}}\right)^2\right),$$ (6.8)

where L is the instantaneus muscle length and F_{max} is the maximal muscle force generated by the fully tetanised muscle during isometric contraction at $N_a = 1$.
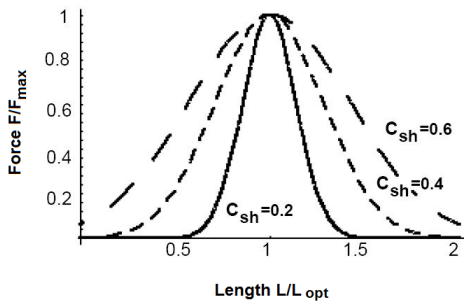
FIGURE 6.2: Active force-length characteristic of the skeletal muscle, [106].
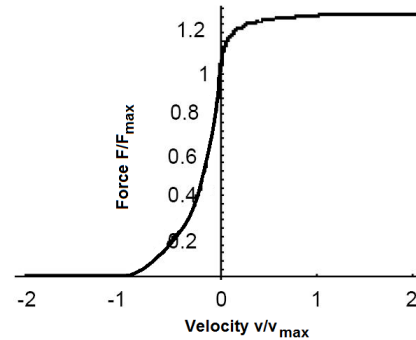
FIGURE 6.3: Active force-velocity characteristic of the skeletal muscle, [106].

As shown in Fig. 6.3, the active force-velocity property should be divided into two parts - the process of shortening and the lengthening. During the shortening, the muscle force is decreased. During the lengthening, the force reaches the plateau. This property can be explained with the cross-bridge theory. At shortening, one part of the cross-bridges is attached in positive tensile force generating position and the other part is in negative. The total force decreases. At the lengthening, the number of attached cross-bridges decreases and however, the higher forces are generated because, the cross-bridges are stretched to larger displacement. As mentioned in the literature [7, 24, 103, 105], at the high lengthening velocity, the force may be below the isometric value. I.e. the force F_ν is less than one. Nevertheless, in this kind of basic Hill-type model, the drops of F_ν are not directly introduced. The force-velocity relation is calculated with the equations

$$F_\nu\left(\nu_n\right) = \begin{cases} 0 & \nu_n \leq -1 \\ \\ \frac{C_{short}(1+\nu_n)}{C_{short}-\nu_n} & -1 < \nu_n \leq 0 \\ \\ \frac{C_{leng}+C_{mvl}\nu_n}{C_{leng}+\nu_n} & \nu_n > 0 \end{cases} \qquad (6.9)$$

where v_n is the muscle shortening of lengthening velocity normalized to the maximal values, v_{max}. The parameter C_{sh} describes the muscle shortening. The range for this is approximately $C_{sh} = 0.1 - 0.25$ depending on numbers of fast and slow muscle fibers. The parameter C_{mvl} determinates the ratio of ultimate force at full activation, usually $C_{mvl} = 1.3 - 1.5$. The last parameter C_{leng} characterize the muscle lengthening. It is calculated from the parameters C_{short} and C_{mvl} to keep the continuous slope of F_ν at $v_n = 0$ as

$$C_{leng} = \frac{C_{mvl} - 1}{1 + \frac{1}{C_{short}}}, \qquad (6.10)$$

The maximal shortening velocity, v_{max}, can be written as

$$v_{max} = 2l_{fib} + 8l_{fib}C_{fast}, \qquad (6.11)$$

where C_{fast} is the fraction of fast muscle fibers in a given muscle and l_{fib} is the length of muscle fibers in the relaxing position.

The passive muscle force F_{PE} is obtained from the formula published in [105] as

$$F_{PE} = \frac{F_{max}}{exp\left(C_{PE}\right) - 1}\left(exp\left(C_{PE}\frac{x}{L_{O_{fib}}PE_{max}}\right) - 1\right), \qquad (6.12)$$

where $L_{O_{fib}}$ is the rest length of muscle, C_{PE} is the shape parameter of the force-elongation characteristic shown in Fig. 6.4, x is the elongation element $x = L - L_{O_{fib}}$, PE_{max} is the elongation of

the parallel component at F_{max}. Usually, PE_{max} is between 0.5 and 0.8, C_{PE} is in range of 4 and 10.

The last model element is F_{DE}. This damped part is given by following relationship

$$F_{DE} = k_{DE}\nu, \tag{6.13}$$

where k_{DE} is the linear coefficient of dashpot.

In used implementation, the muscle deformation rates are calculated as the sum of rates of all elements that are used to model a given muscle.

In reality, muscles are attached to the bones by tendons. Therefore, the muscle complex includes the muscle part and tendon part, see Fig. 6.5. The tendon represents the connection of muscle into a mechanical system and thus, the tendon should influence the muscle properties. For the given muscle-tendon complex, the muscle part connected with the elastic tendon is shorter than the muscle with the stiff tendon. In most cases, the tendon part is modeled much stiffer than the muscle. Therefore, the muscle model neglecting the tendon part gives the acceptable values of force peaks. Otherwise, the tendon is mostly modeled by linear behavior. The stiffness can be calculates as follows

$$k_T = 37.5\frac{F_{max}}{L_{ST}}, \tag{6.14}$$

where L_{ST} is a tendon slack length in meters and F_{max} is given in N. According to the literature [42, 81], the commonly reported values for tendon stiffness are $0.2 - 0.5$ Ns/m. Therefore, the tendon part is often neglected. For the purpose of this study, the tendon part has also been left out.
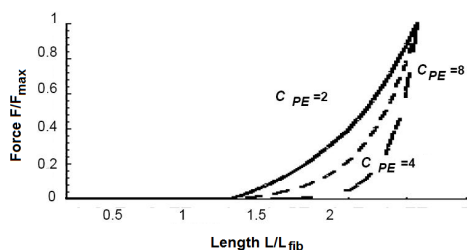
FIGURE 6.4: Pasive force-length characteristic of the skeletal muscle, [106].
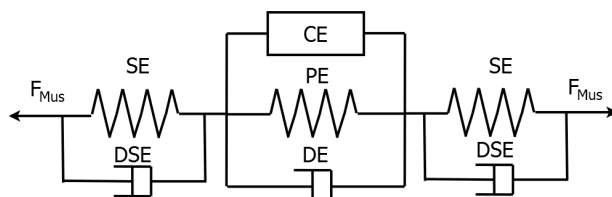
FIGURE 6.5: Muscle model involving the tendon part.

6.3 K-Means Method

The k-means method is a clusterin of vector quatization. The method aims to divide nodes into several groups (clusters) in which each observation belongs to the cluster with the nearest mean. In general, the problem is computationally demanding. However, there are efficient numerical algorithms that are commonly used and that converge quickly to the local optimum. One of these efficient method is called *standard algorithm* [63], often so called *k-means algorithm* and also referred to as *Lloyd's algorithm*. The algorithm is based on Euclidean distance and respects the following form

- Input parameters are observed points $x_1, x_2, \ldots, x_m$, where m is a total number of points. The points are defined by their position in 3D local space - each observation is a 3-dimensional real vector.

- In the initial step, the positions of starting centroids $c_{10}, c_{20}, \ldots, c_{n0}$ are guessed, where n is a number of sets.

- For each point, the centroid in shortest distance is found. All points are distributed into the sets $S_1, S_2, \ldots, S_n$ according to the assigned centroids. The points x_p belonging into the set S_i are given by following prescription

$$S_i^{(t)} = \{x_p : ||x_p - c_i^{(t)}||^2 \leq ||x_p - c_j^{(t)}||^2; \forall 1 \leq j \leq n\}, \tag{6.15}$$

where t is an observed number of iteration.

- Repeatedly, new centroids $c_1, c_2, \ldots, c_n$ of each set of points are found as follows

$$c_i^{(t+1)} = \frac{1}{|S_i^{(t)}|} \sum_{x_j \in S_i^{(t)}} x_j. \tag{6.16}$$

The algorithm converges when the positions of centroids aren't longer changed, i.e. when the differences of centroids positions in the iteration sequence are smaller than arbitrary chosen parameter, $\varepsilon << 1$. In this case, the mentioned steps minimize the within-cluster sum of squares (WCSS) given by

$$argmin \sum_{i=1} \sum_{\mathbf{x} \in \mathbf{S_i}} ||\mathbf{x} - \mathbf{\mu_i}||^2, \tag{6.17}$$

where μ_i is the means of points in S_i.

The algorithm is very often presented as assigning objects to the nearest cluster by distance. It minimize the WCSS objective and thus, assigns by least sum of squares, which is exactly equivalent to assigning by the smallest Euclidian distance. Various modifications of k-means method such as spherical k-mean or k-medoids have been already proposed to allow using other distance measures.

6.4 Muscle Moment Arm

Moment arm calculation is a simple task for mechanical engineering. In general, this is a perpendicular distance between the force line-of-action and the axis of rotation. For simple cases of biomechanics, when the muscle is just the straight-line, this calculation is the same. However, in the opposite cases, this approach is deficient. The muscle lines may change the length as they wrap around the obstacles, they may span several joints, etc. Therefore, few clinically-useful definitions of muscle moment arms have been already introduced. From the biomechanical point of view, the muscle moment arm, M, is an instantaneous measure of the effectiveness with which the muscle contraction force can generate a torque at the given joint, while in a given joint configuration, as explained in [85]. The resulting moment arms are then the scalars with the units of length and depending on the muscle geometry (not on material and mass properties).

In the literature, there is a lot of methods how to calculate the muscle moment arm such as so called *Partial velocity method* [26, 54], *Generalized force method* used in open software OpenSim 3.0 [85], etc. The most popular method is the *Perturbation method* based on direct finite differencing [12, 85]. The muscle moment arm is given by following

$$M = \frac{dL}{d\theta}, \tag{6.18}$$

where L is the muscle length and θ is the angle of rotation. This method is very simple − the muscle moment arm is the partial derivation of the muscle length with respect to the joint angle in the direction of the joint degrees of freedom (just make a small perturbation $\triangle\theta$ and find the resulting changes $\triangle L$). This method is also used in laboratories very often [3, 5].

Chapter 7

The new torus-obstacle method

The musculoskeletal models of human body are commonly used to calculate the forces transmitted by the skeletal muscles. The results of these studies are significantly sensitive to the muscle path modeling. For the given configuration of the joints, the muscle paths determine the forces, moment arms, lengths, torques as well as fatigue of the muscles [14, 44]. Existing virtual models are limited by many factors such as unreal muscle shapes, excessive muscle sliding over the neighboring obstacles, high computation time, large range of input parameters, low number of validated joint movements, etc. as already discussed in Chapter 4. Therefore in this study, the new approach of muscle path modeling is developed. The algorithm is based on the obstacle-set method originally presented by Garner and Pandy [37]. In this work, the new torus-obstacle is implemented instead of the spheres, cylinders and ellipsoids to ensure the suitability of this method for all complex joints and their arbitrary movements.

The main aim of this torus-obstacle method is to eliminate the limits of existing models. The most important advantages of this new method are the followings

- satisfying simulation of muscle shapes corresponding to the reality

- usable for all arbitrary movements of each joint complex

- unreal muscle sliding over the obstacles limited

- only few input arguments needed

- not time-consuming

- muscle bulging up considered; muscle volume changes depending on the actual muscle length

- 3D implementation of the positions of obstacles and the muscle attachments

- easy to add other lines-of-action; automatic recalculation of positions of attachments and obstacles

The torus-obstacle method is based on few assumptions such as

1. The muscle complex is represented by set of lines-of-action. The number of lines for individual muscle corresponds with its cross section area (PCSA).

2. The muscles are represented by frictionless elastic bands.

3. The muscle force is the same along the whole muscle line-of-action.

4. The muscle bands move freely over the neighboring anatomical structures such as bones, organs, joints, other muscles, etc.

5. The surrounding structure constraining the muscle path is replaced by regular torus.

6. The muscle bulking up depends linearly on the actual muscle length.

7. Each muscle line is held by own torus obstacle - at least one torus for each muscle line of action. Each muscle line goes through the torus center and wraps around its surface.

8. The torus is situated in the local coordinate system of individual segment and thus, its position and orientation corresponds to the current joint configuration.

7.1   Torus-Obstacle Algorithm

The torus-obstacle method is developed to find the correct muscle trajectory wrapping the other tissues. It is primarily used to build the musculoskeletal structures. In this case, the skeleton is modeled by a set of rigid bodies representing the bones connected by real mechanical joints. For a given joint configuration, the relative positions and orientations of all bone segments are well described. The muscle path is defined by a series of three parts − the straight-line from muscle origin to the torus, the curved-line wrapping around the torus and passing the torus center and the straight-line going from the torus to the muscle insertion. The muscle path is simulated by the shortest connection of muscle attachments fitting closely to the torus surface. And thus, the straight-lines are tangential to the torus and the curved-line find the shortest way for the muscle wrapping.

In this method, few coordinate systems are used − always given by a set of orthogonal unit vectors. The global reference frame is fixed in space. The local bone coordinate systems are attached to the bone segments - their origins are situated in the center of gravity of individual segment, the orientation of the axes are the same as defined for the global reference frame in the rest position of the human body (i.e. whole upper arm hanging freely along the thorax, elbow joint fully extended, the palm turn forward). The torus obstacle coordinate system is fixed to the torus and its origin agrees with the center of torus. The axes orientation respect the same condition defined for the bone coordinate systems. In these local systems, the points of contacts of muscle straight-lines and torus surfaces as well as the curved-line are defined.

The positions of muscle attachments correspond to the real anatomy. They are fixed to the local coordinate system of the individual bone. Their 3D position is based on data from in-vivo MRI scans and on k-means method mentioned in section 6.3. When the input number of muscle lines is changed by the user, the position of new muscle attachments are automatically recomputed.

The torus obstacles are also situated in the local systems of bones. Their actual position is changed depending on the actual joint movement. Therefore, the muscle bulging up is ensured and moreover, that prevents the overlapping of the torus with the other structures during the motion. The 3D position of torus is again based on in-vivo MR images and k-means method. In addition, when the number of lines is changed, the position of new toruses are also automatically recalculated.

The process of torus-obstacle method can be explained in following steps in more details:

INPUT

The input parameters for the torus-obstacle method are the radius of torus, R, the position and orientation in global reference frame, XYZ, the actual location of the torus, the muscle attachment (origin or insertion), in general called $\mathbf{P}$, given in torus reference frame, $\mathbf{P}_t$. The torus local coordinate system is called $X_t Y_t Z_t$. The origin is situated in the torus center based on MRI. The orientation is the same as defined for the local system of corresponding bone, $X_b Y_b Z_b$. The torus is situated in the plane $X_t Y_t$. The major radius (the distance from the center of the torus to the center of the tube) and the minor radius (the radius of the tube) are the same. The original configuration as well as position and orientation of torus are depicted in Fig. 7.1.
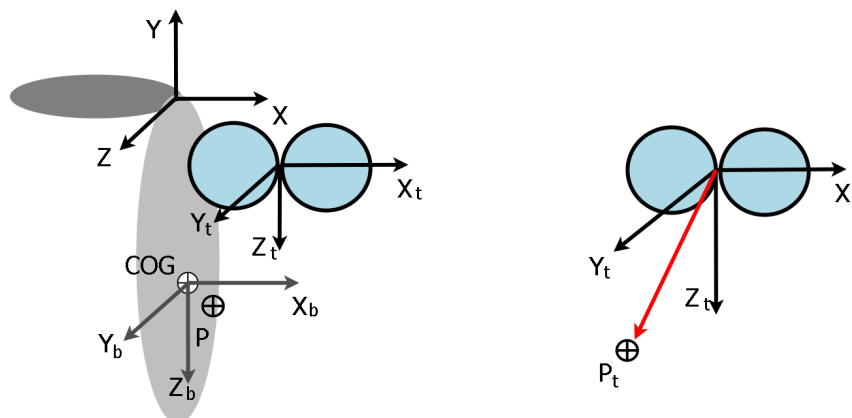
FIGURE 7.1: The expression in torus local coordinate system, where COG is the segment center of gravity, XYZ is the fixed reference frame, $X_b Y_b Z_b$ is the bone segment system, $X_t Y_t Z_t$ is the torus system and $\mathbf{P}_t$ is the muscle attachment fixed to the local system of torus.

STEP I.

For the given joint configuration, the regular torus obstacle can be replaced by the sphere surface, see Fig. 7.2. The radius of sphere is equal to the radius of the torus, R. The center of the sphere is given by intersection of the center circle of the tube and the plane defined by three points - $\mathbf{P}_t$, $\mathbf{P}_{surf}$ and $\mathbf{C}_t$, where $\mathbf{C}_t$ is the center of torus local frame and $\mathbf{P}_{surf}$ is the orthogonal projection of the point $\mathbf{P}_t$ onto the plane X_t, Y_t given by

$$\mathbf{P}_{surf} = [P_{torus_X}; P_{torus_Y}; 0]. \tag{7.1}$$

The first step of presented method is to express $\mathbf{P}_t$ and $\mathbf{C}_t$ in the local sphere coordinate system, $\mathbf{P}_s$ and $\mathbf{C}_s$, respectively. The axes of this local system are parallel to the torus system. The origin, $\mathbf{O}_s$, is situated in the center of sphere. The points are translated using the unit vector, $\mathbf{u}$, and translation vector, $\mathbf{trans}$, in the following forms

$$\mathbf{u} = \frac{\mathbf{P}_{surf}}{\|\mathbf{P}_{surf}\|} \quad and \quad \mathbf{trans} = \mathbf{u}R, \tag{7.2}$$

$$\mathbf{P}_s = \mathbf{P}_t - \mathbf{trans} \quad and \quad \mathbf{C}_s = \mathbf{C}_t - \mathbf{trans}. \tag{7.3}$$
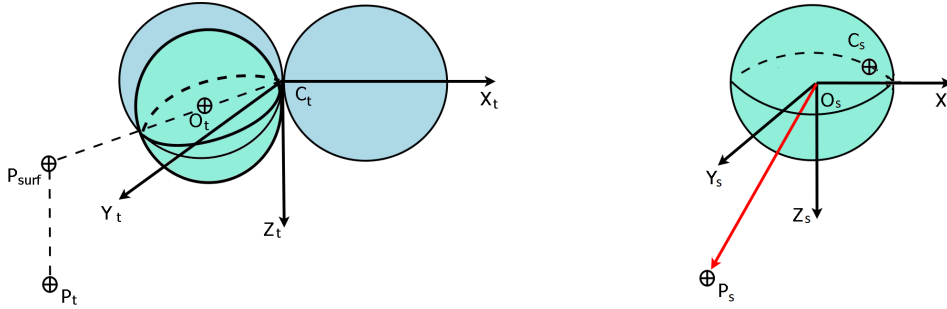
FIGURE 7.2: The expression in sphere local coordinate system, where $X_tY_tZ_t$ is the torus system, $X_sY_sZ_s$ is the sphere system, $\mathbf{P}_{surf}$ is the orthogonal projection of the point $\mathbf{P}_t$ defined in the torus system, $\mathbf{O}_t$ is the center of sphere system defined in torus system and $\mathbf{P}_s$, $\mathbf{O}_s$, $\mathbf{C}_s$ are the points transformed in sphere system.

STEP II.

Considering the fact that the sphere is circular in cross-section, the circle local coordinate system is implemented, $X_cY_cZ_c$, see Fig. 7.3. The second step is to express the points in plane reference frame given by center O_s, P_s and C_s. The transformed points, P_c and C_c, meet the following forms

$$\mathbf{P}_c = [-\|P_sO_t\|; P_{s_z}; 0], \tag{7.4}$$

$$\mathbf{C}_c = [R; 0; 0]. \tag{7.5}$$
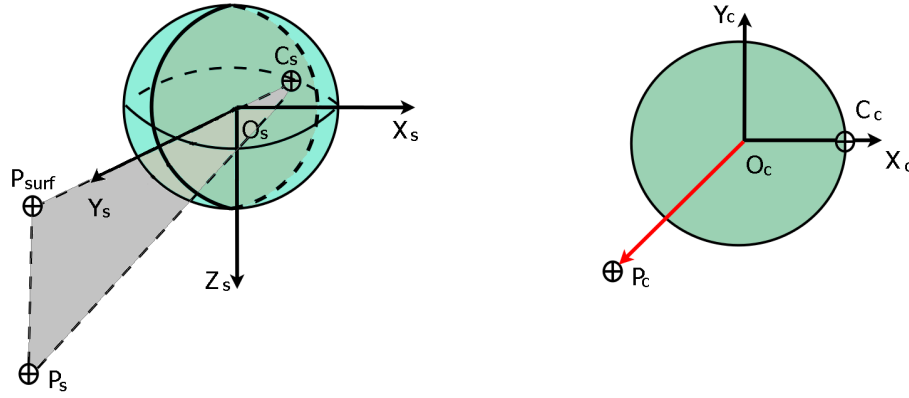
FIGURE 7.3: The expression in circle local coordinate system, where $X_s Y_s Z_s$ is the sphere system, $X_c Y_c Z_c$ is the circle system, $\mathbf{P}_{surf}$ is the orthogonal projection of the point $\mathbf{P}_s$, $\mathbf{O}_s$ is the center of sphere system defined there and $\mathbf{P}_c$, $\mathbf{O}_c$, $\mathbf{C}_c$ are the points transformed in circle system.

STEP III.

The third step is to find the location of point of tangent, $\mathbf{Q}_c$, associated with the torus obstacle. According to the method assumptions, this point is placed on the surface of torus. To ensure the minimum muscle length, straight-line part of the muscle must be tangent to its torus surface. Moreover, each muscle line goes directly through the torus center to be hold in correct position. Therefore, the curved-line part joints the point of tangent with the neighboring torus center, $\mathbf{C}_c$, see Fig. 7.4.

The next task is to find the coordinates XY of point of tangency in local coordinate system of circle. According to the geometric conditions, two constraint equations are derived, [37]

$$R^2 = Q_{c_X}^2 + Q_{c_Y}^2, \qquad R^2 + (P_{c_X} - Q_{c_X})^2 + (P_{c_Y} - Q_{c_Y})^2 = P_{c_X}^2 + P_{c_Y}^2. \tag{7.6}$$

These equations may be combined, squared, rearranged and changed using quadratic formula. After that operations, the final solution for Q_{c_X} and Q_{c_Y} can be expressed

$$Q_c = \begin{cases} Q_{c_X} = \dfrac{P_{c_X} R^2 - R P_{c_Y}\sqrt{P_{c_X}^2 + P_{c_Y}^2 - R^2}}{P_{c_X}^2 + P_{c_Y}^2} \\[2em] \qquad\qquad\qquad\qquad\qquad\qquad\qquad\quad P_{c_Y} < 0 \\[1em] Q_{c_Y} = \dfrac{P_{c_Y} R^2 + R P_{c_X}\sqrt{P_{c_X}^2 + P_{c_Y}^2 - R^2}}{P_{c_X}^2 + P_{c_Y}^2} \\[3em] Q_{c_X} = \dfrac{P_{c_X} R^2 + R P_{c_Y}\sqrt{P_{c_X}^2 + P_{c_Y}^2 - R^2}}{P_{c_X}^2 + P_{c_Y}^2} \\[2em] \qquad\qquad\qquad\qquad\qquad\qquad\qquad\quad P_{c_Y} > 0 \\[1em] Q_{c_Y} = \dfrac{P_{c_Y} R^2 - R P_{c_X}\sqrt{P_{c_X}^2 + P_{c_Y}^2 - R^2}}{P_{c_X}^2 + P_{c_Y}^2} \end{cases} \tag{7.7}$$
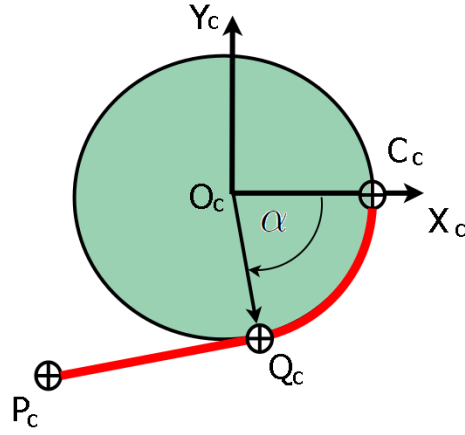
FIGURE 7.4: The torus-obstacle method used for muscle wrapping, where $\mathbf{Q}_c$ is the point of tangent, $\mathbf{P}_c$ is the muscle attachment, $\mathbf{C}_c$ is the center of torus and α is the angle of arc.

STEP IV.

The fourth step is to compute the curved-line part of the muscle − the length of arc between tangent point, Q_c, and center of torus, C_c, see Fig. 7.4. Before that, the actual angle, α, of the arc may be computed using these conditions

$$\alpha = \begin{cases} -arccos\left(\frac{Q_{c_X}}{R}\right) & Q_{c_X} > 0, Q_{c_Y} < 0 \\[2ex] -\left(\pi - arccos\left(\frac{Q_{c_X}}{R}\right)\right) & Q_{c_X} < 0, Q_{c_Y} < 0 \\[2ex] arccos\left(\frac{Q_{c_X}}{R}\right) & Q_{c_X} > 0, Q_{c_Y} > 0 \\[2ex] \pi - arccos\left(\frac{Q_{c_X}}{R}\right) & Q_{c_X} < 0, Q_{c_Y} > 0 \end{cases} \tag{7.8}$$

The arc length, $\|Q_c C_c\|$, is then found using the law of cosines, [37]:

$$\|Q_c C_c\| = R cos^{-1}\left(1 - \frac{(Q_{c_X} - C_{c_X})^2 + (Q_{c_Y} - C_{c_Y})^2}{}\right). \tag{7.9}$$

STEP V.

The fifth step is to express all nodes in torus reference frame as

$$Q_s = [Q_{c_X}(-u_X); Q_{c_X}(-u_Y); Q_{c_Y}], \qquad Q_t = Q_s + \mathbf{trans}. \tag{7.10}$$

OUTPUT

The output of the torus-obstacle method are the parts of muscle lines - the straight-lines and the curved-line. The whole muscle length is a sum of length of strait-line parts and curved-line part. The process od muscle wrapping described above may be also performed for the second part

of muscle line (from the origin to torus or on the contrary from insertion to the torus). The muscle length is then given by

$$L_{muscle} = \|OQ_O\| + \|Q_OC\| + \|CQ_I\| + \|Q_II\|, \tag{7.11}$$

where O is the muscle origin, Q_O is the point of tangent located on the torus and belongs to the straight-line from origin, C is the center of torus, Q_I is the point of tangent located on the torus and belongs to the straight-line from muscle insertion and I is the muscle insertion.

7.2 Torus Obstacle Geometry

The input parameters essential for the torus-obstacle method are the position of torus, $\mathbf{T}_b = [T_{b_X}; T_{b_Y}; T_{b_Z}]$, located in coordinate system of given bone and the radius of torus, R. In most studies, the position and radius of obstacles are fixed during the joint movements, such as mentioned in [12, 38, 71]. These studies usually provide satisfying results describing the muscle forces, moments arms, etc. However, they are mostly limited by a low number of validated movements. This attitude does not work correctly for many joint configuration - especially for complex joints like shoulder or for the extreme joint positions. In these cases, the obstacle can be driven in same improper position negatively influencing the results. Therefore, the new approach of torus position and radius corresponding to the actual joint configuration is developed in this study. Moreover, this method considers the muscle bulging up caused by muscle contraction.

This method is based on well known definition of the muscle physiological cross-section area (PCSA). Most authors such as [44, 79, 111] use the formulas published by Alexander and Vernon [1]

$$PCSA = \begin{cases} \frac{m}{\rho L} & notpennate \quad muscles, \\ \\ \frac{m}{2\rho t}sin(2\alpha) & pennate \quad muscles, \end{cases} \tag{7.12}$$

where m, ρ, L, t, α are the muscle mass, density, length, layer thickness of pennation and pennation angle, respectively. That means that PCSA is defined as the volume of muscle devided by its gross muscle length or its fiber length with or without the pennation. For the purpose of this work, the muscle pennation is neglected. In addition, it is assumed that the muscle mass, m, and the muscle density, ρ, are constants - they are not changed during the muscle contraction or elongation. And thus, it is suppose that the changes of muscle volume and also PCSA depend linearly on the changes of muscle length. The process of torus position and radius computation can be explained in following steps:

STEP I.

The first step is to find the original position and orientation of torus obstacle. In-vivo MRI data in rest anatomical position of human body are recorded. It is assumed that the torus center as well as the middle circle of its tube lie in the horizontal plane (parallel to the transversal plane) going through the middle point of given joint (center of rotation). Therefore, the muscle cross section area is found exactly in this plane, see Fig. 7.5. That created plane, Ω, defining the torus position is represented by the regular mesh, see Fig. 7.6. The final original position of torus centers are computed using the k-means method explained in Section 6.3 and the location of nodes given by mesh of Ω plane.
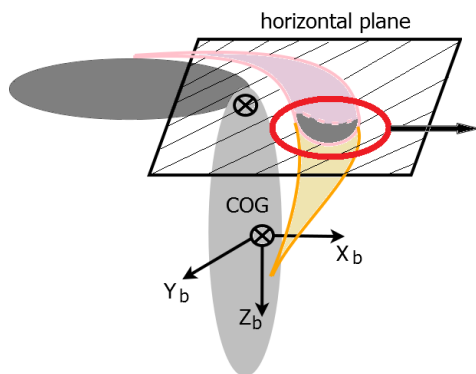
FIGURE 7.5: The muscle cross section area in the horizontal plane defining the torus center positions.
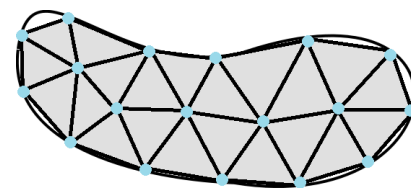
FIGURE 7.6: The regular mesh characterizing the plane Ω defining the torus center positions.

The original positions of torus, $\mathbf{T}_{orig}$, are transformed to the local coordinate system of given bone, $\mathbf{T}_{b_{orig}}$, to ensure the following the actual joint configuration. The original position and orientation of torus is depicted in Fig. 7.7.
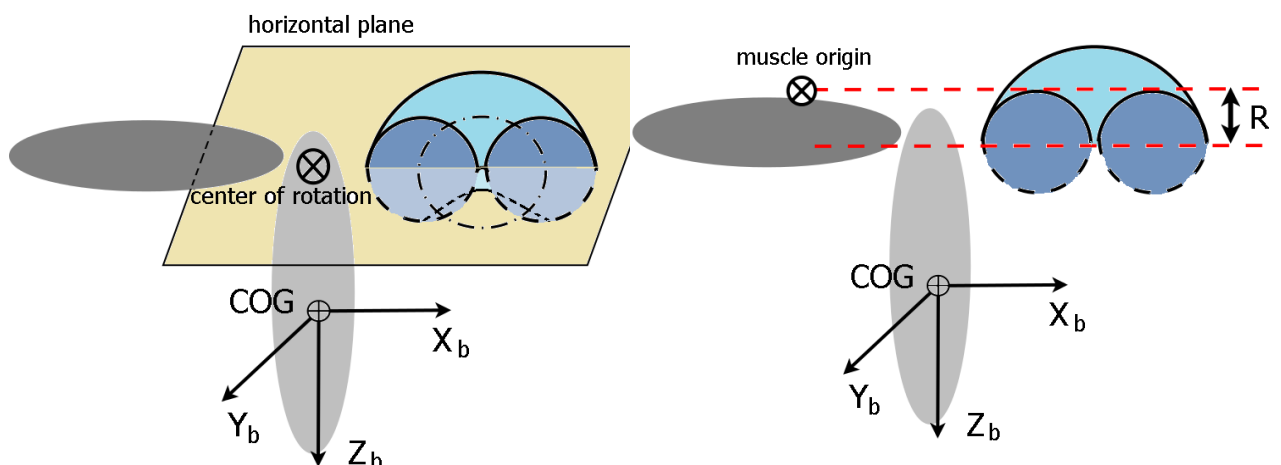
FIGURE 7.7: Calculation of the torus location and orientation.

FIGURE 7.8: Calculation of the torus radius, R.

STEP II.

The second step is to calculate the radius of torus, R. This is the distance between the torus center and the muscle origin in the vertical direction (proximo-distal direction) - the absolute difference of the Z component of position vectors of the torus center and the muscle origin, see Fig. 7.8.

STEP III.

The third step is to compute the original muscle length, L_{orig}, using the torus-obstacle method in rest anatomical position of human body and the Eq. 7.11, see Fig. 7.9.

STEP IV.

The fourth step is to find the parameter K describing the muscle PCSA changes during its contraction or elongation. For each joint configuration and each muscle line-of-action, the muscle length, L, is computed using the torus-obstacle method and the original torus position, $\mathbf{T}_{b_{orig}}$, see Fig. 7.10. The parameter K is also defined for all muscle line-of-action and in each joint configuration. The parameter is given by

$$K = \frac{L_{orig}}{L}. \tag{7.13}$$
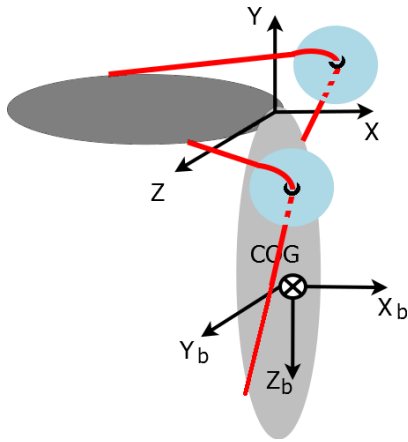
FIGURE 7.9: The original muscle length, L_{orig}.
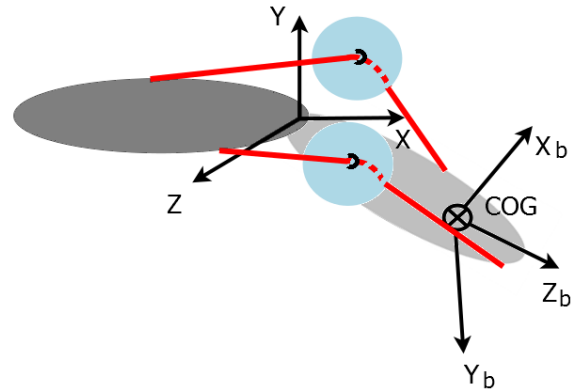
FIGURE 7.10: The actual muscle length using the torus-obstacle method and the original position of torus obstacles.

STEP V.

The next step is to recalculate the torus position for the given joint configuration. The position of midpoint in the bone local system, $\mathbf{M}_b$, is computed as the arithmetic mean of the torus center positions. The midpoint is find for each muscle cross section area and meets the following form

$$\mathbf{M}_b = \frac{1}{N} \sum_{i=1}^{N} \mathbf{T}_{b_{orig\,i}}, \tag{7.14}$$

where N is the number of torus centers. The vector of muscle bulging up given in the local bone coordinate system, $\mathbf{v}_b = [v_X; v_Y; v_Z]$, is then given by the midpoint and the original position of torus centers given by

$$\mathbf{v}_b = \mathbf{T}_{b_{orig}} - \mathbf{M}_b. \tag{7.15}$$

The new torus position is in following expression

$$T_{b_X} = T_{b_{X_{orig}}} + v_{b_X}(K - 1), \tag{7.16}$$

$$T_{b_Y} = T_{b_{Y_{orig}}} + v_{b_Y}(K - 1), \tag{7.17}$$

$$T_{b_Z} = \begin{cases} T_{b_{Z_{orig}}} & \|F_{Z_{orig}} - T_{b_Z}\| \geq R, \\[2ex] T_{b_{Z_{orig}}} + \left(R - \|F_{Z_{orig}} - T_{b_Z}\|\right) & \|F_{Z_{orig}} - T_{b_Z}\| < R, \end{cases} \tag{7.18}$$

where $\mathbf{T}_b = [T_{b_X}; T_{b_Y}; T_{b_Z}]$, K, $\mathbf{F}_{orig} = [F_{X_{orig}}; F_{Y_{orig}}; F_{Z_{orig}}]$, R are the position of torus obstacle in bone local system, parameter of bulging given by Eq. 7.13, position of muscle origin given in bone local system and radius of torus, respectively. These process is shown in Fig. 7.11.
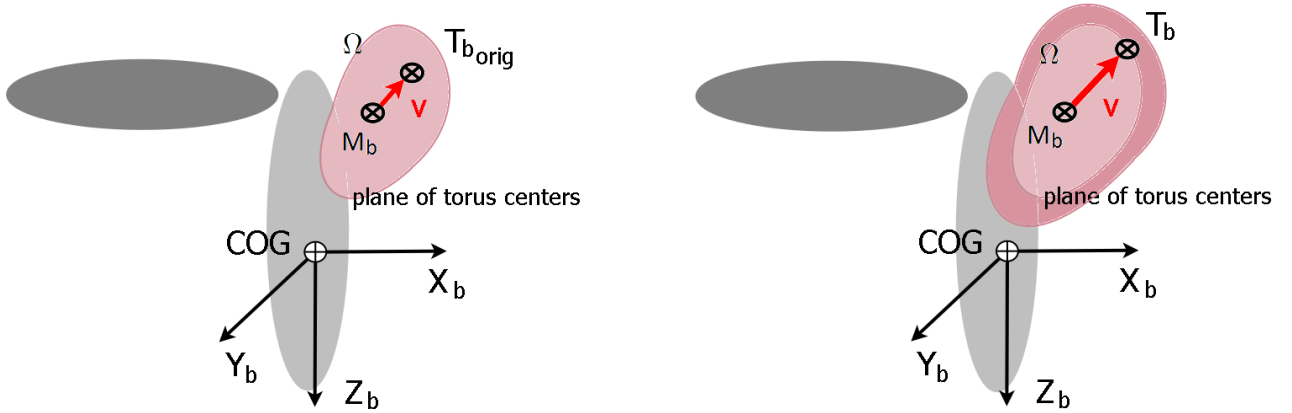
FIGURE 7.11: The process of muscle bulging up. Where $\mathbf{M}_b$ is the midpoint of the torus centers, $\mathbf{T}_{b_{orig}}$ is the example of original position of torus center, $\mathbf{u}$ is the vector of muscle bulging up.

STEP VI.

The final step is to correct the position of torus centers. The muscle complex is always tightly surrounded by other structures such as bones and muscles. Therefore, each muscle bulging causes that the calculated torus centers, T_b *in STEP V.*, intersect these neighboring objects. And thus, some other modification of torus center positions is required. The process of rectification can be divided in two causes and explained in few steps as described below.

CASE (A)

The first case is that the muscle wraps directly around the bone surface. It means that there is no other underlying muscle between the describing muscle and bone. The intersection of the bone is then considered. The whole process can be introduced in following steps.

STEP (1)

The first step is to find the midpoint, $\mathbf{C}_b$, of cross section are of the neighboring bone situated in the plane of torus centers and expressed in the bone coordinate system, see Fig. 7.12. This point is simply given by

$$\mathbf{C}_b = [upper_x; upper_y; M_{b_z}], \tag{7.19}$$

where *upper* is the top point of the bone that defines together with the low point the bone length. The *upper* point is also expressed in the bone local system.

STEP (2)

The second step is to find all torus centers situated inside of bone. The bone cross section area is replaced by ellipse having the center point $\mathbf{C}_b$, major axis a_b in the X_b axis direction and minor axis b_b in the Y_b direction, all depicted in Fig. 7.13. The torus positions respect the following conditions

$$
if \begin{cases}
\dfrac{\left(T_{b_{xi}}-C_{b_x}\right)^2}{a_b^2} + \dfrac{\left(T_{b_{yi}}-C_{b_y}\right)^2}{b_b^2} - 1 > 0 & i = 1, 2, \ldots, N \\[3em]
& \textit{the points } \textbf{outside} \textit{ the ellipse} \\[2em]
\dfrac{\left(T_{b_{xi}}-C_{b_x}\right)^2}{a_b^2} + \dfrac{\left(T_{b_{yi}}-C_{b_y}\right)^2}{b_b^2} - 1 < 0 & i = 1, 2, \ldots, N \\[3em]
& \textit{the points } \textbf{inside} \textit{ the ellipse}
\end{cases} \tag{7.20}
$$

STEP (3)

The third step is to find one point, from those inside the ellipse, that is the farthest from the point $\mathbf{M}_b$. This point is called $\mathbf{T}_{bF}$ and it respects the following condition

$$\|\mathbf{T}_{bF}\mathbf{M}_b\| > \|\mathbf{T}_{b_i}\mathbf{M}_b\|. \tag{7.21}$$

STEP (4)

The fourth step is to compute the direction vector $\mathbf{C}_b\mathbf{M}_b$ also called $\mathbf{u}$, see Fig. 7.14. This vector defines subsequently the movement of all torus centers.
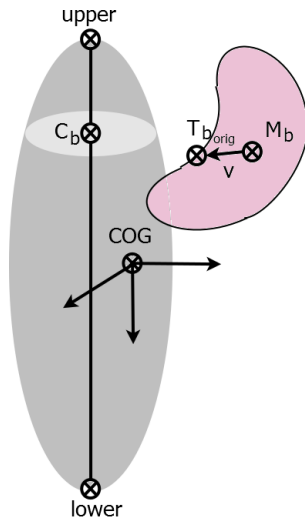
FIGURE 7.12: The bone cross section area situated in the plane of torus centers.
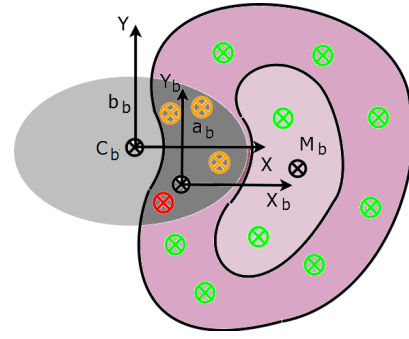
FIGURE 7.13: The muscle bulging up. The green points represents torus centers outside the ellipse and the orange points are founded centers inside the ellipse, aixs X_b, Y_b represents the local coordinate system of given bone, a_b is the major axis of bone ellipse and b_b is its minor axis. This ellipse replace the bone cross section area.

STEP (5)

The fifth step is to find the straight line, p, parallel to the vector $\mathbf{u}$ and going through the point $\mathbf{T}_{bF}$, see Fig. 7.14. The next step is to calculate the intersection, $\mathbf{I} = [I_x; I_y]$, of the bone ellipse and the straight line p given by following equations

$$I_x = T_{bF_x} + u_x t, \tag{7.22}$$

$$I_y = T_{bF_y} + u_y t, \tag{7.23}$$

$$\frac{\left(I_x - C_{b_x}\right)^2}{a_b^2} + \frac{\left(I_y - C_{b_y}\right)^2}{b_b^2} = 1. \tag{7.24}$$

This system of equations has two different solutions, $\mathbf{I}_1$ *and* $\mathbf{I}_2$, as shown in Fig. 7.14. The solution closer to the point $\mathbf{M}_b$ is considered to be the final solution, $\mathbf{I}_T$, the new position of torus center $\mathbf{T}_{bF}$.

STEP (6)

The sixth step is to find the direction vector $\mathbf{m} = \mathbf{T}_{bF}\mathbf{I}_T = \mathbf{I}_T - \mathbf{T}_{bF}$. This vector defines the final displacement of whole group of torus centers, see Fig. 7.15.

STEP (7)

The final step is to check, is there is no point left inside the bone ellipse. If so, the correct position of torus centers were found. Otherwise, the process of torus positions correction has to be repeated.
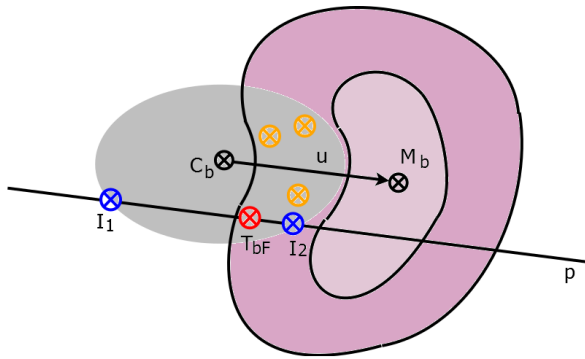
FIGURE 7.14: The muscle bulging up. The vector **u** represents the direction of torus centers movement, the straight line p is parallel to the vector **u**, points I_1 and I_2 show the intersection of the bone ellipse and the straight line, T_{bF} is the torus center lying inside the ellipse and the farthest from the reference point $\mathbf{M}_b$.
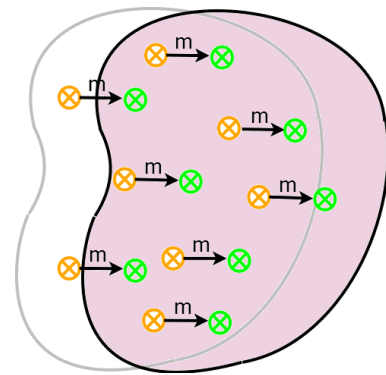
FIGURE 7.15: The final movement of original torus centers in **m** direction. The process ensures no intersection of tissues during the muscle bulging up.

CASE (B)

The second case is that these are some other underlying or neighboring muscles. The bulging of the internal muscles influences the position of covered muscles, as seen in Fig 7.16. The resulting displacement vector of the covered muscle is then given by the sum of the own vector of translation and the vector of the underlying muscle. However, this problem is not considered in this study and thus, it is not explained in more details.
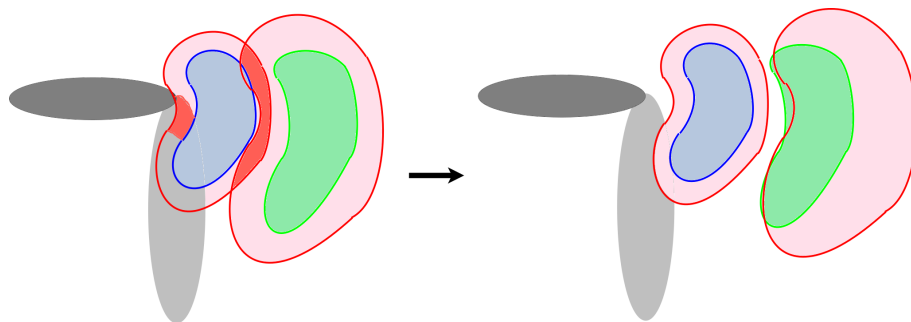
FIGURE 7.16: The dependence of the displacement vector of the cover muscle by the vector of underlying muscle. The blue plane represents the original position of PCSA of the inner muscle while the green one is the cover muscle. The pink area shows the muscle bulging up and the red one is the intersection of the muscle caused by the bulging. The left picture represents the situation before the position correction while the right picture is the situation after the process.

Part IV

RESULTS

Chapter 8

A Case Study: Model of Human Deltoid Muscle

The main aim of this study was to develop the new method for muscle wrapping process to find the real muscle trajectories for all arbitrary movements of musculoskeletal models. Presented method called *torus-obstacle method* consists of three main parts - the new process of (1) muscle trajectory computation, (2) automatic calculation of 3D position of muscle attachments and the obstacles, (3) muscle bulging up. A case of study was to use this method to model the simple musculoskeletal model of the shoulder complex.

The model involves three bones - the clavicle, the scapula and the humerus, one shoulder joint - glenohumeral (GH) and one muscle - the deltoid muscle. The bones were modeled by rigid bodies with the real shapes obtained from MRI. The GH joint was modeled by spherical joint with three degrees of freedom. The other joints such as sternoclavicular, acromioclavicular as well as the connection between the scapula and the thoracic cage are neglected. Therefore, the model is limited to move only to the level of the elevation plane (90° of abduction or flexion). In reality, the next range of motion is ensured by motion of scapula and clavicle - so called shoulder rhythm. Fibers of three heads of deltoid (acromial, scapular and clavicular part) were represented in the 3D model. The muscle was split in few muscle lines-of-action modeled by frictionless elastic bands without any mass or density and wrapping around the neighboring structures. The muscle behavior is simulated by three elemental Hill-type model, see Chapter 6.2. The muscle volume changes caused by its contraction is also considered.

The model performed the simple anatomical movements - humeral abduction and forward flexion. The inverse dynamics was used to calculate the muscle forces and muscle moment arms necessary for the given movement. At the end of work, the model was validated using the data from literature, the measured EMG signal or the results obtained from shoulder models developed in AnyBody Modeling System. The muscle shapes in different joint positions were checked using the MRI. The dynamic equations of motion were estimated as described in Chapter 5.

8.1 Coordinate Systems

The rigid frame is represented by the scapula and the clavicle. It forms the global coordinate system. Its origin is located in the middle of humeral head. The X-axis is oriented in the medio-lateral direction of human body, the Y-axis is in the caudo-cranial and the Z-axis in anterio-posterior (ventral-dorsal) direction, see Fig. 8.1. The upper arm is connected by the humeral head to the fixed reference frame. The connection is represented by spherical GH joint. The origins of deltoideus muscle fixed to the scapula and clavicle are located in the global coordinate system. Their position is not changed during the joint movement.

The local coordinate system is fixed to the upper arm. Its origin is situated in the center of gravity (COG) of this body part. The axes orientation is depicted in Fig. 8.2. The X-axis is in medio-lateral, the Y-axis in anterio-posterior and the Z-axis is in proximo-distal direction of the humerus. The insertions of deltoid attached to the humerus and also the position of torus obstacles are located in the local coordinate system. Their position is changed depending on humeral movement.
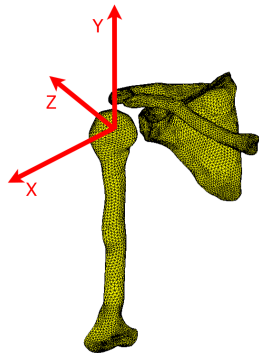
FIGURE 8.1: The global coordinate system fixed to the reference frame.
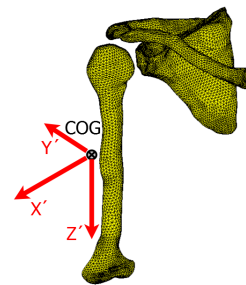
FIGURE 8.2: The local coordinate system fixed to the upper arm.

8.2 Model Geometry

The model geometry is based on one subject specific dataset. For now, the model is not scalable. Nevertheless, it is already prepared to be improved in near future. The asked volunteer was 57 years old man, healthy without any pathological changes, the weight about 95 kg. The anthropometry measurements as well as MRI scanning used for model geometry reconstruction were performed at the City Hospital Pilsen, PRIVAMED Inc.

8.2.1 Magnetic resonance imaging - MRI processing

The MR images of the right shoulder complex were in vivo recorded to get the real model geometry, see Fig. 8.3. The subject was lying in the anatomical rest position - on his back, the upper arm freely

lying along the body, the elbow fully extended, the palm turn up. The MRI *GE Medical Systems - GE Signa Excite* 1.5T and the circle electromagnetic coil originally designed for shoulder joint was used. Obtained slices were 2 *mm* thick and scanned in sagittal, coronal and transversal direction. The surface mesh consisting of triangles was automatically created in free software 3D Slicer (BWH, 3.0, Boston, United States), see the example of deltoid muscle - acromial part in Fig. 8.4a. However, this mesh is not smooth enough. It is full of protuberances, depressions, protrusions and holes. In addition, it involves very small elements (c. hundredths of millimeters). Such a small elements usually cause huge computation time without any big improvement of results quality, especially in the musculoskeletal modeling. Thus, obtained mesh was modified using HyperMesh software (Altair, 11.0, Michigan, United States), see Fig 8.4b. At this point, the mesh of bone and muscle envelopes were considered to be finished.

FIGURE 8.3: MR slices of deltoid muscle (acromial part) in coronal plane.
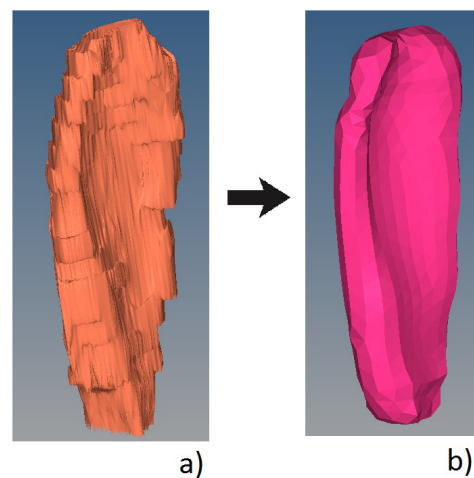
FIGURE 8.4: 2D mesh of deltoid muscle (acromial part) - a) original mesh obtained from MRI automatically generated by 3D Slicer, b) modified mesh built in HyperMesh software.

8.2.2 The position of muscle attachments

The 2D mesh of muscle and the k-means method already introduced in section 6.3 were used to compute the 3D position of muscle origins and insertions. The high quality regular mesh was constructed to define the areas of muscle attachments. The mesh consists of triangular 2D elements of the edge length 1 *mm*. The process is divided in two following steps.

1. *To find the number of muscle lines-of-action.*

   The number of muscle lines-of-action corresponds to the size of muscle physiological cross section area (PCSA). In this work, the PCSA of deltoid muscle was calculated based on subjects MRI, see Tab. 8.1. Unfortunately, it was not find any published source describing the relation

between the muscle PCSA and its number of lines-of-action. For purpose of this study, the very simple form was used - one line replaces just $1cm^2$ of muscle PCSA. The number of lines is also shown in Tab. 8.1.

TABLE 8.1: The computed size of PCSA of individual parts of deltoid muscle replaced by corresponding number of lines-of-action.

muscle part	PCSA $[cm^2]$	number of lines-of-action
acromial	6.78	7
scapular	1.85	2
clavicular	2.72	3

2. *To find the attachments of obtained muscle lines-of-action.*

The nodes of regular 2D mesh represents the input parameters used for k-means method, see Fig. 8.5. The list of attachment positions are summarize in Tab. 8.2 and 8.3.

TABLE 8.2: The positions of deltoideus origins defined in global coordinate system of the scapula and the clavicle.

muscle part	ID	position [mm]		
		x	y	z
acromial	ACO1	5.569	-5.956	33.613
	ACO2	10.863	1.013	18.618
	ACO3	10.111	-2.746	26.202
	ACO4	8.575	4.672	-1.566
	ACO5	-2.030	-9.345	39.676
	ACO6	11.856	0.270	8.496
	ACO7	8.237	7.083	10.346
scapular	SCO1	-59.314	-5.450	58.383
	SCO2	-21.032	-7.840	46.831
clavicular	CLO1	-51.269	15.472	-37.921
	CLO2	-11.997	9.960	-26.683
	CLO3	-32.446	14.519	-30.401

TABLE 8.3: The positions of deltoideus insertions defined in local coordinate system of the humerus.

muscle part	ID	position [mm]		
		x	y	z
acromial	ACO1	10.475	-8.293	-0.8315
	ACO2	14.998	0.219	-23.780
	ACO3	14.211	-1.416	-12.095
	ACO4	5.846	-11.412	23.824
	ACO5	10.234	-9.452	-13.571
	ACO6	11.388	-8.566	-27.269
	ACO7	9.682	-9.911	11.184
scapular	SCO1	14.496	0.681	-0.313
	SCO2	12.875	-5.552	16.609
clavicular	CLO1	2.260	-13.318	15.205
	CLO2	2.415	-12.555	-3.128
	CLO3	4.124	-12.706	-19.921
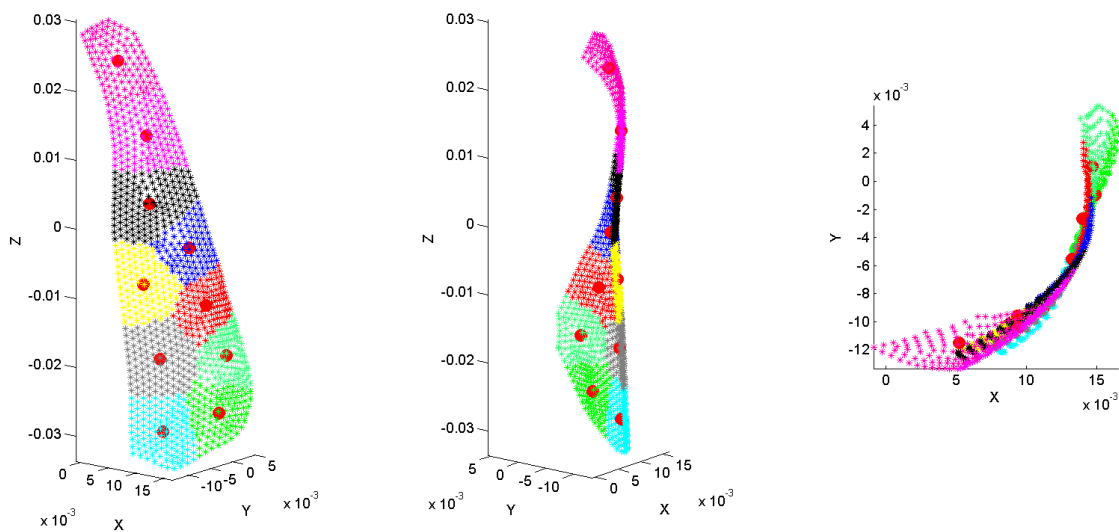
FIGURE 8.5: The positions of muscle lines-of-action represented by red points. The stars are the nodes of regular mesh defining the area of muscle attachments, the colors depict the groups of nodes determining the given attachments. This example demonstrates the case of insertion of acromial part of deltoid muscle situated in the local coordinate system of humerus, the number of lines is $N = 10$ used just for this instance.

8.2.3 The position of torus obstacle

The k-means method introduced in section 6.3 was also used to compute the original position of torus obstacle centers. The centers lye in the area defined by muscle cross section in the horizontal plane going through the center of joint rotation (the center of humeral head). The middle circle of its tube is also positioned in this plane. The toruses are situated in the local coordinate system of the humerus. And thus, their positions respect the actual joint configuration. More over, the actual position is changed as a results of the muscle bulging up as explained in Section 7.2. This continuous control and correction of the torus position ensure that the obstacles avoid the surrounding structure such as muscles and bones. The next task is to calculate the radius of torus, R, as also mentioned in Section 7.2. The list of position and radius of individual torus obstacles is presented in Tab, 8.4.

TABLE 8.4: The original positions of torus centers located in the local coordinate system of humerus.

torus part	ID	position [mm]		
		x	y	z
acromial	T_ACO1	40.141	43.878	-135.510
	T_ACO2	35.164	29.362	-135.510
	T_ACO3	47.603	27.116	-135.510
	T_ACO4	40.065	-17.237	-135.510
	T_ACO5	24.830	45.686	-135.510
	T_ACO6	45.008	-3.708	-135.510
	T_ACO7	44.679	11.450	-135.510
scapular	T_SCO1	-37.437	84.243	-135.510
	T_SCO2	10.480	65.213	-135.510
clavicular	T_CLO1	-18.956	-34.398	-135.510
	T_CLO2	27.848	-32.269	-135.510
	T_CLO3	1.099	-40.702	-135.510

8.2.4 Mass Moment of Inertia

To calculate the mass moment of inertia, the upper arm segment was divided into several parts - the skin, the soft tissue, the bone and the canal in the bony center. Each part was approximated by cylinder with the ellipsoidal cross section area. The process of mass moment of inertia calculation is described in Section 5.1.4 in more details.

Representative external dimensions of male upper arm were measured using the MRI data. The process of measuring is described in Fig 8.6 and obtained values are listened in Table 8.5.
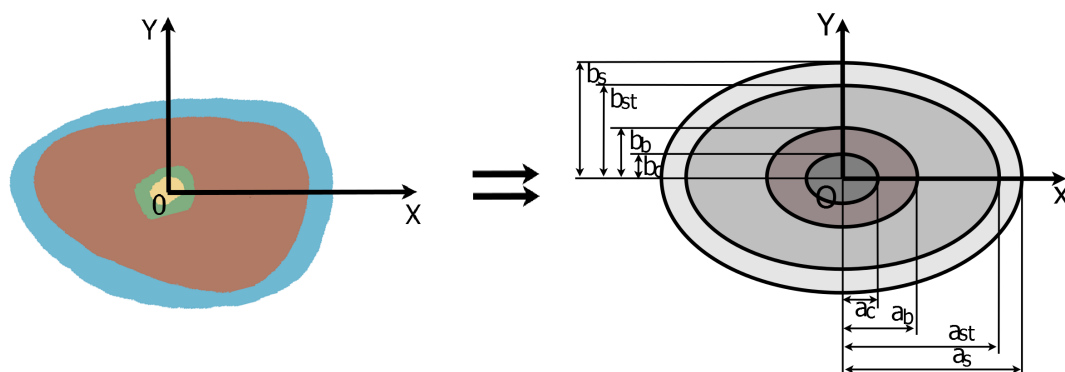
FIGURE 8.6: The upper arm segment is approximated by cylinders. The dimentions are estimated using the male MRI data, as the mean values.

The mass of the upper arm was calculated as the sum of masses of individual cylinders. The general formula was used - $M = \rho V = \rho \pi a b l$, where V is the volume of cylinder, ρ is the density of tissue, a is the semi-major axis, b is the semi-minor axis of the elliptical base and l is its height. The mass, density and the principal mass moment of inertia are listened in Tab 8.5.

TABLE 8.5: Dimensions of upper arm segment used in the current study. The segment consists of the skin, the soft tissue, the bone and the canal, as shown in Fig 8.6. The parameters a, b and l are the half width, the half depth and the lenght of individual cylinder, respectively.

	a[m]	b[m]	l[m]	$\rho[kg/m^3]$ [78]	$I_{xx}[kg/m^2]$	$I_{yy}[kg/m^2]$	$I_{zz}[kg/m^2]$
Skin	0.0717	0.0446	0.3060	940	0.0084	0.0094	0.0028
Soft tissue	0.0611	0.0349	0.3060	1000	0.0156	0.0169	0.0025
Bone	0.0136	0.0098	0.3060	1900	0.0014	0.0014	$1.6 \cdot 10^{-5}$
Canal	0.0075	0.0059	0.2909	-	-	-	-

8.3 Optimization Process

As already described in Section 6.1.1, the inverse dynamics problem with the muscle actuators represents the underdetermined system of equations. This is cased by the fact, that there is more muscle forces than the degrees of freedom in the model. From mathematical point of view, there is more unknowns then the equations. This problem is solved by some optimization method as mentioned in Section 6.1.2. The optimization process used for this study can be expressed by

following formula

$$Control\ variables: \quad \mathbf{F}\left(F_i\right) \qquad\qquad\qquad i = 1, 2, \ldots, 12$$

$$Minimize: \qquad \mathcal{F} = \sum_i \left(\sigma_{CE}^i\right)^3 = \sum_i \left(\frac{F_{CE}^i}{PCSA^i}\right)^3$$

$$(8.1)$$

$$Subject\ to: \qquad \sum_{r=1}^{nF} \left(\mathbf{u}_r \times \mathbf{F}_r\right) = \left(\mathbf{G}^T\right)^{-1} \left(\mathbf{Q}_e\right)_\theta - \mathbf{u}_g \times \mathbf{F}_g$$

$$0 \le F_i \le F_{i_{max}}$$

Exactly this cost function was selected based on the analysis published in [93]. In that work, three cost functions also considered in Section 6.1.2 were used to find the forces generated in the main muscles of the upper extremity. During that simulation, the upper extremity was held in the static position and the palm was loaded by constant external force. The results show, that the muscle forces are the same for all cost functions. Moreover, the cost function used in formula 8.1 has significantly lowest number of iterations and also the smallest computational time. The maximal muscle forces, $F_{i_{max}}$, representing the upper limits are shown in Teb. 8.6.

TABLE 8.6: The maximal muscle forces [47].

muscle part	F_{max} [N]
acromial	1142.6
scapular	259.9
clavicular	1142.6

8.4 Muscle Model

The behavior of deltoid muscle is simulated by Hill-type model explained in Section 6.2. The total muscle force is given by the following form:

$$F_{Mus} = F_{CE} + F_{PE} + F_{DE}. \qquad (8.2)$$

The contractive muscle element, F_{CE}, is the function of many elementary parameters:

$$F_{CE} = f\left(Na, F_{max}, L, L_{opt}, C_{sh}, C_{short}, C_{mvl}, v, l_{fib}, C_{fast}\right) \qquad (8.3)$$

as given by the equation 6.7. Na is the active muscle state, F_{max} is the maximal muscle force, L is the actual muscle length obtained from simulation, L_{opt} is the optimal muscle length (when the muscle generate the maximal force), C_{sh} represents the shape parameters determining the concavity of muscle force-length characteristic (see Fig. 6.2), C_{short} is the Hill-type shape parameter for shortening obtained from the equation [106]

$$C_{short} = 0.1 + 0.4C_{fast}, \tag{8.4}$$

the constant C_{mvl} determines the ration of ultimate force at full activation, v is the actual velocity of muscle shortening/elongation, l_{fib} is the length of muscle fibers in the muscle rest position and C_{fast} is the fraction of fast muscle fibers in given muscle.

The passive muscle force, F_{PE}, is the function of following parameters

$$F_{PE} = f\left(F_{max}, C_{PE}, L, L_{ofib}, PE_{max}\right), \tag{8.5}$$

where C_{PE} is the shape parameter that determines the concavity of the muscle force-length characteristic (see Fig. 6.4), L_{ofib} is the rest muscle length and PE_{max} is the elongation of the parallel component at F_{max}. With respect to the literature [105], the passive force, F_{PE}, is zero when $L \leq L_{ofib}$. Finally, the dumping element F_{DE}, given by the equation 6.13 is the function of followings

$$F_{DE} = f\left(k_{DE}, v\right), \tag{8.6}$$

where k_{DE} is the parameter of dashpot usually computed by following equation [68]

$$k_{DE} = 0.3\frac{F_{max}0.25}{l_{opt}2.25}. \tag{8.7}$$

The values of muscle active state, Na, is obtained from equation 6.7. The actual velocity of muscle shortening/elongation, v, is based on the muscle force. The force-velocity characteristic defines this dependence is shown in Fig. 6.3. The all needed input parameters are summarized in Tab. 8.7.

8.5 Muscle Moment Arm

The clinically used definition of muscle moment arm explained in Section 6.4 was used instead of the general mechanical expression. Polynomial regression was used to find the relationship between muscle shortening/lengthening and the angle of each step of humeral movement (abduction, flexion). A limit of the polynomial order was considered (fourth order) to avoid the data overfitting. Obtained regression was differentiated to give the actual muscle moment arm. The moment arm is given by the simple fraction - the small change of the muscle shortening/lengthening versus small change of actual joint angle given in radius. Moment arms were calculated at one-degree intervals.

TABLE 8.7: The essential input parameters.

parameter	units	acromial part	clavicular part	scapular part	source
C_{fats}	-	0.467	0.390	0.390	[52]
l_{fib}	m	0.108	0.098	0.137	[47]
C_{length}	-	0.089	0.082	0.082	Eq. 6.10
C_{mvl}	-	1.400	1.400	1.400	[106]
C_{PE}	-	5.000	5.000	5.000	[106]
C_{sh}	-	0.400	0.400	0.400	[106]
C_{short}	-	0.287	0.256	0.256	Eq. 8.4
F_{max}	N	1142.600	1142.600	259.900	[47]
k_{DE}	Ns/m	230.980	196.860	44.780	Eq. 8.7
L_{ofib}	m	0.151	0.176	0.173	[111]
L_{opt}	m	0.165	0.194	0.191	[107]
PE_{max}	-	0.600	0.600	0.600	[106]
v_{max}	m/s	0.619	0.504	0.704	Eq. 6.11

8.6   Simulations

Presented simulations were computed on a standard desktop PC (Intel(R) Core(TM) i7 CPU, 2.80 GHz, 8.00 GB RAM). The MATLAB (MATLAB R2013a(32-bit).Inc, MathWorks, Inc.) software was used. The computation time was $9.97s$ for abduction and $9.78s$ for forward flexion. When considering the results plotting, the final computation time was significantly increased - $65.62s$ for abduction and $65.56s$ for flexion.

Presented shoulder model involving the new torus-obstacle method was used to simulate two anatomical movements of the right upper extremity - the abduction (elevation in the coronal plane) and forward flexion (elevation in the sagittal plane), always from 0° to 90°. For both movements, the initial position of the upper arm is the rest position - the upper extremity hanging freely along the human body, the elbow joint fully extended, the palm turn forward (the thumb oriented to the right). For both cases, the following outputs are calculated - muscle forces, muscle moment arm and actual muscle length.

The model situated in the initial rest position is depicted in Fig. 8.7 and Fig. 8.8. The bones are represented by yellow 2D triangular elements. The length of edge is about 2mm. The center of

rotation is located in the center of humeral head. The muscle lines-of-action are shown by red lines.

For better orientation in the results, each muscle line-of-action was marked using unique identification. The code corresponds with the markers used for muscle attachments established in Tab. 8.2 and Tab. 8.3. Thus, the markers used for muscles of acromial, clavicular and scapular part are called $AC1$, $AC2$, ..., $AC7$; $CL1$, $CL2$, $CL3$ and $SC1$, $SC2$, respectively, see Fig. 8.9.
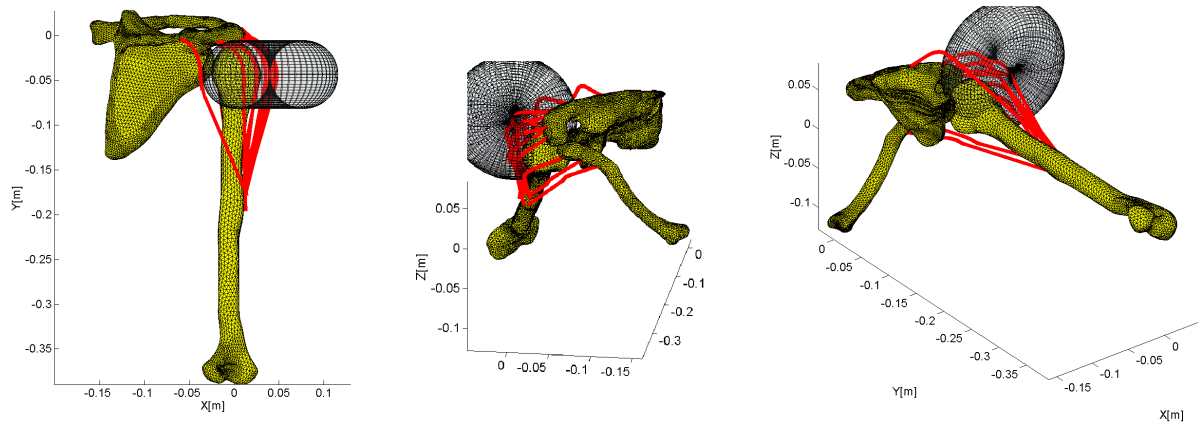
FIGURE 8.7: The final representation of the shoulder model including the new torus-obstacle method. One obstacle belonging to the muscle line $AC1$ depicted.
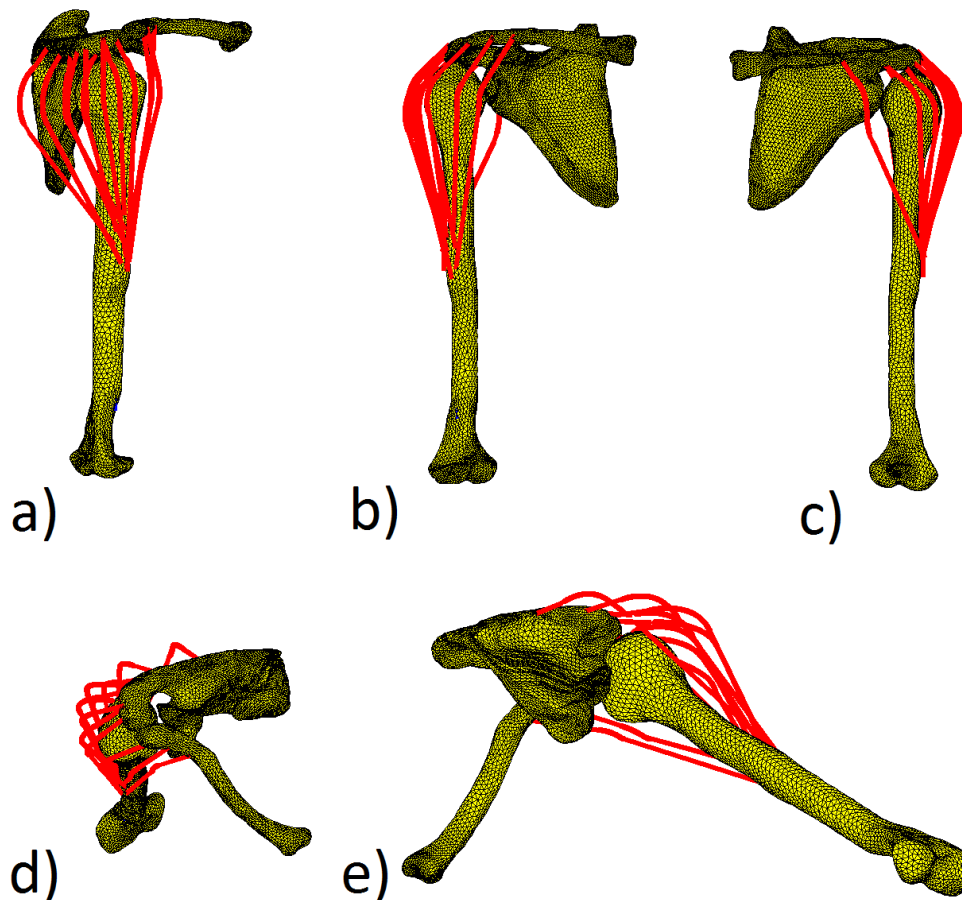
FIGURE 8.8: The final representation of the shoulder model including the new torus-obstacle method. The model shown from five different views - a) right side, b) front, c) back, d) top, and e) general.
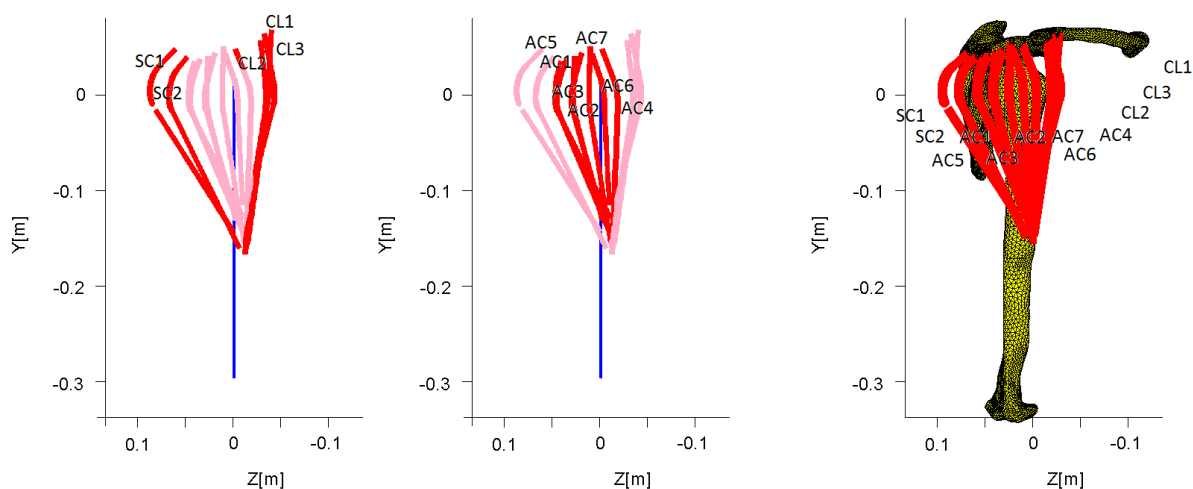
FIGURE 8.9: The identification of muscle lines-of-action for better orientation in results.

8.6.1 Abduction

The abduction of the shoulder joint (elevation in coronal plane) was simulated using the new torus-obstacle method. The shoulder complex is depicted in Fig. 8.10 in three joint positions - 0°, 45° and 90°. During whole movement, the scapula is fixed in the original position. The internal rotation of humerus is also neglected. Fig. 8.10 also shows that the predicted muscle path generate anatomically reasonable results without any muscle penetration of surrounding structures such as bones, joints and other muscles.
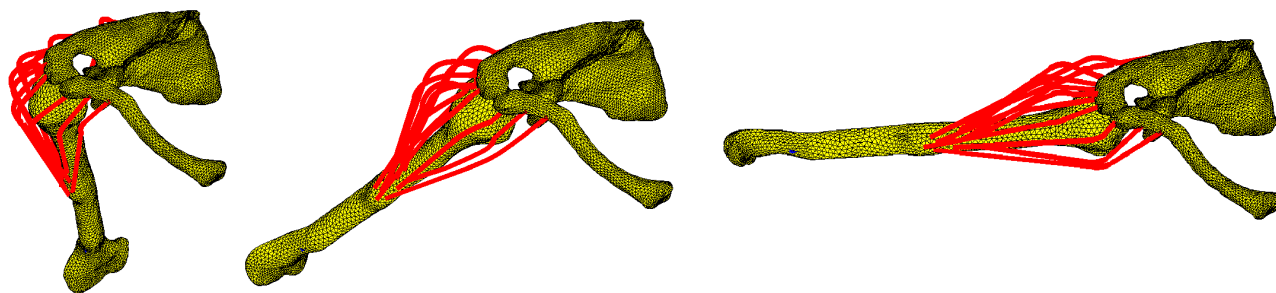
FIGURE 8.10: The process of abduction; from left: 0°, 45° and 90°.

Muscle Forces

The Fig. 8.11 presents the final distribution of the muscle forces between 12 muscle lines of action (the acromial, clavicular and scapular part represented by 7, 3 and 2 lines of action, respectively). In general, the deltoid muscle is the main agonist of abduction. Therefore, almost all muscle lines generate significant force. The results highlight the acromial part (except the line $AC5$) as the most active - the maximal force is almost $50N$. It can be concluded that exactly this muscle part is mainly responsible for abduction motion and its activity is the most important for abduction till 90°. The line $AC5$ generates the lower force in comparison with the others from acromial part, around $5N$ in maximal. This is caused by the position of its attachments that are closer to the scapular part.

The scapular part of the deltoid muscle does not contribute to the shoulder abduction too much. Its maximal activity is about $0.23N$ and appears only at the beginning of the movement. The clavicular part of the muscle also shows quite low activity - about $8N$ in maximal. Moreover, the muscle lines $CL1$ and $CL3$ are not even active at all. The acromial muscle part (except the line $AC5$ again) reaches the maximal force values at the end of abduction, i.e. at $90°$. However, the clavicular part shows the maximals at about $60°$, the scapular at about $20°$ and finally the muscle line $AC5$ at about $60°$.

FIGURE 8.11: Resulting muscle forces generated in acromial, clavicular and scapular part of the deltoid muscle during humeral abduction till $90°$.

Actual Muscle Length

The process of muscle path shortening/elongation corresponds well with the muscle forces. Almost all muscle lines are shortened respecting the growth of the joint rotation angle, see Fig. 8.12. Nevertheless, the results show that the lines $CL1$, $CL3$ and also $SC1$ are elongated again caused by the position of lines attachments and toruses prescribing the actual muscle path. And thus, these muscles represent the insignificant antagonists of the abduction. The mean original muscle lengths calculated in the starting rest position of the shoulder are $197.6 \pm 26.9mm$, $211.15 \pm 18.55mm$ and $221.2 \pm 0.1mm$ for acromial, clavicular and scapular part, respectively.

FIGURE 8.12: Resulting muscle length of acromial, clavicular and scapular part of the deltoid muscle during humeral abduction till $90°$.

Muscle Moment Arms

The abduction moment arms in coronal plane are shown in Fig. 8.13. Overall, the muscle lines of acromial part, the lines $CL2$ and also $SC2$ have the largest agonist (elevator) moment arm. Conversely, the lines $CL1$, $CL3$ and $SC1$ are found to have antagonist (depressor) moment arms. The muscle moment arms of all agonists in each muscle part are comparable.

FIGURE 8.13: Resulting muscle moment arms for acromial, clavicular and scapular part of the deltoid muscle during humeral abduction till 90°.

8.6.2   Flexion

The forward flexion of the shoulder joint (elevation in sagittal plane) was modeled using developed torus-obstacle method. The shoulder model is shown in Fig. 8.14 in three different joint positions - 0°, 45° and 90° of flexion. During whole motion, the scapular movements as well as the internal rotation of the humerus were again neglected. The Fig. 8.14 also confirms that the muscle lines of action do not penetrate any surrounding structures.
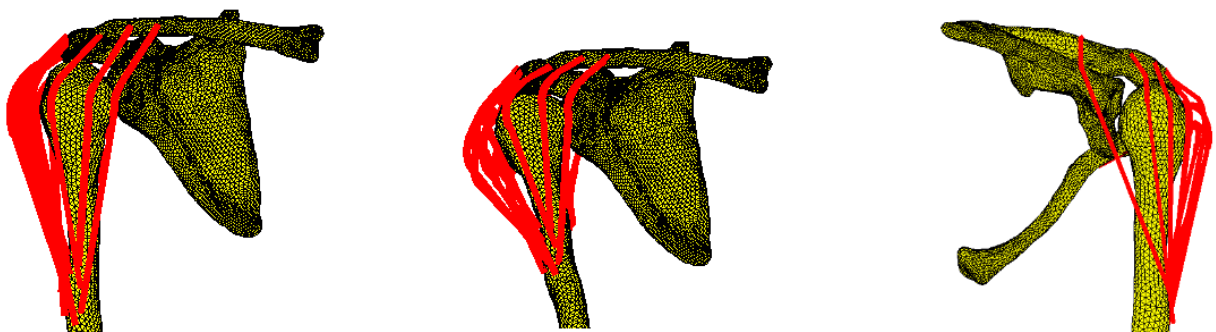
FIGURE 8.14: The process of flexion; from left: 0°, 45° and 90°.

Muscle Forces

The Fig. 8.15 shows the muscle forces generated in the all 12 muscle lines of action, see Tab. 8.1. As already mentioned, the deltoid muscle represents the main agonist of humeral abduction. And thus, only few muscle lines are active during this kind of motion. The results show that the clavicular muscle part is the most active. The maximal forces are reached at the end of flexion - almost $45N$

at 82°. The comparable forces are also found in the lines $AC4$ and $AC6$ that are in close proximity to the clavicular part. The other lines of acromial part and also the whole scapular part do not contribute to much. That is naturally given by the geometry of the deltoid muscle and the shoulder joint.
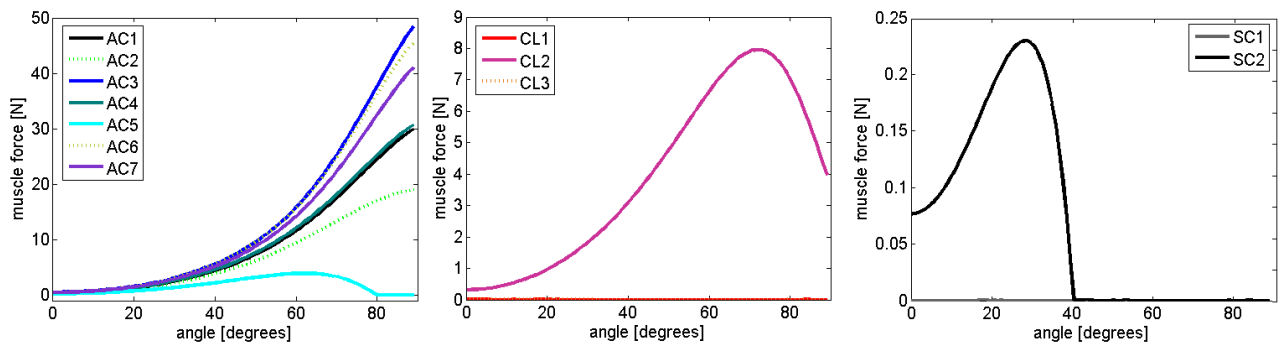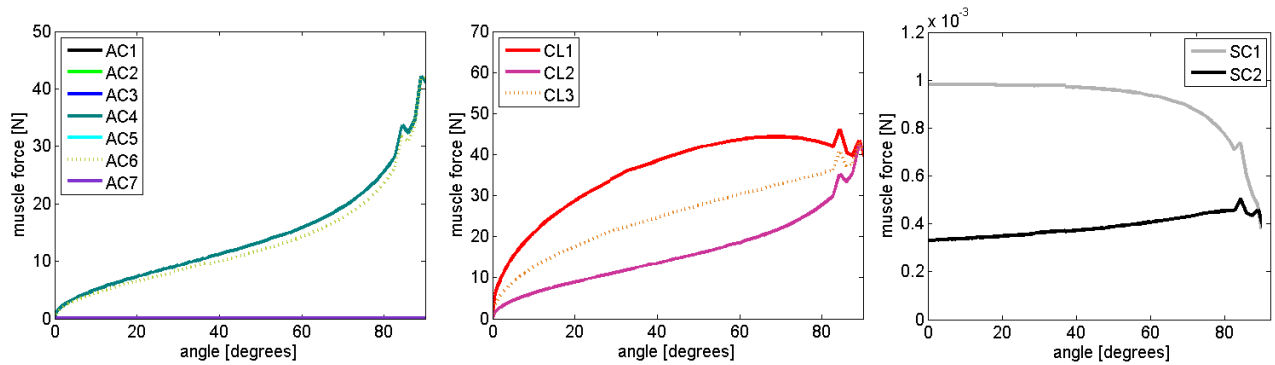

FIGURE 8.15: Resulting muscle forces generated in acromial, clavicular and scapular part of the deltoid muscle during humeral flexion till 90°.

Actual Muscle Length

The actual muscle lengths are shown in Fig. 8.16. The process of muscle shortening/elongation corresponds again well with the graphs of muscle forces - the assumption that the muscle can only pull, i.e. the muscles produce the active force while they are shortened, is fulfill. The muscle lines $AC4$, $AC6$ and the whole clavicular part are shortened during the flexion. Therefore, these muscle lines represents the main agonists. The other lines are elongated. The mean muscle lengths in original rest position are the same as written in abduction section.
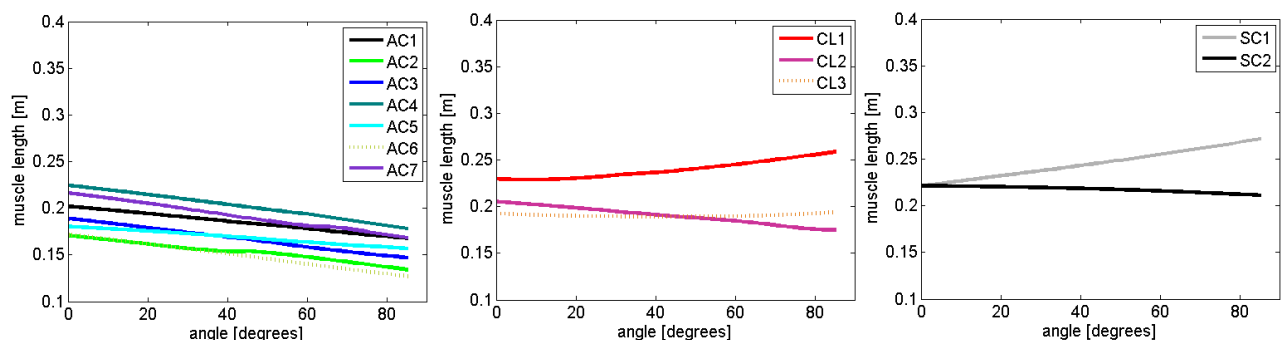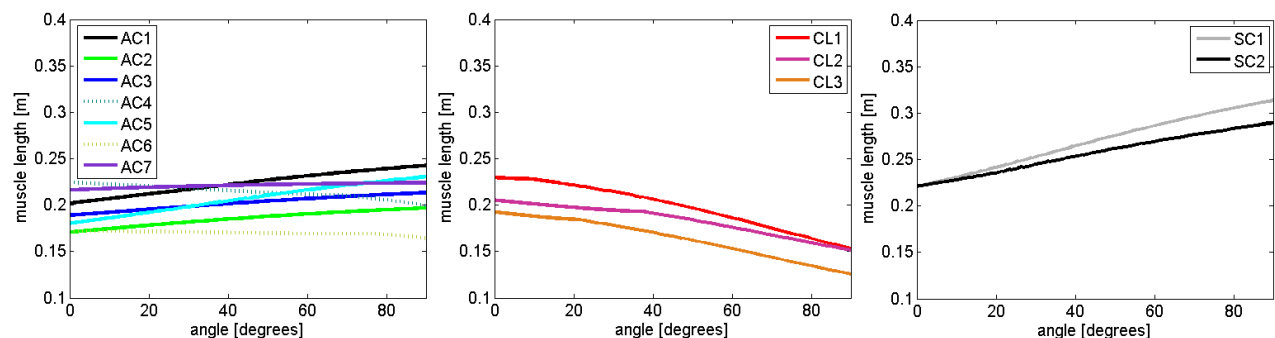

FIGURE 8.16: Resulting muscle length of acromial, clavicular and scapular part of the deltoid muscle during humeral flexion till 90°.

Muscle Moment Arm

The muscle moment arm for the forward flexion are shown in Fig. 8.17. The muscle lines of clavicular part and the lines $AC4$ and $AC6$ have the agonist moment arms, while the other lines have the antagonist moments arm.
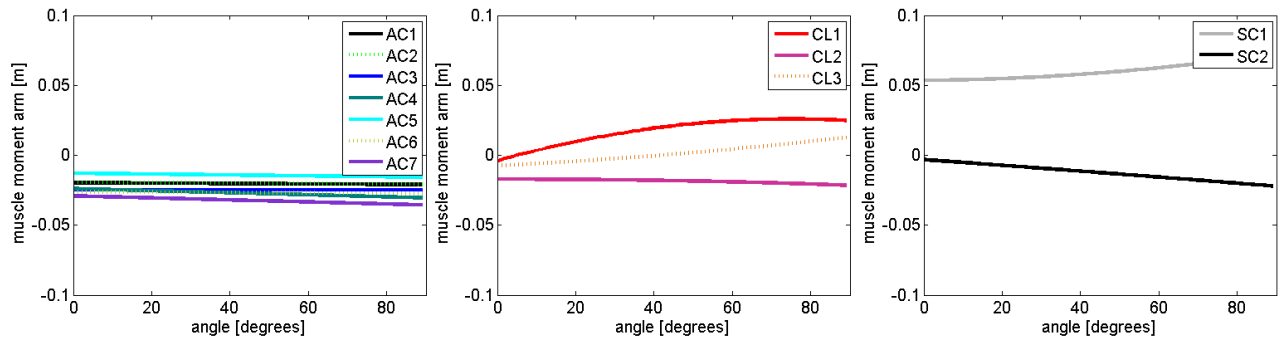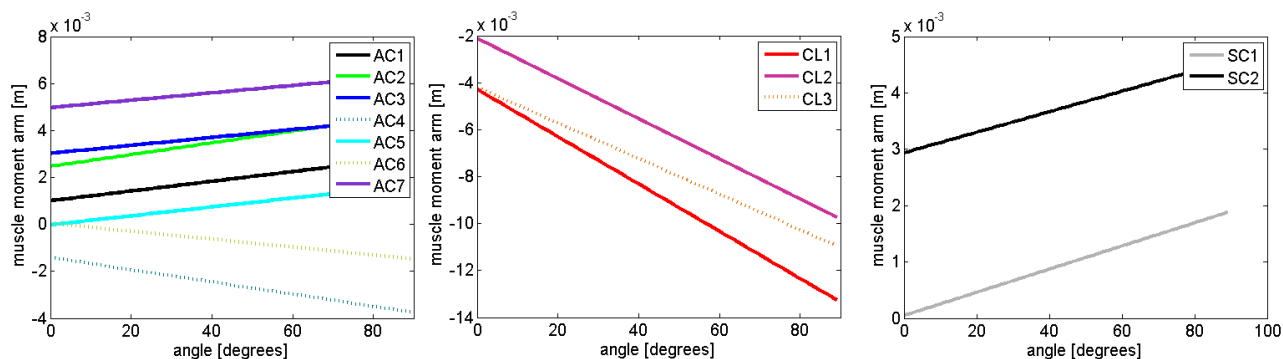
FIGURE 8.17: Resulting muscle moment arm for acromial, clavicular and scapular part of the deltoid muscle during humeral flexion till 90°.

8.7 Motion Capture Data and EMG Processing

Two laboratory measurements were performed to validate developed shoulder model - motion capture data measurement and elecromyography (EMG). Three right-hand-dominant male subjects (mean age 38 years, mean weight 82 kg, mean height 175 cm) without any pathological changes volunteered to participate in this work. For all cases, the initial rest position of each subject was following - the arms hanging vertically by the sides, the elbow fully extended and the hand in neutral position, palm turned to the body. The subjects were always asked to performed the abduction till 90°. The kinematic data as well as the EMG were measured in the Motion Capture Laboratory at the Faculty of Physical Education and Sport, Charles University, Prague.

The opto-electric motion capture system called Qualisys (Qualisys AS, Göteborg, Sweden) was used to record the 3D movements of the right upper arm. 15 high-visible skin markers (balls, diameter 2 cm) were used to monitor the motion. The location of markers respect the standards of International Society of Biomechanics [108], see Fig. 8.18. The coordinate system was always situated on the right side in front of subjects body. The orientation of the axis X, Y and Z were in the posterior, lateral to the right and in the superior direction, respectively. Mentioned motion capture data were already presented at the conference Computed Mechanics, 2013, Špičák, Czech Republic, [95] and accepted in journal Kinanthropologica [94].

The surface EMG technique was used to determine the function of the neuromuscular compartments within the deltoid muscle of three mentioned volunteers during the humeral abduction till 90°. Four pairs of bipolar surface electrodes were applied to each subject. The position of each electrode was estimated using the study [101], see Fig. 8.18. The electrodes were sticked to the subjects by double-sided tape. Before that, the skin has been shaved, abraded and washed with alcohol to minimize the skin resistance. The special electrode gel (called E.C.G. cream) was used to improve conductance. The reference surface electrode was situated on the chest on the right side, in the area of the muscle pectoralis major. The 4 bipolar surface electrodes and their reference electrodes were connected to the differential amplifiers - signal-to-noise ratio 1 : 3. The raw EMG signal was amplified and filtered - 10 Hz low-pass and 1 kHz high-pass filters, at a sample rate of 1000 Hz over a 1000 ms recording

period. The obtained EMG signal was rectified, averaged and normalized to the maximal recorded EMG value. The raw EMG signal is depicted in Fig. 8.19. For the model validation, the mean values of three measured datasets were used.
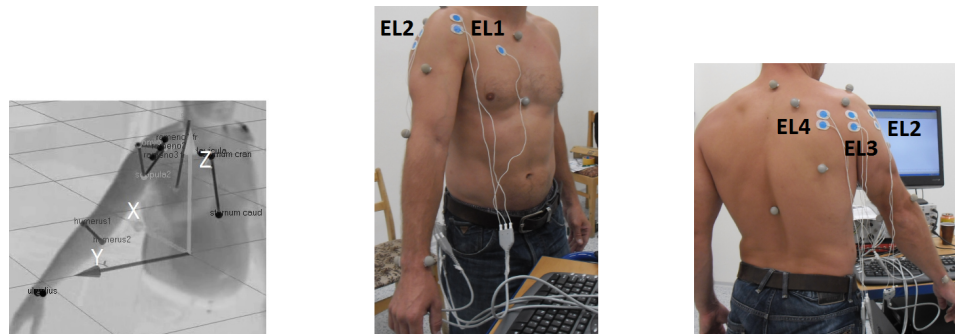
FIGURE 8.18: The motion capture data and EMG signal processing. On the left picture, the orientation of coordinate system depicted.
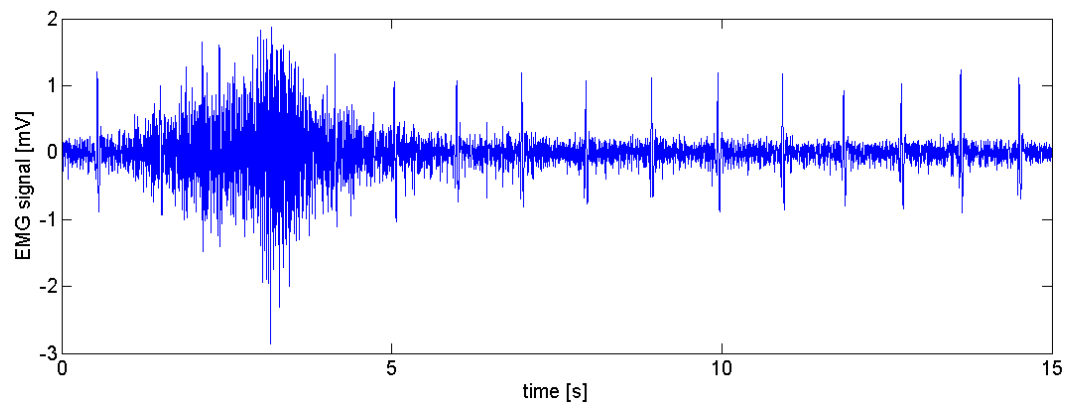
FIGURE 8.19: The example of raw EMG signal measured during humeral abduction till 90°.

8.8   AMS Shoulder Model

The new musculoskeletal shoulder model was built in AnyBody Modeling System (AMS; AnyBody 5.3, AnyBody Technology, Aalborg, Denmark). This model is originally available in the open free repository of AMS. It consists of 118 muscle fascicles; of three bones - the clavicle, the scapula and the humerus; of 5 joints - acromioscapular, glenohumeral, sternoclavicular and of two other joints so called scapulo-thoracic consisting of 2 points of scapula gliding over the thoracic cage represented by ellipsoid. The optimization technique and the inverse dynamics are used to calculate muscle forces, muscle activity, muscle moment arms, reaction forces, etc. generated during the given shoulder movements. Originally, the muscle path are computed by via-points method. The Hill-type muscle model is used to simulate the active muscles. All bones are modeled by rigid bodies with the real geometry based on MRI data.

For the purpose of this work, the AMS shoulder model was little bit adapted. (1) All muscle lines of action even the deltoid muscle were removed. To ensure the model stability, the all joints even the gleno-humeral were locked. (2) The real motion capture data of shoulder abduction till 90° were recorded and after that used to drive the AMS model. (3) The muscle paths were modeled using the obstacle-set method as presented in [37]. The neighboring anatomical structures were replaced by spheres, ellipsoids and cylinders. The muscle lines slide over these obstacles to avoid the intersection with other tissues and to fit the more anatomically correct shapes. The final modified AMS model is depicted in Fig. 8.20.
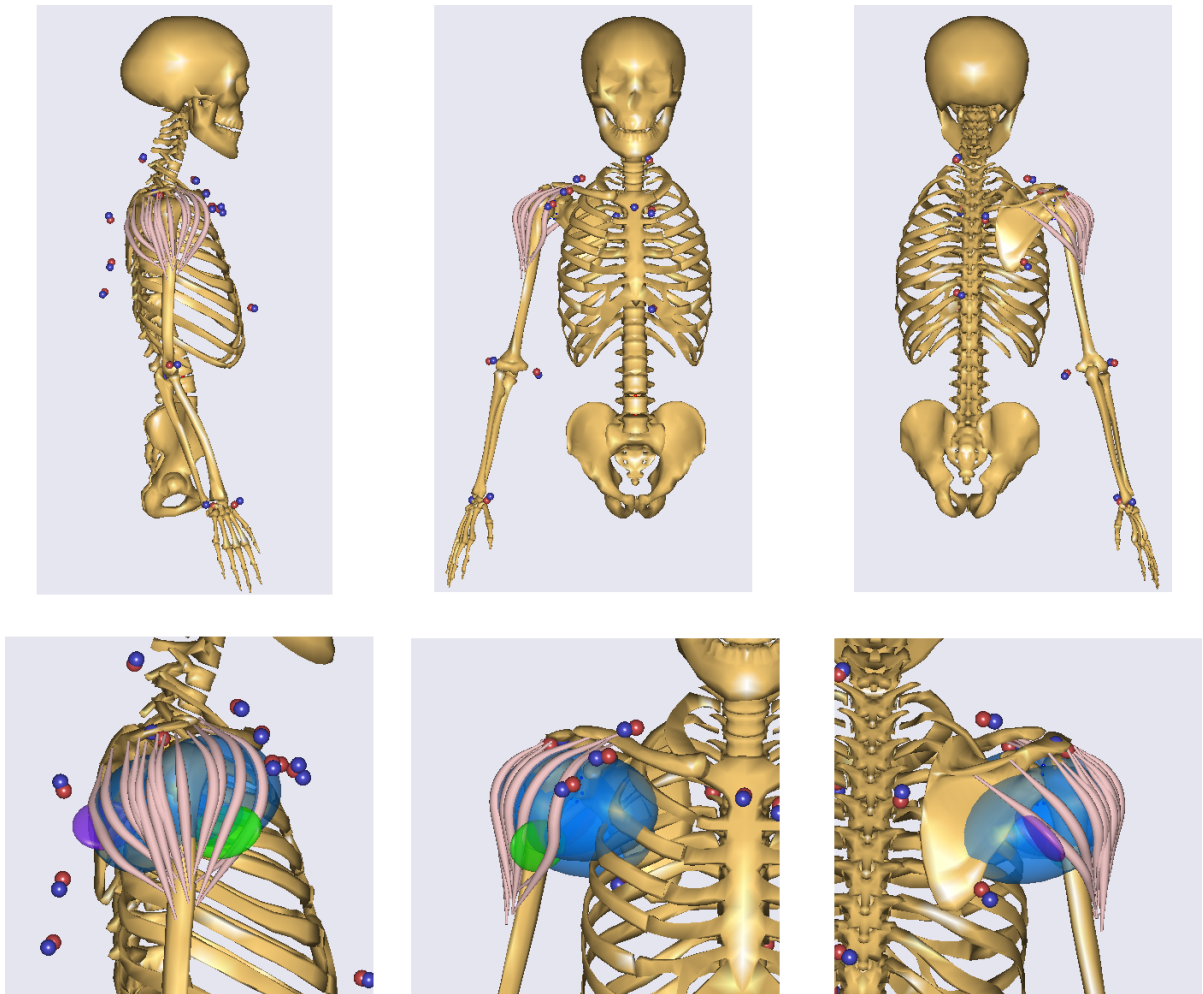
FIGURE 8.20: The shoulder model included the deltoid muscle modeled in AMS. The obstacle-set method used to find the more correct muscle trajectory.

Chapter 9

Validation

The computational models need the justified confidence that they are adequate representation of the real systems they simulate. Moreover, the next necessarity is to estimate how the model can by critically evaluated. The efforts, procedures, methodologies and process representing the model testing is formalized into the field of validation and verification [64]. The verification says how the model is implemented and describes the numerical accuracy of the obtained solution. While the model validation is how well the model represents the real system or how it fills experimental data. Validation process is open-ended. This is always linked with the evaluation of the given model and the algorithm. Each model is validated for specific use. In general, it is nor relevant to refer to a model as being validated for all arbitrary use [64].

In this study, the main aim was to developed the new torus-obstacle method for muscle path calculation. In addition, very simple 3D model of the shoulder complex (involving just the humerus, the scapula, the clavicle, the glenohumeral joint and the deltoid muscle) was built to demonstrate how the new torus-obstacle method is implemented, how it works, which are its advantages and disadvantages, etc. The model was also verified and validated to ensure that the new method of muscle wrapping works well and that the obtained results are correct. The computed values such as muscle forces, actual muscle lengths and muscle moment arms were compared with the existing literature. Moreover, the method was checked by the process of initial sensitivity analysis. Finally, the model was compared with the corresponding models built in AnyBody Modeling System and with in vivo measured EMG signals. The shoulder model was validated for humeral abduction and forward flexion both till 90°.

9.1   Muscle Path

The muscle path calculated by presented method were validated using the MR images. The reconstructed muscle shapes were scaled to fit the existing musculoskeletal model with respect to

the positions of muscle attachments and PCSA. For the original rest position of the upper arm, the MRI were scanned using *GE Medical System − GE Signa Excite*, $1.5T$. The comparison of the muscle lines trajectories and the simplified muscle mesh is shown in Fig. 9.1, on the left. Almost all muscle lines are situated in the area defined by the bone surfaces and the upper external cover of the deltoid. Only one single line $SC1$ get out little bit. Nevertheless, as shown further, this line is otherwise in correct position for the other movements and thus, this inaccuracy does not have any importance. The mentioned measuring system *GE Signa Excite* provides the images with the high definition. Moreover, it scans quite large region of shoulder joint. Nevertheless, the circle electromagnetic coil limits the joint position that are suitable to measure. And thus, the shoulder in forward flexion or abduction was absolutely impossible to scan.

Therefore, these two positions were recorded using another system *MAGNETOM C!*, $0.35T$. Unfortunately, this machine does not offer such a high definition and so, the images are hard to read. The validations of the muscle lines path in the abduction and forward flexion till 90° are depicted in Fig. 9.1 in the middle and on the right side, respectively. The comparison of computed muscle trajectories and the mesh representing the upper cover of the real deltoid muscle is satisfying. As obvious in the figure, the meshes of real muscles for abduction and flexion are not complete (muscle insertions on humerus not shown). This is cased by the limits of machine to scan the whole shoulder complex.
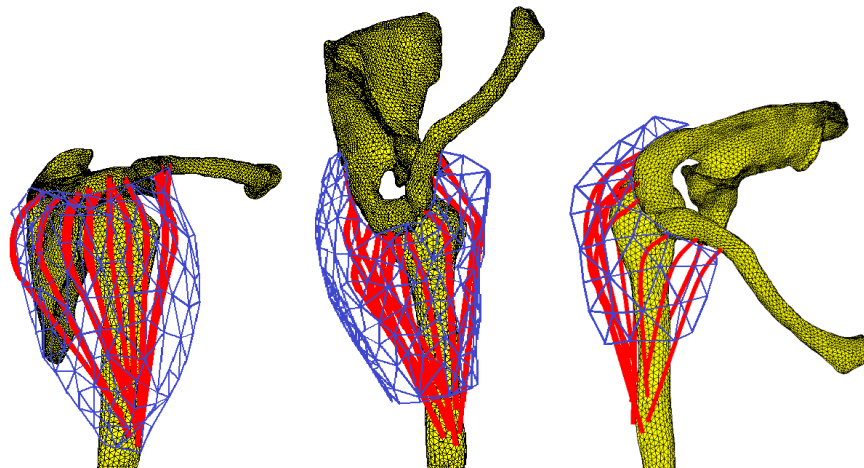
FIGURE 9.1: From left: the right side view of muscle bands for original rest joint position; the top view of abduction and the top view of forward flexion. All muscle lines lying within the deltoid muscle reconstructed from in vivo measured MRI.

9.2   Positions of Muscle Attachments

The positions of model muscle attachments are checked using the pictures of real anatomy, [87] and [66]. The Fig. 9.2 proves that the positions are correct. The origins of the acromial, claviculaer and scapular part are situated on the scapular acromion, clavicular deltoid tubercle and scapular spine, respectively. The insertions are fixed to the humeral deltoid tubersity.
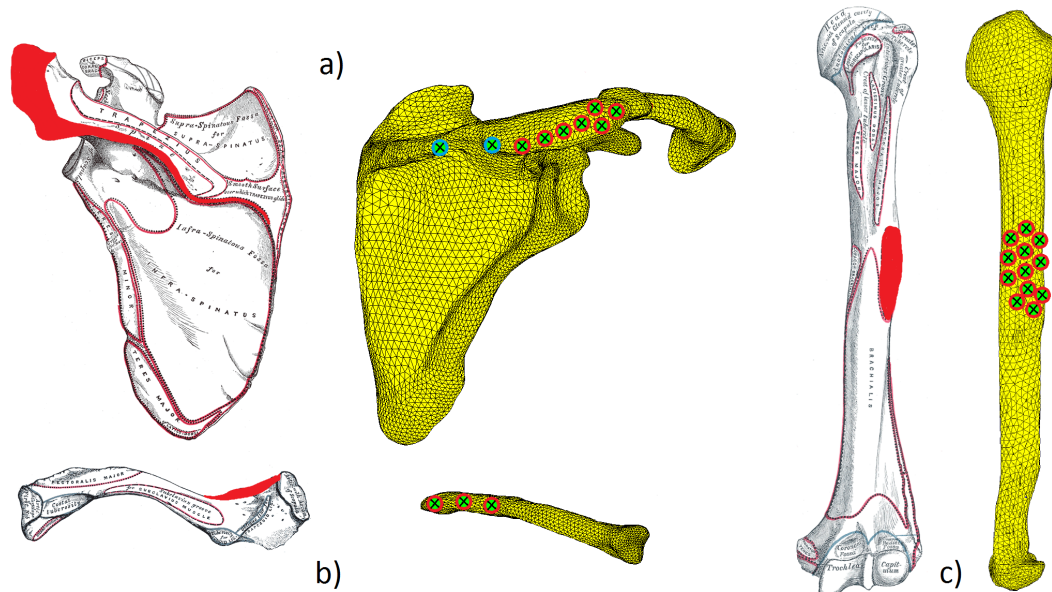
FIGURE 9.2: The comparison of computed and real positions of muscle attachments. (A) The red markers demonstrate the acromial muscle part; the blue markers are the scapular. (B) The origins of clavicular part. (C) The insertions of all muscle parts.

9.3   Results of Simulations

As the next test of model accuracy, the muscle forces, actual muscle length as well as muscle movement arms were compared with experimental data or by the results of corresponding musculoskeletal models already published in research sources.

Muscle Forces

Appropriate muscle forces generated during the shoulder abduction were predicted using the new torus-obstacle method and then compared by the experimental dataset as well as published modeling results, [2, 70, 96, 98, 110], see Fig. 9.3. The results show that the calculated muscle forces of 10 lines fit well the corridors built by the literature datasets. The only one line $AC5$ goes absolutely out of the marked area. This line is extremely closed to the scapular part and thus, these values are more comparable with the SC lines. In comparison with this group, the values achieve the highest muscle forces limits.

FIGURE 9.3: Muscle forces during the humeral abduction compared to the corridors based on literature [2, 70, 96, 98, 110]. The joint angles are given for fixed scapula.

The muscle forces produced by shoulder flexion were also validated using the literature [98]. The final comparison is summarized in Tab 9.1.

TABLE 9.1: The comparison of muscle forces generated in shoulder flexion.

muscle part	Helm [98]		**present study**	
	max muscle force [N]	corresponding angle [°]	max muscle force [N]	corresponding angle [°]
AC	39.58	89.9	43.90	90.00
CL	12.08	62.14	36.60	82.60
SC	57.08	60.58	$9.80 \cdot 10^{-4}$	$1 \cdot 10^{-4}$

Muscle Length

The original muscle lengths in the initial rest position of the shoulder joint at 0° of elevation were compared with the published data obtained by in vivo measured MRI [48] or from cadaver dissections [16, 32, 61, 98]. The results were also in agreement with precious modeling approaches, as shown in Tab. 9.2.

TABLE 9.2: Comparison of calculated muscle length while the resting arm position.

author	AC[mm]	CL[mm]	SC[mm]
Breteler [16]	-	151.938 ± 39.535	-
Langenderfer [61]	134.884 ± 22.480	125.581 ± 42.636	151.938 ± 17.828
Holzbaur [48]	-	181.395 ± 8.605	-
Favre [32]	154.264 ± 0.000	166.667 ± 0.000	154.264 ± 0.000
Helm [98]	162.426 ± 9.763	175.150 ± 18.863	148.225 ± 9.763
presented study	$\mathbf{197.600 \pm 26.900}$	$\mathbf{211.150 \pm 18.550}$	$\mathbf{221.200 \pm 0.100}$

Muscle Moment Arm

In most studies, the Standardization and Terminology Committee (STC) of the International Society of Biomechanics (ISB) is used to define the local and global coordinate systems, as published in [108]. According to this terminology, the X, Y and Z axis are oriented in anterior, superior and in lateral direction to the right, see Fig. 9.4. And thus, the backward flexion has the positive angle of rotation, however, the forward flexion has the negatives.

In presented work, the standards of STC were not respected. The coordinate system was based on in vivo MR images of developed shoulder model. Thus, the X, Y and Z axis are directed in

lateral to the right, in superior (proximo-distal) and in posterior direction, respectively, see Fig. 9.5. Because of this fact, the muscle moment arms of this study were transformed to ensured the correct validation with the given literature datasets.
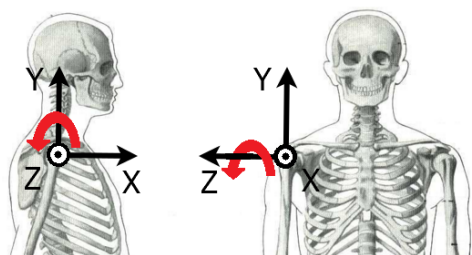
FIGURE 9.4: The coordinate system defined by the standards of the International Society of Biomehcanics.
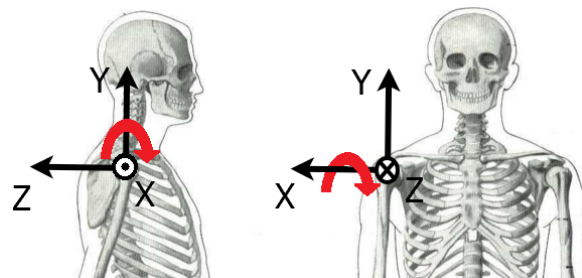
FIGURE 9.5: The coordinate system defined in presented study and based on MRI dataset.

Quantitative comparison of computed muscle moment arms predicted during humeral abduction and forward flexion to data from corresponding experiments or modeling results was performed, see Fig. 9.6 and Fig. 9.7. In both cases, the results of presented study fit well the corridors. However in few cases (lines $AC7$, $AC5$, $CL2$ for abduction and lines $AC1$, $AC3$, $AC5$, $AC7$, $CL1 - 3$ for flexion), the moment arm curves fell outside of the envelope. Fortunately, the error remained within ranges that have previously been considered tolerable, [5, 11, 47]. Moreover, some muscle lines of action (lines $CL1$, $CL3$, $SC1$ for abduction and lines $SC1$, $SC2$ for flexion) show absolutely different values of moment arms with opposite curve trend. Nevertheless, this corresponds with the process of muscle elongation.
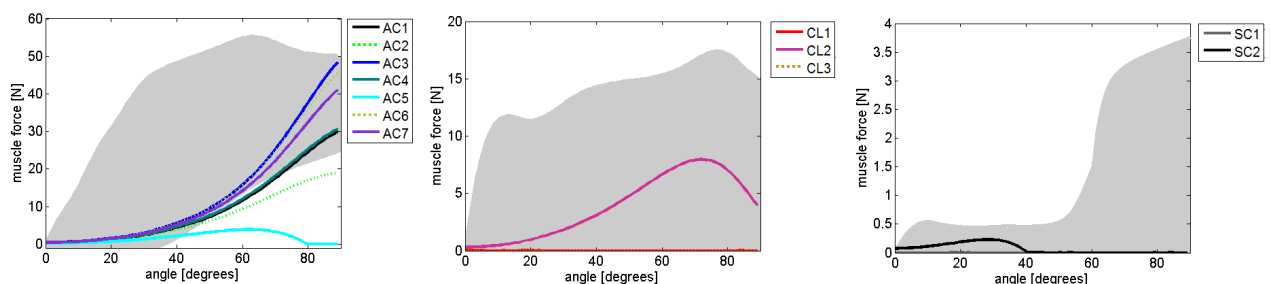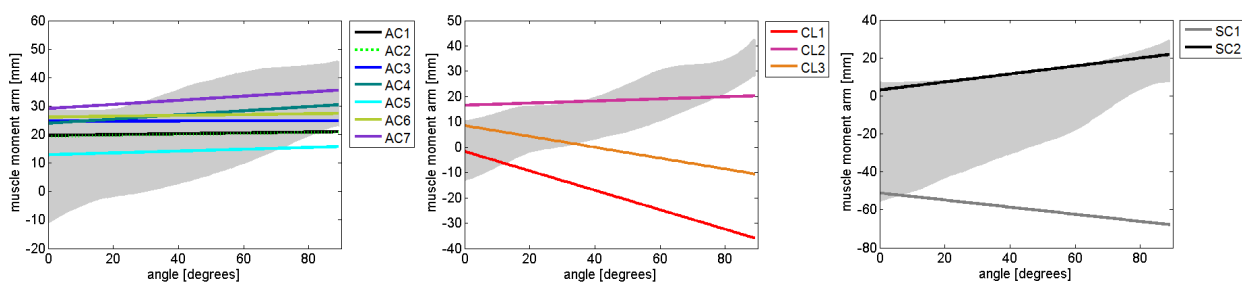

FIGURE 9.6: Muscle moment arms during the humeral abduction compared to the corridors based on literature [32, 50, 60, 62, 73, 74, 76, 110]. The joint angles are given for fixed scapula.
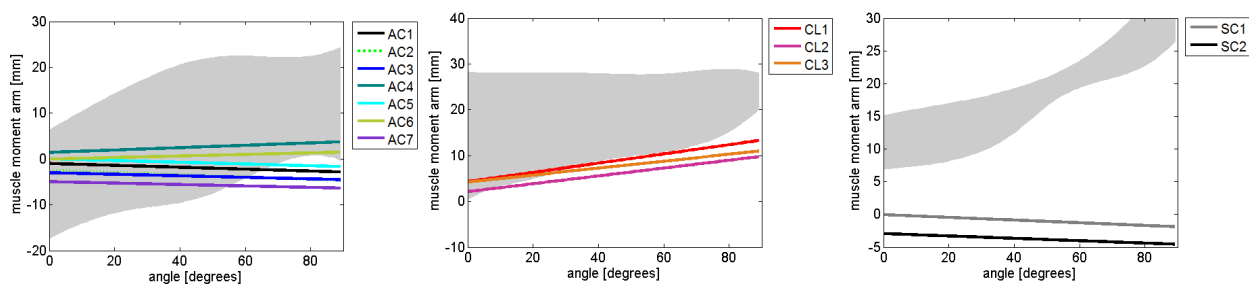
FIGURE 9.7: Muscle moment arms during the humeral forward flexion compared to the corridors based on literature [32, 39, 60, 98]. The joint angles are given for fixed scapula.

9.4   Initial Sensitivity Analysis

The initial sensitivity analysis was performed to find out how sensitive an output is to the changes in an input while keeping the other inputs without any changes. In other words, this method tells the model user how depends the output on each individual input. So, that helps to assess the risks.

The input parameters were little bit changed. For each of them, 50 different random values in range of $\pm$ 0.1 - 5% of original value was considered. The following changes were tested subsequently:

- *mass* - the mass of the whole upper arm was changed.

- *positions of muscle insertions* - the local positions of muscle insertions fixed to the humerus were changed in the direction of Z axis in the local coordinate system, see Fig. 8.2.

- *ellipse dimension* - the semi-major and semi-minor axes of elliptical base of cylinder representing the upper arm segment were changed. Thank that, the mass moments inertia were also changed.

- *toruses position* - the local positions of torus obstacles given in coordinate system of humerus, see Fig. 8.2, was also changed in the direction of Z axis.

For instance, one resulting comparison of muscle forces calculated with 50 different input positions of muscle insertion are depicted in Fig. 9.8, for the case of humeral abduction, muscle forces generated in line $AC1$. The results show that these changes do not cause such a big differences in outputs, i.e. muscle forces. The outputs increase or decrease is absolutely smooth, no local peaks appear, no step response of the shoulder model to the input changes shown. The effects of the input changes
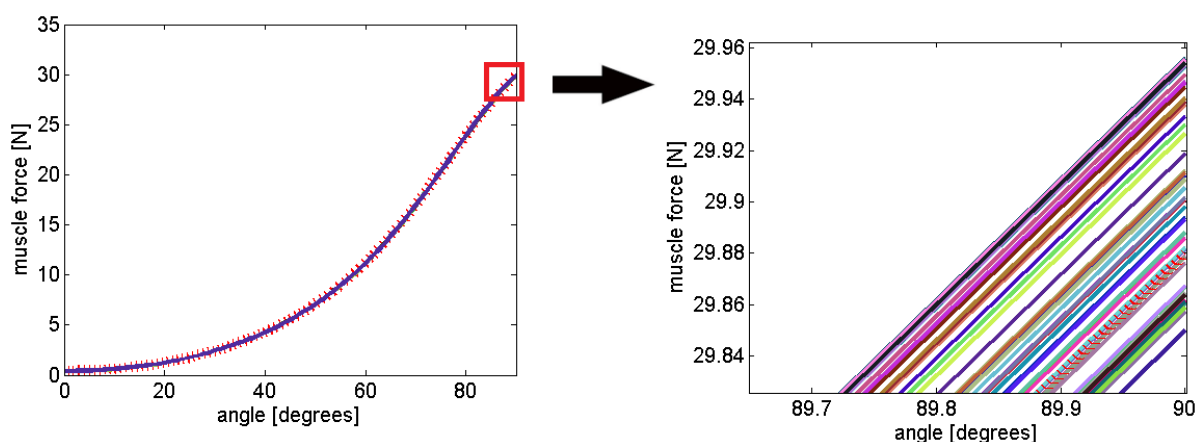
FIGURE 9.8: Initial sensitivity analysis.

to the outputs are summarized in Tab. 9.3, where 50 different values of 4 different input parameters are subsequently considered. The results confirm that chosen input parameters (mass, positions of muscle insertions, positions of torus obstacles and the mass distribution) have significant influence

on the output results. Therefore, the correct estimation of these data are essential for right use of the model.

TABLE 9.3: The internal sensitivity analysis. 4 input parameters changed - the mass, the positions of muscle insertions, the dimensions of ellipse representing the upper arm segment, the positions of toruses. For each that case, 50 different random values in range of $\pm$ 0.1 - 5% of original value considered. The results expressed as a percentage of change. In some cases ($CL1$, $CL3$, $SC1$ and $SC2$), no significant changed found (changes in thousandth of percent) - represented by expression NS (nonsignificant).

| muscle ID	changed input parameter							
	mass		insertion position		ellipse dim.		torus position	
	mean[%]	SD[%]	mean[%]	SD[%]	mean[%]	SD[%]	mean[%]	SD[%]
AC1	2.70	0.09	0.44	0.04	4.09	0.88	4.36	0.60
AC2	3.80	0.53	1.85	0.01	3.85	0.66	4.28	0.40
AC3	2.90	0.14	0.63	0.01	4.93	0.86	3.99	0.31
AC4	3.80	0.51	1.91	0.06	3.89	0.67	4.39	0.38
AC5	2.70	0.16	0.63	0.18	4.87	0.86	4.52	0.64
AC6	4.80	0.84	2.79	0.01	3.55	0.60	4.29	0.02
AC7	3.20	0.32	1.30	0.04	4.39	0.74	4.35	0.48
CL1	NS	NS	NS	NS	NS	NS	NS	NS
CL2	3.90	0.61	1.99	0.07	3.72	0.67	3.41	0.19
CL3	NS	NS	NS	NS	NS	NS	NS	NS
SC1	NS	NS	NS	NS	NS	NS	NS	NS
SC2	NS	NS	NS	NS	NS	NS	NS	NS

9.5 EMG-Force Comparison

The surface EMG was measured for the deltoid muscle during the shoulder abduction and forward flexion. The raw signal was filtered, rectified (the absolute values were calculated), smoothed and the root mean square method was in addition used. After that, the averaged modified EMG patterns were normalized to the maximal EMG recorded for individual signal. These results were compared with the muscle forces calculated by the model and also normalized by the maximal muscle forces of given muscle line.

The EMG signal can only be used for qualitative validation of the model. Particularly, the on/off EMG patterns during humeral abduction and forward flexion as well as the trend of curves shoulder correspond with the force calculation. The results show that the forces of acromial part in abduction and flexion corresponds well with EMG. The same situation is also for clavicular part for flexion. However, the clavicular part has the comparable EMG and force pattern till 70°. The other muscle lines have different EMG and force patterns. The final results are shown in Fig. 9.9, 9.10 and 9.11.
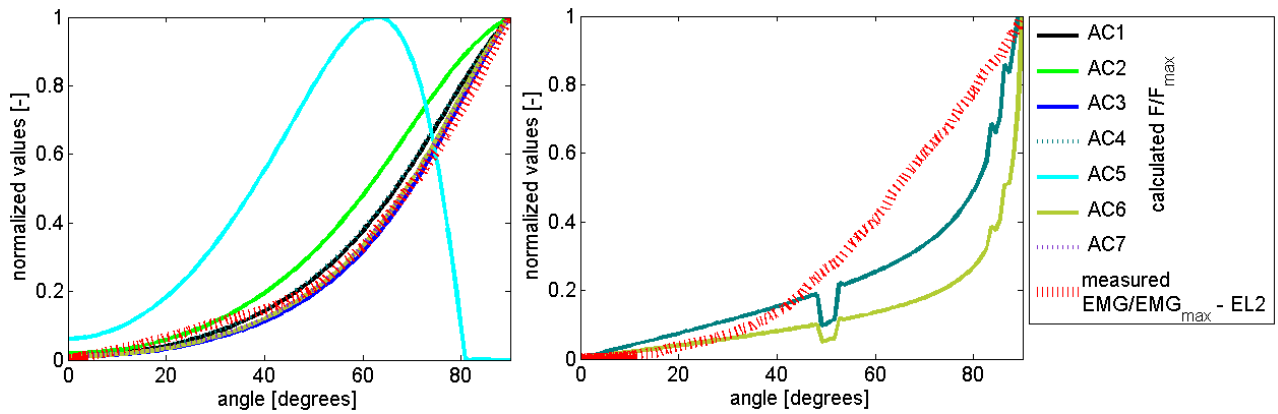
FIGURE 9.9: The comparison of EMG and force patterns during humeral abduction (left picture) and forward flexion (right picture) of the deltoid acromial part.
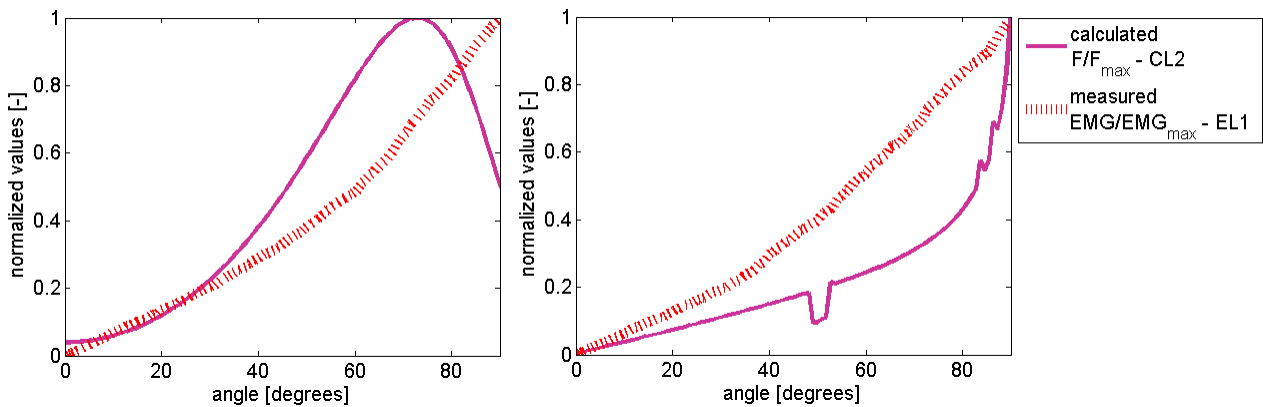
FIGURE 9.10: The comparison of EMG and force patterns during humeral abduction (left picture) and forward flexion (right picture) of the deltoid clavicular part.
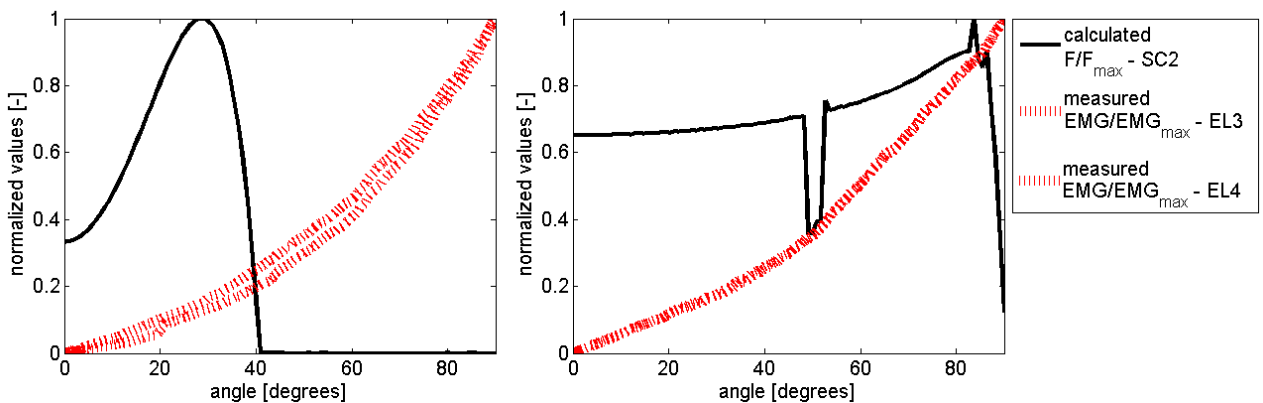
FIGURE 9.11: The comparison of EMG and force patterns during humeral abduction (left picture) and forward flexion (right picture) of the deltoid scapular part.

For the case of insignificant muscle forces, such as $CL1$, $CL3$ and $SC1$ for abduction, the comparison was not presented.

9.6 AMS Shoulder Models

The comparison of three musculoskeletal shoulder models was performed. The following models were considered: (1) the presented model developed by new torus-obstacle method and built in MATLAB, (2) the model built in AMS and using the via-point method, available free in repository of AMS and (3) the AMS model using the standard obstacle-set method, the modified AMS model. The resulting muscle forces and actual muscle lengths during the humeral abduction till 90° were compared, see Fig. 9.12 and 9.13.
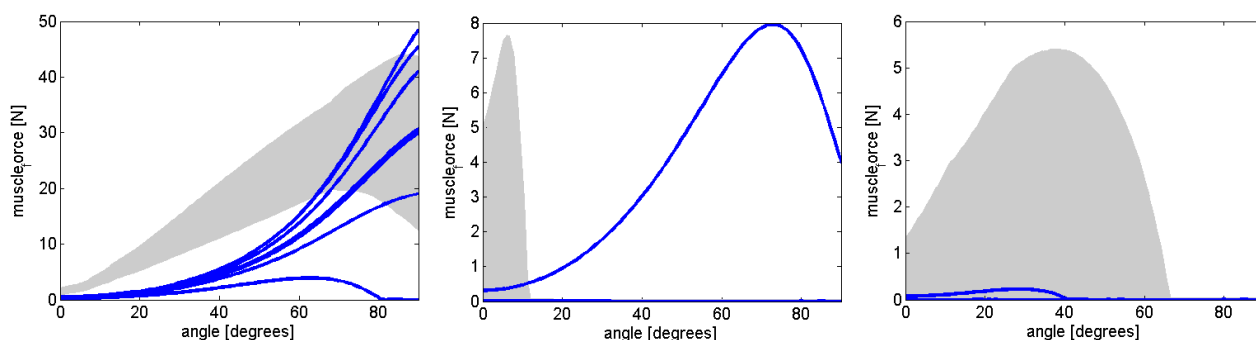
FIGURE 9.12: The comparison of muscle forces computed by model considering the new torus-obstacle method (blue lines) with the results from AMS models using the via-points and the obstacle-set method (gray corridors). From left: the acromial, the clavicular and the scapular part, respectively.
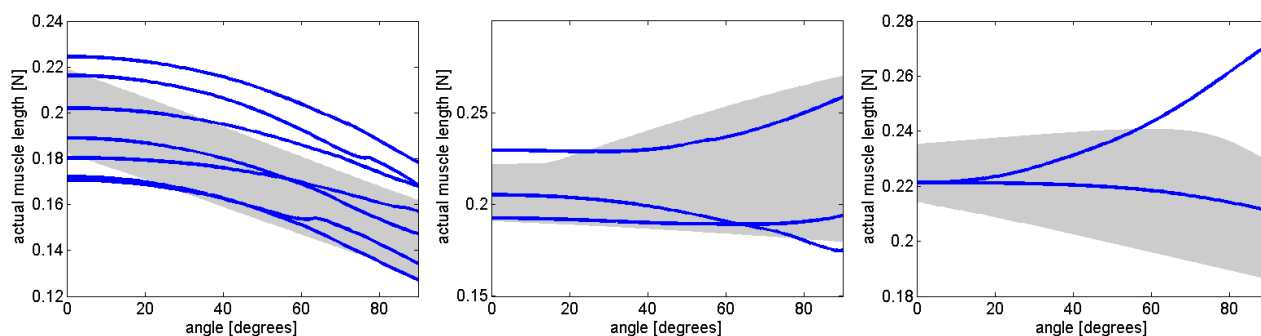
FIGURE 9.13: The comparison of actual muscle lengths computed by model considering the new torus-obstacle method (blue lines) with the results from AMS models using the via-points and the obstacle-set method (gray corridors). From left: the acromial, the clavicular and the scapular part, respectively.

The results show that the muscle forces generated in acromial part are comparable. The maximal muscle forces achieved at the end of abduction are similar. However, the increase of muscle forces in AMS models are significantly faster. The maximal forces in clavicular part are almost the same for AMS and presented models. Nevertheless, in the case of presented model, the maximal muscle forces are generated at the end of abduction while in the other cases, the maximals are shown at the beginning. The maximal forces produced by scapular muscle part are significantly higher for AMS models compared with the presented model. The actual muscle length shown in presented model and AMS models are well comparable.

Part V

DISCUSSION AND CONCLUSION

The shoulder mechanism represents very complex system with huge range of motion. Even if a model simulates a simplification of the reality, the model still remains very complicated. In the shoulder complex modeling, the existing methods for muscle path definition cease to be sufficient. They are not useful for all arbitrary movements, they cannot provide the real muscle shapes, etc. Therefore, the new torus-obstacle method was developed in this work to limit the lacks of existing methods. This algorithm adopts the main advantages of two already presented methods. It holds the muscle lines in given position as defined in via-points method [27, 84, 104] and it maintains the real muscle trajectory as supposed in obstacle-set method [37].

The method assumes that the muscle complex is represented by frictionless elastic bands having the same forces along the whole line. The neighboring structures are replaced by rigid torus having the distance from the center of the tube to the center of the torus equal to the radius of tube. The muscle has than prescribed path going straightly from origin perpendicularly to the torus surface, wrapping over the torus and intersecting the torus center, going perpendicularly from torus straightly to the muscle insertion. The geometry and the position of torus obstacles are automatically calculated respecting the MRI data and the actual joint position. The method considers the simplified muscle bulging up as well as changes of positions of underneath muscles. According to the research of corresponding studies, similar method including such a complex and automatic tools has never been presented. The torus-obstacle method has a lot of advantages. The main of them are summarized below:

- *the muscle shape comparable with real anatomy* The condition of muscle wrapping around the torus obstacle ensures the smooth curve of muscle path. Moreover, the center intersection guarantees the holding of muscle in correct position. Thanks that, the excessive muscle sliding over the obstacles, as founded in few studies [37, 38], is eliminated.

- *suitable for all arbitrary joint movements* The position, rotation as well as geometry of individual torus obstacles are recalculated for each joint position. In addition, the muscle lines are hold by torus to avoid the falling down while still keeping the real muscle path.

- *muscle bulging up considered* During the muscle contraction, the muscles change their shapes to save the volume. This process is significant and should not be neglected in the muscle path modeling [115]. Simplified muscle bulging up is also considered depending on actual muscle length.

- *automatic recalculation of model geometry* The positions of muscle attachments are automatic calculated respecting the muscle lines number set by user. This process is based on surfaces of muscle attachments originated from MRI and on the k-means method. Therefore, the user does not need to use the long list of input parameters such as expected in many studies [110] to add some other muscle line. The next advantage of this method is that the positions of muscle attachments and torus are defined in 3D.

- *fast computational performance and hight flexibility* As already noted in this work, the inter-connectivity between lines when modeling the path of broad muscles is important [110]. This is represented very well using the finite element method [11, 58]. In fact, the computation time to solve e.g. the muscle forces during the humeral abduction is on the order of tens of minutes to hours. In contrast, the computation time for the same task using the torus-obstacle method is less than 10 seconds.

  Presented algorithm offers also great flexibility. Theoretically, this method could be used for any number of muscle bands and for any kind of skeletal muscle.

The case of study was also to build the simplified shoulder model in MATLAB including the deltoid muscle. For the purpose of this work, the clavicle and the scapula were fixed. The complex of deltoid muscle was modeled by 12 lines of action (7 for acromial, 3 for clavicular and 2 of scapular part). Thanks that, the new torus-obstacle method was shown in practice. Thereafter, the abduction and the forward flexion till 90° were simulated to calculate the muscle forces, the actual muscle length and the muscle moment arm generated during these movements. The angle limitation was caused by the fact that the scapula movements were neglected.

Any model is as good as its validation [96]. Therefore, this model was also compared to the MRI data, literature and other shoulder models developed in AMS. One general problem of validation of musculoskeletal models is that the computed muscle forces cannot be measured directly. Only the qualitative comparison could be done. One method of accessing the individual contribution of muscles is to compare predicted forces with EMG signal. However, this comparison is influenced by the dependence of EMG on the muscle length [43]. To eliminate that, the EMG data were normalized to the maximal measured value and compared to the muscle forces normalized to the maximal calculated force. Just the trend validation was performed. The final results of method and model validation are discussed following in more details:

- *muscle path* The muscle trajectory for 0°, 45° and 90° were shown and thus, their real shapes were proved. The results were validated using the deltoid muscle contour based on MRI in the maximal considered abduction/flexion.

- *positions of muscle attachments* The positions of muscle attachments were compared to literature [66, 87]. The values were similar.

- *muscle forces* For the humeral abduction, the AC muscle part was found to be the main actuator. The CL part produces much lower activity (almost one tenth) and moreover, the SC part generates almost no activity. The maximal AC forces are achieved at the end of movement, almost $50N$. From ca. 50° of abduction, the muscle forces increase significantly faster. Firstly, the results were validated using the literature describing the similar models namely [2, 67, 96, 98, 110]. The muscle forces generated in AC and CL part were well comparable. However, the SC part is different. While the corridors indicate the force increase,

the presented work shows the decrease of values. Nevertheless, it still meets the limits of corridor.

In the case of humeral forward flexion, the main actuator is naturally the CL muscle part and also two lines of AC part - $AC4$ and $AC6$. The CL part reaches the maximal forces at 83.6° of flexion, almost $44N$, and the AC part at the end of movement, almost $44N$. Only the values of maximal muscle forces were compared with the study [96]. The AC part has the similar results. The CL part generates three times bigger forces compared with the study. On the contrary, the SC part of this work has negligible forces instead of the high values from [96] almost $60N$.

- *muscle length* The muscle lengths are based by the position of attachments given by MRI and by the parameters of torus obstacles. The muscle lengths in original rest position of the upper arm were validated using the literature such as [16, 32, 61, 98]. Respecting the given subject, the validation was successful.

- *muscle moment arm* The clinically-useful definition for muscle moment arm calculation was used as published in [3, 5]. In general, the muscle moment arms computed in this study shown significantly slower increase in comparison with the conclusions of literature [32, 60, 76]. The biggest differences were founded for lines $CL1$, $CL3$, $SC2$ of abduction and $SC1$, $SC2$ for flexion. In these cases, the calculated moment arms decrease caused by the muscle elongation, while in mentioned literature, these values increase significantly.

- *initial sensitive analysis* Four input parameters of presented shoulder model were changed (mass of the upper limb, the position of muscle insertions, the dimensions of ellipse representing the upper arm segment, the positions of torus) also to validate the model. For each change, 50 different random values in range of $\pm$ 0.1 - 5% of original value was considered. The results shown that the changes of output parameters reach as well 5% at the maximum. The outputs were smooth, without any local peaks and there were no step response.

- *EMG comparison* The normalized EMG signal and the normalized muscle forces were compared. In the AC and CL part, the values were comparable. However, for the $CL2$ muscle line of the abduction, the maximal muscle force was reached at 70° instead of 90° as measured. Nevertheless, this are the tolerable differences as concluded in [5, 11].

  The differences for SC part are more considerable. In this case, the processed EMG signal starts at the zero, the output curve is smooth and the maximal value is shown at the end of movement. In the presented study, the muscle forces get the step increase at the beginning and the maximal values are shown at 30° and 80° of abduction and flexion, respectively.

- *AMS shoulder models* The abduction and forward flexion is also simulated using the AMS shoulder models considering the via-point and obstacle-set method. The results shown that the AC part in abduction have slower increase of muscle forces in comparison with AMS models. In the CL part, the muscle forces reach the maximal values at about 80° of abduction. While the

AMS models have the maximal values at the beginning. Nevertheless, the values of maximal forces are quite the same. The actual muscle lengths of presented model and the AMS models are similar.

In summary, the validation of major actuators of given movements was successful. The *AC* and *CL* muscle parts were checked for humeral abduction and forward flexion till 90°. Nonetheless, the *SC* muscle part brought few problems. This could be caused by the new geometry based on the individual subjected MRI. But, the presented results confirmed that some muscle lines of this part are shortened during the movement and thus, calculated results are naturally expected. Fortunately, this part contributes not so much to the mentioned movements (e.g. muscle force - $0.3N$ for abduction, $1 \cdot 10^{-5}N$ for flexion). So, there is no significant influence of results. Maybe, this should be the topic for the next model improvements.

The next point is that few muscle lines where assign to the part according to the MRI slices (e.g. *AC*5) but they correspond better with some other part (*SC*, respectively). This is caused by the model geometry this line is too close to the second part.

Presented torus-obstacle method as well as modeled shoulder joint has some significant limits. The first one is that the scaling has not yet be included. For now, the model is strictly based on the subject dataset. The second one is that the position, rotation and the size of torus obstacles are estimated by the author based on the shoulder geometry. However, that should be more tested, discussed and alternatively modified. Up to now, this approach is considered to be the pilot. The third limitation is that the model, as well as method, was validated only for two simple movements humeral abduction and forward flexion. This was caused by three main facts (1) the new torus-obstacle method was validated and implemented for the first time and thus, it was necessary to start the testing with the simply movements; (2) the scapula and the clavicle were fixed and therefore, the motion was limited; (3) the effort was to compare the results with as many studies as possible, most of comparable studies are focused exactly on these two movements. Nevertheless, the validation should be extended at least, the backward flexion should be tested. Right in this movement, the *SC* deltoid muscle part, causing the problems in this study, represents the main actuator. Thanks that, this muscle part could be precisely tested. The final limitation is that the model is not prepared for motion capture data and that the scapular and clavicular movements are still neglected. This should be also improved.

Presented new torus-obstacle method designed for muscle path modeling in musculoskeletal models seems to be useful tool. The future steps are (1) to extended the method validation for other movements; (2) to use this method for next joints of human body; (3) to implement the method into some full body model that was already developed (e.g. AMS models); (4) and then to use that in practice for example to simulate some orthopaedic injuries or diseases, to optimize the rehabilitation, to help with diagnoses, and many others.

Bibliography

[1] ALEXANDER, R., AND VERNON, A. The dimension of knee and ankle muscles and the forces they exert. *Journal of Human Movement Studies 1* (1975), 115–123.

[2] AMBRÓSIO, J., QUENTAL, C., PILARCZYK, B., FOLGADO, J., AND MONTEIRO, J. Multibody biomechanical models of the upper limb. *Procedia IUTAM, 2011 Symposium on Human Body Dynamics 2* (2011), 4–17.

[3] AN, K., UEBA, Y., CHAO, E., COONEY, W., AND LINSCHEID, R. Tendon excursion and moment arm of index finger muscles. *Journal of Biomechanics 16(6)* (1983), 419–425.

[4] ANDREYKIV, A., PRENDERGAST, P., VAN KEULEN, F., SWIESZKOWSKI, W., AND ROZING, P. Bone ingrowth simulation for a concept glenoid component design. *Journal of Biomechanics 39* (2005), 1023–1033.

[5] ARNOLD, A., SALINAS, S., ASAKAWA, D., AND DELP, S. Accuracy of muscle moment arm estimated from mri-based musculoskeletal models of the lower extremity. *Comput. Aided Surg. 5(2)* (2000), 108–119.

[6] ARORA, J. *Introduction to Optimum Design*. McGraw-Hill Book Company, New York, NY, 1989.

[7] AUDU, M. The influence of muscle model complexity in musculoskeletal motion modeling. *Journal of Biomechanical Engineering 107* (1985), 147–157.

[8] BAO, H., AND WILLEMS, P. Y. Parameter estimation of fixed-distance joints. *Archive of Applied Mechanics 69* (1999), 465–479.

[9] BHAT, R. *Advanced Dynamics*. Alpha Science, Pngbourne, 2001.

[10] BIGLIAMI, L., POLLOCK, R., SOSLOWSKY, L., FLATOW, E., PAWLUK, R., AND MOW, V. Tensiel properties of the inferior glenohumeral ligament. *J Orthop Res 10* (1992), 187–197.

[11] BLEMKER, S., AND DELP, S. Three dimensional representation of complex muscle architectures and geometries. *Annals of Biomedical Engineering 33* (2005), 661–673.

[12] Bo Xu, B. *A Linked-plane Obstacle-set Algorithm for Modeling Broad Muscle Paths: Application to the Deltoid Muscle*. PhD thesis, Graduate Faculty of Baylor University, Waco, Texas, 2008.

[13] Brand, R., Crowninshield, R., Wittstock, C., Pedersen, D., Clark, C., and van Krieken, F. A model of lower extremity muscular anatomy. *Journal of Biomechanical Engineering 104* (1982), 304–310.

[14] Brand, R., Pedersen, D., Davy, D., Kotzar, G., Heiple, K., and Goldberg, V. Comparison of hip force calculations and measurements in the same patient. *Journal of Arthroplasty 9* (1994), 45–51.

[15] Brát, V. *Maticové metody v analýze a syntéze prostorových vázaných syst´mu*. Academia, 1981.

[16] Breteler, M., Spoor, C., and Van der Helm, F. Measuring muscle and joint geometry parameters of a shoulder for modeling purposes. *Journal of Biomechanics 32* (199), 1191–1197.

[17] Buchler, P., and Farron, A. Benefits of an anatomical reconstruction of the humeral head during shoulder arthroplasty: a finite element analysis. *Clinical Biomechanics 19* (2004), 16–23.

[18] Charlton, I. W., and Johnson, G. R. A model for the prediction of the forces at the glenohumeral joint. *Proceedings of the Institution of Mechanical Engineers 220* (2006), 801–812.

[19] Collins, J. The redundant nature of locomotor optimization laws. *Journal of Biomechanics 28(3)* (1995), 251–267.

[20] Couteau, B., Mansat, P., Estivalezes, E., Darmana, R., Mansat, M., and Egan, J. Finite element analysis of the mechanical behaviour of a scapula implanted with a glenoid prosthesis. *Clinical Biomechanics 16* (2001), 566–575.

[21] Crowninshield, R., and Brand, R. Physiologically based criterion of muscle force prediction in locomotion. *Journal of Biomechanics 14(11)* (1981), 793–801.

[22] Crowninshield, R., Johnston, R., Andrews, J., and Brand, R. A biomechanical investigation of the human hip. *Journal of Biomechanics 11* (1978), 75–85.

[23] Da Silva, M. *Human Motion Analysis Using Multibody Dynamics and Optimization Tools*. PhD thesis, Universidade técnica de Lisboa, 2003.

[24] De Jager, M. *Mathematical Head-Neck Models for Acceleration Impacts*. PhD thesis, Technical University of Eindhoven, 1996.

[25] DE LUCA, C. J., AND FORREST, W. J. Force analysis of individual muscles acting simultaneously on the shoulder joint during isometric abduction. *Journal of Biomechanics 6* (1973), 385–393.

[26] DELP, S., AND LOAN, J. A graphics-based software system to develop and analyze models of musculoskeletal structures. *Comput. Biol. Med. 25(1)* (1995), 21–34.

[27] DELP, S., LOAN, J., HOY, M., ZAJAC, F., TOPP, E., AND ROSEN, J. An interactive graphics-based model of the lower extremity to study orthopedic surgical procedures. *IEEE Transactions on Biomedical Engineering 37* (1990), 757–767.

[28] DICKERSON, C. R., MARTIN, B. J., AND CHAFFIN, D. The relationship between shoulder torques and the perception of muscular effort in load transfer tasks. *Ergonomics 49* (2006), 1036–1051.

[29] DOSTAL, W., AND ANDREWS, J. A three-dimensional biomechanical model of hip musculature. *Journal of Biomechanics 14* (1981), 803–812.

[30] EDELSON, J., ZUCKERMAN, J., AND HERCHKOVITZ, I. Os acromiale: anatomy and surgical implications. *J Bone Jt Surg 74 (B)* (1993), 551–555.

[31] ERDEMIR, A., MCLEAN, S., HERZOG, W., AND VAN DEN BOGERT, A. Model-based estimation of muscle forces exerted during movements. *Clinical Biomechanics 22(2)* (2007), 131–154.

[32] FAVRE, P., GERBER, C., AND SNEDEKER, J. Automated muscle wrapping using finite element contact detection. *Journal of Biomechanics 43* (2010), 1931–1940.

[33] FAVRE, P., SHEIKH, R., S.F., F., AND JACOB, H. An algorithm for estimation of shoulder muscle forces for clinical use. *Clin. Biomechanics 20* (2005), 822–833.

[34] FICK, A. E., AND WEBER, E. A. Anatomisch mechanische studie über die schultermuskeln. *Verh. d. phys. med. Ges. zu Würzburg 11* (1877), 123–152.

[35] FOX, B., JENNINGS, L., AND ZIMAYA, A. *Constrained Dynamics Computations, Models and case studies.* Word Scientific, Singapore, 2000.

[36] GARNER, B., AND PANDY, M. A kinematic model of the upper limb based on the visible human projects (vhp) image dataset. *Computer Methods in Biomechanics and Biomedical Engineering 2* (1999), 107–124.

[37] GARNER, B., AND PANDY, M. The obstacle-set method for representing muscle path in musculoskeletal models. *Computer Methods in Biomechanics and Biomedical Engineering 3* (2000), 1–30.

[38] GARNER, B., AND PANDY, M. Musculoskeletatl model of the upper limb based on the visible human male dataset. *Computer Methods in Biomechanics and Biomedical Engineering 4* (2001), 93–126.

[39] GATTI, C., DICKERSON, C., CHADWICK, E., MELL, A., AND HUGHES, R. Comparison of model-predicted and measured moment amrs for the rotator cuff muscles. *Clinical Biomechanics 22* (2007), 639–644.

[40] GUPTA, S., VAN DER HELM, F. C. T., AND VAN KEULEN, F. The possibilities of uncemented glenoid component - a finite element study. *Clinical Biomechanics 19* (2004), 292–302.

[41] HAJŽMAN, M., AND POLACH, P. Application of stabilization technique in the dynamic analysis of multibody systems. *Applied and Computational Mechanics 1* (2007), 479–488.

[42] HATZE, H. *Control Models of Skeletal Muscle. Characteristics and Applications.* PhD thesis, University of South Africa, 1991.

[43] HECKATBORNE, C., AND CHILDRESS, D. Relationship of the surface electromyogram to the force, length, velocity, and contraction rate of the cineplastic human biceps. *Am. J. Phys. Med. 60* (1981), 1–19.

[44] HERZOG, W. Sensitivity of muscle force estimation to changes in muscle input parameters using nonlinear optimization. *Journal of Biomechanical Engineering 114* (1992), 267–268.

[45] HILL, A. The heat of shortening and the dynamic constants of muscle. *Proceedings of Royal Society 126B* (1938), 136–195.

[46] HÖGFORS, C., KARLSSON, D., AND PETERSON, B. Structure and internal consistency of a shoulder model. *Journal of Biomechanics 28*, 7 (1995), 767–777.

[47] HOLZBAUR, K., MURRAY, W., AND DELP, S. A model of the upper extremity for simulating musculoskeletal surgery and analyzing neuromuscular control. *Biomedical Engineering 33(6)* (2005), 829–840.

[48] HOLZBAUR, K., MURRAY, W., GOLD, G., AND DELP, S. Upper limb muscle volumes in adult subjects. *Journal of Biomechanics 40* (2007), 741–749.

[49] HOPKINS, A. R., HANSEN, U. N., AND AMIS, A. Finite element model of total shoulder replacement: application of boundary conditions. *Comput. Methods Biomech. Biomed. Eng. 8* (2005), 39–55.

[50] HUGHES, R. E., NIEBUR, G., LIU, J., AND AN, K. Comparison of two methods for computing abduction moment arms of the rotator cuff. *Journal of Biomechanics 31* (1998), 157–160.

[51] HVORSLEV, C. M. Studien über die bewegungen der schulter. *Skand. Arch. f. Physiol. 53* (1927), 1–136.

[52] Johnson, M., Polgar, J., Weightman, D., and Appleton, D. Data on the distribution of fiber types in thirty-six human muscles. *J. Neurol. Sci. 18* (1973), 111–129.

[53] Kaftka, R., and Gurdal, Z. *Elements of Structural Optimization.* Kluwer Academic Publisher, 1992.

[54] Kane, T., Likins, P., and Levinson, D. *Spacecraft Dynamics.* Mcfraw-Hill, 1983.

[55] Kapandji, I. *The physiology of the joints. Annotated diagrams of the mechanics of the human joints.* Churchill Livingstone, Edinbourg, 1974.

[56] Karlsson, D., and Peterson, B. Towards a model for force predictions in the human shoulder. *Journal of Biomechanics 25* (1992), 189–192.

[57] Klopčar, N., Tomšič, M., and Lenarcic, J. A kinematic model of the shoulder complex to evaluate the arm-reachable workspace. *Journal of Biomechanics 40* (2007), 86–91.

[58] Kohout, J., Clapworthy, G., Zhao, Y., Tao, Y., Gonzalez-Garcia, G., Dong, F., Wei, H., and Kohoutova, E. Patient-specific fibre-based models of muscle wrapping. *Interface Focus 3* (2013), 1–8.

[59] Kraft, D. *A Software Package for Sequential Quadratic Programming.* Technical Report DFVLR-FB, DLR German Aerospace Center - Institute for Dynamics of Flight Systems, Germany, 1988.

[60] Kuechle, D., Newman, S., Itoi, E., Morrey, B., and An, K. Shoulder muscle moment arms during horizontal flexion and elevation. *Journal of Shoulder and Elbow Surgery 6* (1997), 429–439.

[61] Langenderfer, J., Jerabek, S., Thangamani, V., Kuhn, J., and Hughes, R. Musculoskeletal parameters of muscles crossing the shoulder and elbow and the effect of sarcomere length sample size on estimation of optimal muscle length. *Clinical Biomechanics 19* (2004), 664–670.

[62] Liu, J., Hughes, R., Smutz, W., Niebur, G., and Nan-An, K. Roles of deltoid and rotator cuff muscle in shoulder elevation. *Clinical Biomechanics 12* (1997), 32–38.

[63] Lloyd, S. Least squares quantization in pcm. *IEEE Transactions of Information Theory 28* (1982), 129–137.

[64] Lund, M., Zee, M., Anderson, M., and Rasmussen, J. On validation of multibody musculoskeletal models. *Journal of Engineering in Medicine 226(2)* (2012), 82–94.

[65] Maurel, W., and Thalmann, D. Human shoulder modeling including scapulo-thoraxis constrain and joint sinus cones. *Computer & Graphics 24* (2000), 203–218.

[66] MOELLER, T., AND REIF, E. *Pocket Atlas of Sectional Anatomy, Computer Tomography and Magnetic Resonance Imaging.* Thieme, Germany, 2007.

[67] MOLLIER, S. Über die statik und mechanik des menschlichen schultergürtels unter normalien und patholohischen verhältnissen. *Festschr. f. C. v. Kupffer* (1899).

[68] MÖRL, F., SIEBERT, T., SCHMITT, J., BLICKHAN, R., AND GÜNTHER, M. Electro-mechanical delay in hill-type muscle models. *J. Mech. Biol. 12(5)* (2012).

[69] MURPHY, L. A. Prendergast, p. j., acromion-fixation of glenoid components in total shoulder arthroplasty. *Journal Biomechanics 38* (2005), 1702–1711.

[70] NIEMI, J., NIEMINEN, H., TAKALA, E., AND VIIKARI-JUNTURA, E. A static shoulder model based on a time-dependent criterion for load sharing between synergistic muscles. *Journal of Biomechanics 29(4)* (1996), 451–460.

[71] NIKOOYAN, A., AND VEEGER, H. Development of a comprehensive musculoskeletal model of the shoulder and elbow. *Med Biol Eng Comput 49* (2011), 1425–1435.

[72] NIKOOYAN, A. A., VEEGER, H. E. J., WESTERHOFF, P., BOLSTERLEE, B., GRAICHEN, F., BERGMANN, G., AND VAN DER HELM, F. An emg-driven musculoskeletal model of the shoulder. *Human Movement Science 31* (2012), 429–447.

[73] NYFFELER, R., SHEIKH, R., JACOB, H., AND GERBER, C. Influence of humeral prosthesis height on biomechanics of glenohumeral abduction. an in vitro study. *Journal of Bone and Joint Surgery American 86-A* (2004), 575–580.

[74] OTIS, J., JIANG, C., WICKIEWICZ, T., PETERSON, M., WARREN, R., AND SANTNER, T. Changes in the moment arms of the rotator cuff and deltoid muscles with abduction and rotation. *Journal of Bone and Joint Surgery American 76* (1994), 667–676.

[75] PEDOTTI, A., KRISHMAN, V., AND STARK, L. Optimization of muscle force sequencing in human locomotion. *Mathematical Bioscience 38* (1978), 57–76.

[76] POPPEN, N. K., AND WALKER, P. S. Forces at the glenohumeral joint in abduction. *Clin. Orthop. Relat. Res. 135* (1978), 165–170.

[77] RAU, G., DISSELHORST-KLUG, AND SCHMIDT, R. Movements biomechanics goes upwards: from the leg to the arm. *Journal of Biomechanics 33* (2000), 1207–1216.

[78] ROBERTSON, D., HAMILL, J., KAMEN, G., CALDWELL, G., AND WHITTLESEY, S. *Research Methods in Biomechanics.* Human Kinetics Publishers, 2004.

[79] SACKS, R.D., R. R. Architecture of the hind limb muscles of cats: Functional significance. *Journal of Morphology* (1982), 185–195.

[80] SCEPI, M., FAURE, J., RIDOUX, N., KAMINA, P., AND RICHER, J. A three-dimensional model of the shoulder girdle. forces developed in deltoid and supraspinatus muscles during abduction. *Surg Radiol Anat. 26* (2004), 290–296.

[81] SCHNECK, D. *Mechanics of Muscle.* PhD thesis, New York, NY: New York University Press, 1992.

[82] SEIREG, A., AND ARVIKAR, R. A mathematical model for evaluation of forces in the lower extremities of the musculoskeletal system. *Journal of Biomechanics 6* (1973), 316–326.

[83] SHABANA, A. A. *Computational Dynamics.* JOHN WILEY & SONS, INC., 2001.

[84] SHELBURNE, K., AND PANDY, M. A musculoskeletal model of the knee for evaluating ligament forces during isometric contraction. *Journal of Biomechanics 30* (1997), 163–176.

[85] SHERMAN, M., SETH, A., AND DELP, S. What is a moment arm calculating muscle effectiveness in biomechanical models using generalized coordinates. *Proc ASME Des Eng Tech Conf.* (2013).

[86] SHIINO, K. Schultergelenkbewegungen und schultermuskelarbeit. *Arch. u. Physiol. Anat. Abt. (Suppl)* (1913).

[87] SINĚLNIKOV, R. *Atlas anatomie člověka I.* AVICENUM, 1980.

[88] SNYMAN, J. *Practical mathematical optimization.* Springer, 2005.

[89] SPENCER, J., AND TURKEL, M. Stabilising mechanismus preventing anterior dislocation of the glenohumeral joint. *J. Bone Jt Surg 63 (B)* (1981), 1208–1217.

[90] STRASSER, H. *Lehrbuch der Muskel- und Gelenkmechanik, Die obere Extremität.* Springer, 1917.

[91] TONDU, B. *Modelling of the Shoulder Complex and Application to the Design of Upper Extremities for Humanois Robots.* Proceedings of 2005 5th IEEE-RAS International Conference of Human Robots, 2005.

[92] TSIRAKOS, D., BALZOPOULUS, V., AND BARTLETT, R. Inverse optimization functional and physiological considerations related to the force-sharing problem. *Critical Reviews in Biomedical Engineering* (1997), 371–407.

[93] VALDMANOVÁ, L. *Kosterně svalová rovnováha horní končetiny.* PhD thesis, University of West Bohemia, Faculty of Applied Sciences, Department of mechanics, 2011.

[94] VALDMANOVÁ, L., AND KUBOVÝ, P. The process of motion capture data and its usage for shoulder modeling. *Acta Universitatic Carolinea Kinanthropologica* (accepted for publication, 2015).

[95] VALDMANOVÁ, L., AND ČECHOVÁ. Three-body segment musculoskeletal model of the upper limb. *Applied and Computational Mechanics 7* (2013), 87–98.

[96] VAN DER HELM, F. A finite element musculoskeletal model of the shoulder mechanism. *Journal of Biomechanics 27(5)* (1994), 551–569.

[97] VAN DER HELM, F., VEEGER, H., PRONK, G., VAN DER WOUDE, L., AND ROZENDAL, R. Geometry parameters for musculoskeletal modelling of the shoulder system. *Journal of Biomechanics 25* (1992), 129–144.

[98] VAN DER HELM, F. C. T. Analysis of the kinematic and dynamic behaviour of the shoulder mechanism. *Journal of Biomechanics 27* (1994), 527–550.

[99] VEEGER, H. E. J., AND VAN DER HELM, F. C. T. Shoulder function: the perfect compromise between mobility and stability. *Journal of Biomechanics 40* (2007), 2119–2129.

[100] ŠPIČKA, J., HAJŽMAN, M., AND HYNČÍK, L. Double pendulum contact problem. *Applied and Computational Mechanics 8* (2014), 115–128.

[101] WICKHAM, J., AND BROWN, J. The function of neuromuscular compartments in human shoulder muscles. *J Neurophysiol 107* (2012), 336–345.

[102] WILLIAMS, P. *Gray's Anatomy: The Anatomical Basis of Medicine and Surgery.* Churchill Livingstone, USA, 1995.

[103] WINTERS, J. Hill-based muscle models: a systems engineering perspective. *Multiple Muscle Systems. Biomechanics and Movements Organization, Edited by J.M. Winters and S.L.-Y. Woo, New York, Springer-Verlag.* (1990), 69–94.

[104] WINTERS, J., AND KLEWENO, D. Effect of initial upper-limb alignment on muscle contributions to isometric strength curves. *Journal of Biomechanics 26* (1993), 143–153.

[105] WINTERS, J., AND STARK, L. Analysis of fundamental human movement patterns. *IEEE Transactions on Biomedical Engineering 12* (1985), 826–839.

[106] WITTEK, A. *Mathematical Modeling of the Muscle Effects on the Human Body Responses under Transient Loads.* PhD thesis, Chalmers University of Technology, 2000.

[107] WOOD, J. E., AND MEEK, S. G. Quatitation of human shoulder anatomy for prosthetic arm control - i., surface modelling. *J. Biomechanics 22* (1989), 273–292.

[108] WU, G., VAN DER HELM, F., VEEGER, H., MAKHSOUS, M., VAN ROY, P., ANGLIN, C., NAGELS, J., KARDUNA, A., MCQUADE, K., WANG, X., WENER, F., AND BUCHHOLZ, B. Isb recommendation on definitions of joint coordinate systems of various joints for the reposting og human joint motion - part ii: shoulder, elbow, wrist and hand. *Journal of Biomechanics 38* (2005), 981–992.

[109] WUELKER, N., WIRTH, C. J., AND PLITZ, W., R. B. A dynamic shoulder model: reliability testing and muscle force study. *Journal of Biomechanics 28* (1995), 489–499.

[110] XU, B. *A Linked-plane Obstacle-set Algorithm for Modeling Broad Muscle Paths: Application to the Deltoid Muscle.* PhD thesis, Baylor University, USA, 2008.

[111] YAMAGUCHI, G., SAWA, A., MORAN, D., AND FESSLER, M.J., W. J. *Multiple Muscle Systems: Biomechanics and Movement Organization.* Springer Verlag, New York, 1990.

[112] YAMAGUCHI, G. T., MORAN, D., AND SI, J. A computationally efficient method for solving the redundant problem in biomechanics. *Journal of Biomechanics 28 (8)* (1995), 999–1005.

[113] YANG, J. J., FENG, X., XIANG, Y., KIM, J., AND RAJULU, S. Determining the three-dimensional relation between the skeletal elements of the human shoulder complex. *Journal of Biomechanics 42* (2009), 1762–1767.

[114] YU, J., ACKLAND, D. C., AND PANDY, M. Shoulder muscle function depends on elbow joint position: An illustration of dynamic coupling in the upper limb. *Journal of Biomechanics* (2001).

[115] ZATSIORSKY, V., AND PRILUTSKY, B. *Biomechanics of Skeletal Muscles.* Thomson-Shore, Inc., USA, 2012.